Exchange of Nutrients and Oxygen between Sediments and Water Column: the Role of the Benthic Boundary Layer

Dissertation
zur Erlangung des
Doktorgrades der Naturwissenschaften
dem Fachbereich Geowissenschaften
der Universität Bremen vorgelegt

von
Moritz Holtappels

Bremen, August 2009

Die vorliegende Arbeit wurde in der Zeit von Dezember 2005 bis August 2009 am Max-Planck-Institut für marine Mikrobiologie in Bremen angefertigt.

Gutachter:
Prof. Dr. Bo Barker Jørgensen
Prof. Dr. Michael Schlüter

Prüfer:
Prof. Dr. Achim Kopf
Priv. Doz. Dr. Volker Brüchert

Weitere Mitglieder des Prüfungsausschusses:
Dr. Heiko Sahling
Meri Eichner

Datum des Promotionskolloquiums: 18. September 2009

Table of Contents

Abstract

This thesis largely focuses on the transport and transformation of nutrients and oxygen across the benthic boundary layer (BBL). The BBL denotes the water layer that is directly influenced by the interface between the sediment and the overlying water column and which is characterized by intense turbulent mixing, gradients in solutes and increased concentrations of suspended particulate matter. So far, the rates and regulation of nutrient exchange across and microbial activity within the BBL are poorly understood. The aim of this thesis is to characterize and quantify the vertical transport of nutrients and oxygen across the BBL as well as the microbial activity within the BBL. The vertical turbulent transport in the benthic boundary layer is subject of two Chapters of which one focuses on the measurement and interpretation of nutrient and oxygen concentration gradients in the BBL while the other focuses on the dynamics of turbulent flow in the BBL and its mixing efficiency. Microbial activity in the BBL is described for several different sites exhibiting oxic as well as suboxic bottom waters.

The thesis presents the first study that evaluates sediment-water fluxes from solute gradient measurements in the BBL. A newly built sampling gear was deployed to measure nutrient and oxygen concentration gradients in the BBL of the Baltic Sea with a high depth resolution. The concentration profiles identified the sediment as a source of ammonium, nitrite and nitrate and a sink for oxygen. These concentration profiles were used to calculate the ratio of nutrient flux to oxygen flux across the sediment water interface. On the basis of nutrient-oxygen flux ratios and sedimentary C/N ratios the amount of sedimentary nitrogen which was nitrified, denitrified and exported to the overlying water column was determined. The results of this study indicate that nitrification at the sediment surface in Baltic Sea is an important source of water column nitrate as well as the sole source of nitrate for sedimentary denitrification.

To study the turbulent diffusive transport a new approach, which is based on Taylor's theory of turbulent diffusion, was developed to calculate turbulent diffusivity from acoustic Doppler velocimetry (ADV) data. The new approach was tested during a study of the dynamics of turbulent diffusivity in the BBL of Lake Constance. With common ADV, flow velocities were measured in the BBL at variable current velocities and density stratifications. Turbulent diffusivities were determined by using three different approaches; first, the new approach based on Taylor's theory, second, the logarithmic Law of the Wall and third, direct

gradient-flux measurements. The results obtained from Taylor's theory agreed well with results from the gradient-flux measurements. In contrast, the logarithmic Law of the Wall failed to predict plausible diffusivities whenever the boundary flow exhibited decreased current velocities or stable density stratification. Under these conditions, the turbulent diffusivities calculated from the gradient-flux measurement and from Taylor's theory were as low as 10^{-6} m^2 s^{-1}. A simple flux model was developed to predict the effect of low diffusivities on the oxygen flux into the sediment. Results from the flux model suggest that low diffusivities in the benthic boundary layer have the potential to decrease oxygen concentrations and oxygen flux at the sediment surface.

As nutrients are transported across the BBL, the microbial processes in the BBL may alter the nutrient flux and the nutrient stoichiometry and as such control the primary production and the species composition of the phytoplankton community in the surface waters. Microbial aerobic respiration and anaerobic nitrogen loss processes in the BBL and the adjacent sediment and water column were studied during a cruise to the Pakistani Margin in the Arabian Sea in Oktober 2007. Anammox and denitrification rates in sediment, benthic boundary layer and overlying suboxic waters were determined from incubation experiments. These experiments indicate that sedimentary nitrogen loss was dominated by denitrification and that the contribution of anammox to the total sedimentary N-loss increased with water depth. The areal rates of nitrogen loss from the Pakistani Margin sediments exceeded those from the overlying suboxic water column. In the water column, anammox was the dominant nitrogen loss process. Anammox rates in the water column were low and were detected exclusively in the benthic boundary layer and in the oxycline of the upper water column. Oxygen consumption rates in the oxygen minimum zone were determined from a simple flux model. The low oxygen consumption rates in the water column corresponded with the low anammox rates.

Aerobic respiration rates were directly measured in the benthic boundary layer of the North Sea and the Baltic Sea. Applying oxygen optodes, oxygen respiration rates were measured in samples from various settings that contained different amounts of particulate organic matter. The results indicate that quantity and quality of particulate organic matter can only partly account for the observed oxygen respiration rates and that a considerable amount of aerobic respiration in the BBL of the Baltic and North Sea is due to the mineralization of dissolved organic matter.

Kurzfassung

Gegenstand der vorliegenden Doktoarbeit ist die benthische Grenzschicht und deren Einfluss auf die mikrobielle Aktivität und den Nährstoff- und Sauerstofftransport zwischen den Sedimenten und der darüberliegenden Wassersäule. In den aquatischen Wissenschaften bezeichnet die benthische Grenzschicht jene Wasserschicht, die durch den Übergang zwischen Sediment und Wassersäule beeinflusst ist. Kennzeichnend für die benthische Grenzschicht sind turbulente Wasserströmungen, hohe Gradienten gelöster Stoffe und erhöhte Partikelkonzentrationen. Der Einfluss dieser Eigenschaften auf den Nährstofftransport und die mikrobielle Aktivität ist wenig bekannt. Ziele der vorliegenden Arbeit sind die Beschreibung und Quantifizierung der mikrobiellen Prozesse und der vertikalen Nährstoff- und Sauerstoffflüsse in der benthischen Grenzschicht. Der turbulent-diffusive Stofftransport in der benthischen Grenzschicht wird anhand zweier Studien beschrieben, von denen sich die erste mit der Messung und Interpretation von Nährstoff- und Sauerstoffgradienten in der benthischen Grenzschicht befasst während eine zweite Studie den turbulent-diffusiven Stofftransport in Abhängigkeit zu den Strömungseigenschaften in der benthischen Grenzschicht beschreibt. In weiteren Untersuchungen werden mikrobielle Prozesse sowohl in oxischen als auch anoxischen benthische Grenzschichten beschrieben.

Im Rahmen der vorliegenden Doktorarbeit konnten erstmalig Nährstoff- und Sauerstoffaustausch zwischen Sediment und Wassersäule anhand von Konzentrationsgradienten in der benthischen Grenzschicht bestimmt werden. Während einer Expedition in die Ostsee wurde ein neu konstruiertes Beprobungsgerät eingesetzt, um in der benthischen Grenzschicht hochaufgelöste Profile von Nährstoff- und Sauerstoffkonzentrationen zu messen. Anhand der Konzentrationsgradienten ließ sich das Sediment als Quelle für Ammonium, Nitrit und Nitrat und als Senke für Sauerstoff bestimmen. Das Verhältnis der Nährstoffflüsse zum Sauerstofffluss konnte aus den Konzentrationsprofilen berechnet werden. Die Stoffflussverhältnisse in der benthischen Grenzschicht und die C/N Verhältnisse im Sediment dienten als Grundlage für das Erstellen einer Stickstoffbilanz, welche die Anteile des mineralisierten Stickstoffes beschreibt, die nitrifiziert, denitrifiziert oder an die Wassersäule abgegeben werden. Es stellte sich heraus, dass die Nitrifizierungraten an der Sedimentoberfläche ausreichend hoch waren, um sowohl die Denitrifizierung im Sediment als auch das Bodenwasser mit Nitrat zu versorgen.

Für die Untersuchungen des turbulent-diffusiven Stofftransports in der benthischen Grenzschicht wurde ein neuartiger Meßansatz entwickelt, der es erlaubt aus Doppler-Geschwindigkeitsmessungen den turbulenten Diffusionskoeffizienten zu bestimmen. Der neue Meßansatz, abgeleitet von Taylors Theorie der turbulenten Diffusion, wurde im Rahmen einer *insitu* Untersuchung über die Variabilität turbulenter Diffusion getestet. In einer benthischen Grenzschicht wurde die turbulente Strömung unter variierenden Fließgeschwindigkeiten und Dichteschichtungen gemessen. Turbulente Diffusions-koeffizienten wurden sowohl über den neuen Meßansatz, als auch über das logarithmische Wandgesetz sowie mit gewöhnlichen Fluss-Gradienten-Messungen bestimmt. Die Werte aus dem neuen Meßansatz stimmten mit denen der Fluss-Gradienten-Messungen überein. Das logarithmische Wandgesetz dagegen ergab stark abweichende Werte bei geringen Fließgeschwindgkeiten und stabilen Dichteschichtungen. Unter solchen Strömungsbedingungen waren die aus Fluss-Gradienten-Messungen und aus dem neuen Meßansatz ermittelten turbulenten Diffusionskoeffizienten auf bis zu 10^{-6} m^2 s^{-1} verringert. Ein einfaches Modell zur Simulation von Sauerstoffflüssen über die benthische Grenzschicht wurde entwickelt, um die Auswirkungen verringerter turbulenter Diffusivität auf den Sauerstofftransport ins Sediment abzuschätzen. Die Modellberechnungen zeigten, dass turbulente Strömungen mit Diffusionskoeffizienten in dieser Größenordnung den Sauerstofftransport zum Sediment kontrollieren können.

Da die Nährstoffe auf ihrem Transport von den Sedimenten in die obere Wassersäule die benthische Grenzschicht passieren müssen, ist es möglich, dass mikrobielle Prozesse in der benthischen Grenzschicht die Flussraten und die Zusammensetzung der Nährstoffe verändern können und damit die Primärproduktion und die Artzusammensetzung des Phytoplanktons in der oberen Wassersäule kontrollieren. Im Rahmen der vorliegenden Arbeit wurden mikrobielle Prozesse in der benthischen Grenzschicht und den angrenzenden Sediment- und Wasserschichten untersucht, wobei aerobe Respiration und anaerobe Stickstoffverlustprozesse im Mittelpunkt der Untersuchungen standen. Während einer Expedition ins Arabische Meer im Oktober 2007, wurden Anammox- und Denitrifizierungsraten in Sedimenten, der benthischen Grenzschicht und der suboxischen Wassersäule mit Hilfe von Inkubationsexperimenten gemessen. Denitrifizierung war überwiegend verantwortlich für den Stickstoffverlust im Sediment, wobei der Anteil von Anammox mit zunehmender Wassertiefe anstieg. Anammox war dagegen fast ausschließlich verantwortlich für den Stickstoffverlust in der suboxischen Wassersäule. Die Anammoxraten in der Wassersäule waren gering und konnten nur in der Sauerstoffsprungschicht der oberen

Wassersäule und in der benthischen Grenzschicht gemessen werden. Ergänzend wurden die Sauerstoffrespirationsraten in der suboxischen Wassersäule modelliert, deren geringen Werte sich mit den geringen Anammoxraten deckten.

In einer weiteren Untersuchung wurden Sauerstoffrespirationsraten in der benthischen Grenzschicht der Nordsee und der Ostsee gemessen. Mit Hilfe von Sauerstoff-Optoden wurden Sauerstoffrespirationsraten in Wasserproben aus verschiedenen Beprobungstationen und mit unterschiedlichem Gehalt an partikulärem organischem Material bestimmt. Die Ergebnisse dieser Untersuchung zeigen, dass die Sauerstoffrespirationsraten in den untersuchten benthischen Grenzschichten nicht alleinig durch den Gehalt oder die Zusammensetzung von partikulärem organischem Material erklärt werden können. Dagegen gibt es Hinweise auf erhöhte Mineralisierungsraten von gelösten organischen Substanzen.

Introduction

Preface

The intention of this introduction is to provide information on the marine carbon and nitrogen cycle as well as to introduce sediment and water column as specific environments for biological production and mineralization processes. In particular, the relevance of the benthic boundary layer as the interface between the sediment and the overlying water column is described. Finally, the physical properties of the benthic boundary layer, its dynamic and turbulent nature, are explained to introduce the field of turbulent diffusive mass transport.

The Carbon Cycle

The increase in the average temperature of the Earth's surface since the mid-20th century has drawn much attention in particular to the greenhouse gas CO_2 and to the global carbon cycle in general. Examination of the global carbon budgets revealed the crucial role of the Ocean for the medium- and long-term storage of carbon (Sarmiento and Sundquist 1992; Volk and Hoffert 1985). The carbon cycle in the Ocean is critically dependent on the net primary production in the euphotic surface waters. The global net primary production is estimated to be 45-50 Pg C per year, driven by a oceanic phytoplankton biomass of only 1 Pg C (Falkowski et al. 1998). The average biomass turnover is, therefore, on the order of once per week, with the result that phytoplankton biomass, and subsequently the biomass of other trophic levels, is extremely sensitive to short-term environmental changes.

Primary production depends on the supply of essential nutrients. In the Ocean, the assimilation of 106 moles of inorganic carbon requires, on average, the uptake of 16 moles of nitrogen and 1 mol of phosphate. This elemental ratio is known as the 'Redfield' ratio and is found highly conserved in most particulate organic matter (Redfield et al. 1963). In steady state, the phytoplankton production is balanced by mortality due to grazing or viral cell lysis (Falkowski et al. 1998). Detritus and excretory products of consumers are rapidly assimilated by nanoflagellates and the microbial community (Banse 1992). The heterotrophic consumption releases dissolved nitrogen and phosphate in the Redfield ratio that, ultimately, sustain primary production. The recycling of nutrients in the euphotic zone can be very efficient. In the gyres of the open Ocean, only little particulate organic matter escapes the euphotic zone (Suess 1980). The exported organic matter is largely mineralized in either subsurface waters or sediments, which results in the build up of a subsurface nutrient pool

(Fanning 1992). The nutrients are transported back into the euphotic surface waters due to diffusion and advection. This return of nutrients more or less balances the export flux of particulate organic matter (Eppley and Peterson 1979). At Ocean margins, physical processes such as upwelling (Gross and Gross 1996), freshwater inflow (Seitzinger et al. 2005), enhanced mixing at continental slopes (McPhee-Shaw 2006), but also aeolian nutrient input (Duce et al. 2008) increase the nutrient flux to surface waters. Phytoplankton blooms occur that, especially when decoupled from zooplankton grazing, form large aggregates and cause high organic matter export to subsurface waters and sediments (Alldredge and Gotschalk 1988; Smetacek et al. 1978).

Although Ocean margins represent only 20% of the Ocean's surface area they sustain 50% of the global marine production (Wollast 1991). Moreover, 25 – 50% of the primary production in the euphotic zone is exported to the margin sediments (Wollast 1991). Of the organic matter that reaches the seafloor, a fraction of 0.5-3% is buried in the sediment for thousands to millions of years (Wollast 1991). In total, more than 90% of all organic carbon burial in the Ocean occurs in margin sediments (Hartnett et al. 1998). Ocean margin sediments are, therefore, a significant carbon sink. However, most of the sedimented organic matter is mineralized, and the released nutrients resupply the production in the surface waters. Mineralization processes in the sediment, the chemical transformation of nutrients and their transport to the upper water column are, therefore, crucial steps in the marine nutrient and carbon cycles.

The Nitrogen Cycle

As the primary production depends on the availability of several nutrients at the same time, the lack of only one nutrient is sufficient to cease the production. Of all nutrients, nitrogen is most often limiting primary production and thus nitrogen cycling is intimately linked to biological CO_2-sequestration (Gruber 2004). Nitrogen has the property of an eight electron difference between its most oxidized and reduced compounds. Thus, the redox cycling between nitrogen compounds is the basis for numerous microbial processes (Figure 1). In the Ocean, the most reduced and the most oxidized form of nitrogen are linked by microbial nitrification (Herbert 1999); that is the biological oxidation of ammonium (NH_4^+) to nitrite (NO_2^-) and ultimately to nitrate (NO_3^-); ($NH_4^+ \rightarrow NO_2^- \rightarrow NO_3^-$). Nitrification is a two step chemolithoautotrophic process mediated by bacteria and in parts by crenarchaeota at oxygen concentrations ranging from saturated to micro-molar concentrations. It is due to nitrification that ammonium, the primary product of nitrogen mineralization, occurs usually at low

concentrations in oxic environments (Canfield et al. 2005). Most inorganic nitrogen circulates in the form of nitrate between sediments, subsurface waters and surface waters.

Microbial processes control the pool of available nitrogen in the Ocean. Of all nitrogen at the Earth's surface, only 0.005 % is biologically available (Canfield et al. 2005). The atmosphere is one of the largest nitrogen pools composed of 78 % of dinitrogen gas (N_2) which is, however, virtually biologically unavailable. The nitrogen flux between the atmospheric reservoir and the bioavailable pool is controlled by prokaryotes. Dinitrogen gas (N_2) becomes utilizable by prokaryotes after the breaking of the strong triple N-N bonds by a process known as N_2-fixation ($N_2 \rightarrow NH_4^+ \rightarrow$ organic N, see Figure 1) (Sprent and Sprent 1990). This bioavailable or 'fixed' nitrogen cycles within the Oceans in various forms – e.g. ammonium, nitrite, nitrate and organic nitrogen – until it is lost to the atmosphere when facultative anaerobic microorganisms respire nitrate and nitrite in the absence of oxygen (Zumft 1997). Fixation of dinitrogen gas takes place in the euphotic zone when primary production is limited by the availability of fixed nitrogen but nutrients such as phosphate and iron are still present (Capone and Carpenter 1982). The loss of fixed nitrogen takes place either in oxygen-deficient subsurface waters or in sediments (Codispoti et al. 2001).

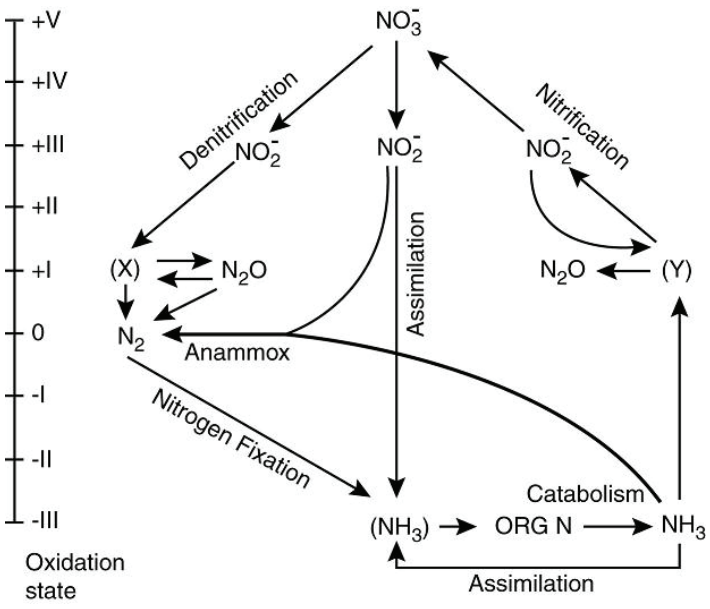

Figure 1: Nitrogen compounds and their respective oxidation state in the marine nitrogen cycle. The arrows mark the major transformation processes. 'X' and 'Y' are intra-cellular intermediates that do not accumulate in water column.
(after Codispoti et al., 2001)

Nitrogen loss processes

Microbial denitrification was generally considered to be the main nitrogen sink in the Ocean (Codispoti et al. 2001). Denitrification includes several respiratory steps, in which nitrate is reduced to dinitrogen gas in the absence of oxygen ($NO_3^- \rightarrow NO_2^- \rightarrow NO \rightarrow N_2O \rightarrow N_2$), (Fig. 1). The vast majority of denitrifying bacteria are heterotrophs, relying on organic carbon sources (Zumft 1997). Denitrification occurs in the suboxic layer of almost any kind of sediment. Denitrification was found in freshwater and marine sediments (Seitzinger et al. 2006), in coastal and deep sea sediment (Glud et al. 2009; Nielsen and Glud 1996), in muddy as well as in sandy sediment (Cook et al. 2006). The total amount of nitrogen that is lost from marine sediments is assumed to be up to 300 Tg N per year (Codispoti 2007). Although sediments of the continental shelves are organic rich and show highest areal denitrification rates, most of the sedimentary nitrogen loss is attributed to the vast area of slope and deep sea sediments (Middelburg et al. 1996).

About 20-40 % of the global oceanic nitrogen loss occurs in the oxygen-deficient waters of the Ocean, which constitute only about 0.1 % of the Ocean volume (Codispoti et al. 2001; Gruber 2004; Gruber and Sarmiento 1997). The major oxygen-deficient water bodies, also known as oxygen minimum zones, are found in the Eastern Tropical North Pacific, the Eastern Tropical South Pacific, the Arabian Sea, as well as in the Benguela upwelling system in the South Atlantic (Gruber 2004). For a long time, the nitrogen loss from oxygen minimum zones was fully attributed to denitrification since denitrification was considered the only microbially mediated nitrogen sink in the Ocean. The conventional nitrogen-cycling paradigm is, however, challenged by the recent findings of anammox, the anaerobic ammonium oxidation by nitrite to yield N_2, as an alternative nitrogen loss pathway ($NH_4^+ + NO_2^- \rightarrow N_2$) (Mulder et al. 1995). Anammox is a chemolithoautotrophic process mediated by bacteria of the order *Planctomycetales* (Strous et al. 1999). In the last decade, anammox was detected in many sediments (Dalsgaard et al. 2005; Thamdrup and Dalsgaard 2002) as well as in most oxygen minimum zones (Hamersley et al. 2007; Kuypers et al. 2005; Thamdrup et al. 2006). In fact, the bulk nitrogen loss in major oxygen minimum zones such as the Eastern Tropical South Pacific and the Benguela upwelling system might be attributable to anammox. The discovery of anammox in the marine environment stimulated once more the ongoing debate on whether the sources and sinks of fixed nitrogen in the Ocean are in balance or if the loss of fixed nitrogen strongly exceeds the input, as proposed by Codispoti et al. (2001) and Codispoti (2007). Recent findings on the regulation of anammox in oxygen minimum zones

(Lam et al. 2009) and sediments (Dalsgaard and Thamdrup 2002) illustrate that the nitrogen cycle is by far more complex than previously assumed.

Mineralization in marine sediments

Sediments and water column represent two distinct physical environments that are characterized by different biological and chemical processes (Figure 2). The transport of solutes in the porous sediments is usually governed by molecular diffusion and is therefore extremely slow compared to convection and turbulent mixing in the water column. Margin sediments receive high inputs of particulate matter and often contain high concentrations of organic matter, whereas the water column is comparatively poor in organic matter. Correspondingly, the average microbial cell density decrease from ~10^9 cells per ml in the sediment to ~10^5 cells per ml in the water column (Canfield et al. 2005). The water column is usually oxygenated, while increased microbial respiration depletes oxygen within the upper first millimeters to centimeters in the sediment (Glud 2008). In the anoxic sediment below this zone, a diverse anaerobic microbial community thrives utilizing a variety of electron acceptors to oxidize organic compounds. The different respiration processes occur at distinct sediment depths where the respective electron acceptor is available and the energy yield is most favorable (Froelich et al. 1979). Typical respiration processes in descending order are denitrification, manganese reduction, iron reduction, sulfate reduction and methanogenesis (Jørgensen 1982). Some of the reduced electron acceptors such as reduced manganese, reduced iron and sulfide are partly reoxidized and recycled or precipitated and trapped within the sediment.

Ammonium and phosphate, as breakdown products of organic matter mineralization, accumulate in the sediment and diffuse towards the sediment surface (Froelich et al. 1979). At the oxic-anoxic interface, some of the ammonium is oxidized by nitrifying bacteria to nitrite and ultimately to nitrate (Rysgaard et al. 1994). From this zone of nitrification, nitrate diffuses upwards into the water column as well as downwards to depths of denitrification, where it is reduced to N_2. How much of the mineralized nitrogen is nitrified and subsequently denitrified and how much is released to the water column depends on the oxygen concentration in the bottom water and the flux of sedimented organic matter (Middelburg et al. 1996).

The nitrate used for denitrification may also originate from the nitrate pool in the overlying water column from where it diffuses into the sediment. Increased sedimentary denitrification is found when the carbon flux to the sediment is high and when the nitrate concentration in the bottom water is high. High oxygen concentrations in the bottom water

may either increase or decrease denitrification. In organic poor sediments, such as found in the deep sea, high oxygen concentrations decrease denitrification rates, because most organic material is mineralized in the oxic zone (Middelburg et al. 1996). In organic rich sediments, such as found at coastal margins, high oxygen concentrations increase denitrification rates due to enhanced coupled nitrification-denitrification rates. In contrast to ammonium, phosphate is not involved in further redox-cycling. However, phosphate is potentially adsorbed onto iron oxides (Sundby et al. 1992), which may account for about 9 % of the phosphorus removed from marine waters (Canfield et al. 2005). How much phosphorus is released from the sediment depends, therefore, on the iron flux towards the sediment, on the iron oxidation state and, thus, on the oxygen concentration in the bottom water.

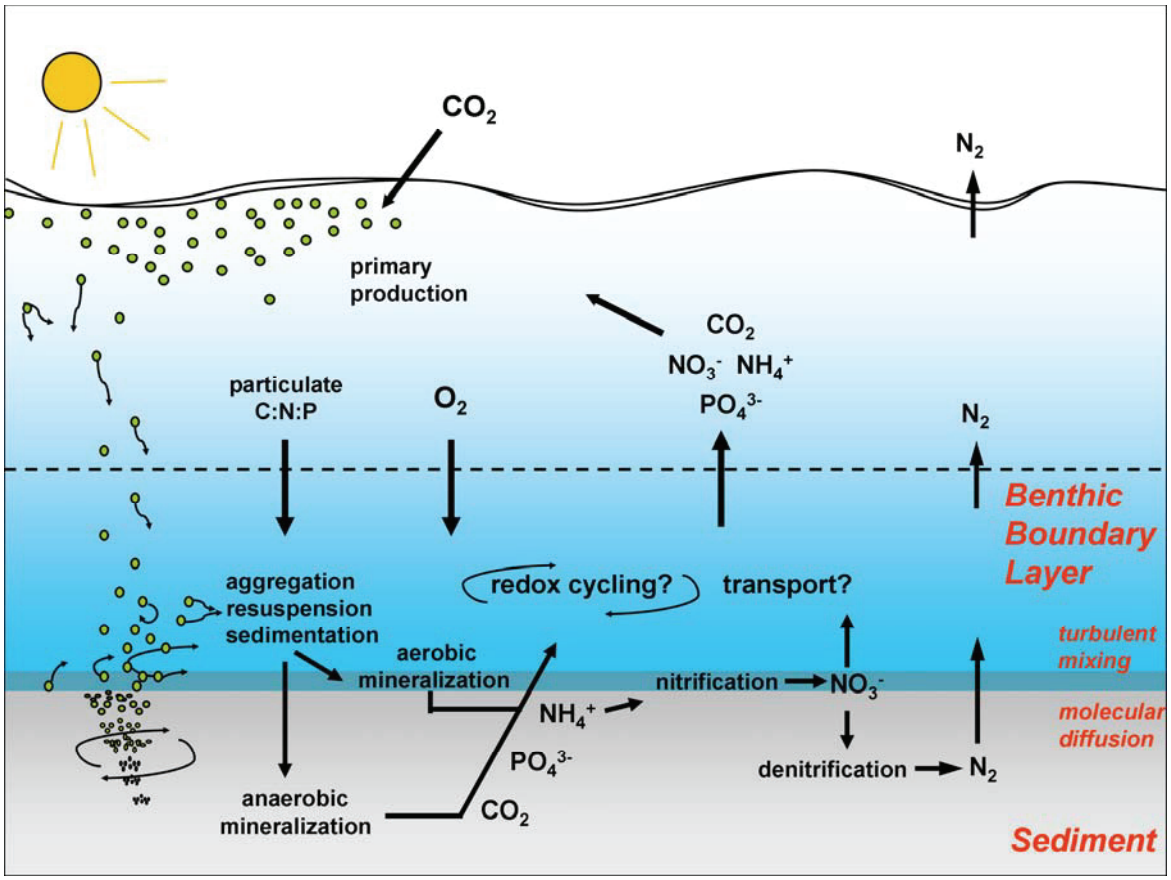

Figure 2: A schematic drawing of the marine nutrient cycling between the water column and the sediment. The benthic boundary layer is the interface between sediment and water column that provides a specific environment for redox cycling and mass transfer: Particulate matter accumulates in the BBL and can increase the mineralization in the BBL. Reduced metabolites diffuse out of the sediment into the oxic water column that may enhance redox processes. The mass transport changes from molecular to turbulent diffusive mixing (see Figure 3).

In summary, mineralization rates in the sediment and the efflux of nutrients is not only determined by the downward flux of organic matter but also dependent on the redox state of the water column. Furthermore, the recycling efficiency and the turnover time of nutrients strongly depend on the transport of electron acceptors in both, water column and sediments. The understanding and quantification of solute transport between the sediment and the water column is, therefore, crucial for the understanding of the marine nutrient cycles.

Measuring the exchange of solutes across the sediment surface

Both, mineralization processes in the sediment as well as the transport of solutes across the sediment-water interface are intensively studied using a diversity of different approaches (Zabel 2000). Well established is the measurement of vertical chemical gradients in the sediment, using microsensors (Jørgensen and Revsbech 1985), optodes (Wenzhoefer et al. 2001) and porewater analysis (Schulz 2000). From concentration maxima and minima, depths of production and consumption may be identified. Solute fluxes can be calculated from concentration gradients with the knowledge of the respective diffusion coefficients and the rates in specific depths can be calculated by using diffusive flux models (Berg et al. 1998). The spatial resolution of the concentration profile depends on the sensor dimension or the required porewater volume. In general, profiles obtained by chemical porewater analysis have a poor vertical resolution of at best several millimeters. In contrast, oxygen microsensors provide highly resolved profiles of a few micrometers (Revsbech and Blackburn 1980). By using microsensors, oxygen gradients in the so called ‘diffusive boundary layer’ just above the sediment surface can be resolved from which the diffusive oxygen flux into the sediment can be calculated (Jørgensen and Revsbech 1985). However, this gradient-diffusion approach does not consider the convective solute flux caused by burrowing fauna in the sediment (i.e bioirrigation) that can considerably exceed the diffusive flux (Glud et al. 1994).

Alternatively, the solute flux across the sediment-water-interface can be determined experimentally by incubating sediment samples and the overlying water as a whole in a closed system (Glud et al. 1995). Solute fluxes can be measured by following the change of the solute concentration in the overlying water over time. The flux due to bioirrigation is taken into account when the incubated sediment area is large enough to include the average diversity of sediment fauna. A drawback of the incubation approach is that the closed system changes the environmental conditions, especially the bottom water flow (Tengberg et al. 2005). The incubated water needs to be mixed artificially, simulating the flow of the bottom water. However, the degree of stirring can change the concentration of suspended particulate

matter, the behavior of the macrofauna or the porewater flux in case of permeable sediments. Both, the gradient-diffusion approach as well as the incubation approach are preferentially applied *in situ*, using well established benthic lander techniques (Reimers et al. 2001). Both approaches have led to a tremendous increase of knowledge about mineralization and transport processes in the sediments (Canfield et al. 2005; Glud 2008; Jørgensen and Boudreau 2001).

The benthic boundary layer - interface between sediment and water column

In recent years increasing attention was paid to the water layer just above the sediment, which is affected directly by the presence of the sediment-water interface and which exhibits its own characteristic features (Boudreau 2001; Dade et al. 2001; Hill and McCave 2001; Jørgensen 2001). This layer, denoted as the benthic boundary layer (BBL) (Figure 2), plays a crucial role in the exchange of particles and solutes between the sediment and the water column. In the turbulent part of the BBL, suspended particles that sink to the seafloor are retained in suspension and accumulate due to the increased turbulence in this layer before they finally settle to the sediment (Thomsen and Graf 1994). The shear stress exerted on the sediment by the moving water column can cause the re-suspension of surface sediments and a significant lateral transport of particulate matter (Inthorn et al. 2006; van Weering et al. 2001). The high particle concentrations in the BBL are associated with enhanced bacterial abundances (Ritzrau and Thomsen 1997), which might suggest that mineralization rates are enhanced and may be exceeding sedimentary mineralization rates (Thomsen et al. 2002).

Because the BBL is the interface between water column and sediment it is a layer where oxidized compounds such as oxygen and nitrate meet reduced metabolites that diffuse out of the sediment. This redox potential can be utilized by microorganisms such as the giant filamentous sulfur bacteria of the genus *Beggiatoa* and *Thioploca* (Jørgensen and Gallardo 1999) that use oxygen and nitrate to oxidize sulfide. Although attached to the sediment the filaments of giant sulfur bacteria can reach out several centimeters into the BBL thus enhancing their supply with oxygen or nitrate (Jørgensen and Gallardo 1999). Next to these rather specialized bacteria, it was suggested that microorganisms might stick to the particulate matter in the BBL to be retained close to the sediment and take advantage of increased substrate concentrations (Woebken et al. 2007) as well as of increased mass transfer rates to the cell surface due to the high shear in the turbulent BBL (Ritzrau 1996). In the BBL, also abiotic processes such as adsorption and desorption of ammonium onto particles (Seitzinger et al. 1991) or the scavenging of dissolved phosphate by iron oxides may occur (Sundby et al.

1986). However, little is known about the biotic and abiotic transformation processes in the BBL and how they alter the quantity and composition of nutrient fluxes from the sediment to the upper water column.

As the BBL intimately links the sediment to water column it should be a favorable place to observe and quantify the flux of solutes between sediment and water column. Flux measurements in the BBL are advantageous because they are non-invasive and integrate the flux over a large surface area (Berg et al. 2007). Flux measurements in the BBL, therefore, integrate the diffusive and advective flux across the sediment surface, which makes them applicable at settings such as sandy sediment or mussel beds. Although the transport of solutes in turbulent boundary flow is well described by laboratory flumes experiments and fluid dynamic theories (Boudreau 2001; Hill and McCave 2001) measurements in the field are scarce. The lack of *in situ* studies can be attributed to the difficulties in sampling of the BBL. Lander techniques measure solute concentration profiles that extend, at most, a few millimeters into the water column. On the other hand, conventional water column gears such as a CTD-Rosette do not allow sampling of the lower most 2-3 meters above the seafloor for technical reasons. Adequate sampling of the BBL was made possible with the development of the so called 'bottom water samplers' (Sauter et al. 2005; Thomsen et al. 1994) that are deployed to the seafloor and take water samples within the lower most meters above the seafloor.

So far, only a few, mainly descriptive studies on particle and solute concentrations are published (Ritzrau 1996; Thomsen and Graf 1994) that, however, do not allow to quantify the flux of solutes and solids between sediment and water column. The only approach that allows estimating fluxes in the turbulent boundary layer is the eddy correlation measurement that was recently introduced to aquatic science by Berg et al. (2003). The eddy correlation technique measures the instantaneous flux in the turbulent flow and requires the combined high resolution measurement of velocities and solute concentrations. To date, only oxygen microsensors fulfill the requirements and thus the eddy correlation technique is only applicable for oxygen flux measurements.

The BBL is a dynamic environment where conditions can change within short time scales due to changes in bottom water flow. A few millimeters above the sediment surface, the bottom water flow is of turbulent nature. In the field of fluid dynamics, this part of the BBL is therefore classified as a turbulent boundary layer (Dade et al. 2001). A thorough understanding of turbulent flow is crucial to understand the significance of the benthic boundary layer for nutrient cycles.

Turbulent flow

Turbulent motion evolves from shear flow (Pope 2000). The shear stress between layers of different current velocities causes abrupt fluid motions that differ in direction and magnitude from the mean current velocity. These motions form eddies that subsequently break up into smaller eddies which break up again into tinier eddies until their kinetic energy is viscously dissipated (Kolmogorov 1962). An essential feature of turbulent flow is that the fluid velocity field varies significantly and irregularly in position and time (Pope 2000). The motion of a fluid parcel is unpredictable even after short time intervals. An important characteristic of turbulence is its ability to transport and mix momentum and solutes much more efficiently than comparable laminar flows. The random nature of turbulent motion allows describing the mixing as a quasi diffusive transport according to Fick's first law of diffusion:

$$J = -D_T \frac{\partial C}{\partial x} \qquad \text{E1}$$

where J denotes the flux, D_T is the turbulent diffusivity (i.e. the turbulent diffusion coefficient) and $\partial C / \partial x$ is the concentration gradient of a solute. In this phenomenological description, however, the turbulent diffusivity is a mere constant of proportionality but an unknown function of the flow field. It was Taylor (1921) who first described the time dependent mean square displacement of a fluid parcel (i.e. the turbulent diffusivity) as a function of its velocity fluctuations. The statistical analysis of the velocity of a fluid parcel allows to derive characteristic length (L_E) and velocity (u_E) scales of eddies that subsequently determine the turbulent diffusivity as follows (Tennekes and Lumley 1972):

$$D_T = u_E \, L_E \qquad \text{E2}$$

It becomes apparent that turbulent diffusivity is a property of the flow only, whereas molecular diffusivity is a property of solute, solvent and temperature. Turbulent diffusivity expressed as $D_T = u_E \, L_E$ can be used to characterize the degree of turbulence. By comparing the inertial forces of eddy motion to the viscous forces in water, a dimensionless turbulent Reynolds number is defined: $\mathrm{Re}_T = D_T / \nu$ (Pope 2000), where ν is the kinematic viscosity. The flow is fully turbulent and viscosity can be neglected when $\mathrm{Re}_T >> 1$, whereas at $\mathrm{Re}_T \approx 1$, viscosity affects the flow.

Turbulent diffusivity is often interpreted as turbulent viscosity ν_T in analogy to the viscosity in laminar flow (Tennekes and Lumley 1972). Viscosity in laminar flow is a measure of the resistance of the fluid which is being deformed by shear stress. In laminar

flow, the shear stress τ between fluid layers is proportional to the velocity gradient $\partial U / \partial z$, with viscosity as the constant of proportionality:

$$\tau = \nu \, \rho \frac{\partial U}{\partial z} \qquad \text{E3}$$

For the sake of simplicity, the dynamic viscosity is expressed as the product of kinematic viscosity and density ($\mu = \nu \rho$). In turbulent flow, the shear stress from viscous forces is negligible. It is the stress due to random fluctuations of fluid momentum that is proportional to the velocity gradient. This stress is denoted as Reynolds stress τ_R and the proportionality factor is denoted as turbulent viscosity v_T, so that (Tennekes and Lumley 1972):

$$\tau_R = \nu_T \, \rho \frac{\partial U}{\partial z} \qquad \text{E4}$$

It should be emphasized that v is a property of the fluid, whereas v_T is a property of the flow.

In the Ocean, $D_T \approx v_T$ for vertical mixing range between 10^{-5} to 10^{-2} m^2 s^{-1} (Wunsch and Ferrari 2004) and, therefore, is 10 to 10^4 times above the kinematic viscosity and 10^4 to 10^7 above the molecular diffusion. Therefore, the mixing of momentum and solutes in the Ocean is dominated by turbulent motion. As mentioned above, turbulent flow is unpredictable. This is because no exact solution of the Navier-Stokes-Equations exists for turbulent motion. Fluid dynamic theories, therefore, aim to link time-averaged properties of turbulent flow such as the mean current velocity to specified boundary conditions. Hence, a variety of flow classifications evolved (Pope 2000), of which the turbulent boundary flow will be described in the following section.

The turbulent flow in the benthic boundary layer

The water column in the Ocean as well as in lakes is rarely stagnant but exhibits currents that are generated by various forces such as the earth's rotation, wind, tides and density differences (Wunsch and Ferrari 2004). The lower boundary of the moving water column is the seafloor. As the current velocity at the seafloor must be zero, a boundary layer is created where current velocities change from zero at the seafloor to what we will call the "free stream" velocity at some distance above the seafloor. By definition, the benthic boundary layer is the water layer that is influenced by the friction between the stationary seafloor and the moving water column (Dade et al. 2001). The lower boundary of the BBL is set by the seafloor but the upper boundary is vaguely defined. In shallow waters such as rivers the upper boundary coincides with the water surface. In deeper water, the upper boundary, by

convention, is set where the current velocity approaches 99% of the free stream velocity (Pope 2000). Yet another definition applies for the Ocean where rotational effects by Coriolis forcing have to be considered. There, the upper boundary is defined as the height where rotational effects by Coriolis forcing dominate the frictional effects (Dade et al. 2001). For free stream velocities ranging from 1 to 15 cm s^{-1}, the thickness of the benthic boundary layer in mid latitudes ranges from 2 to 20 m, respectively (Dade et al. 2001).

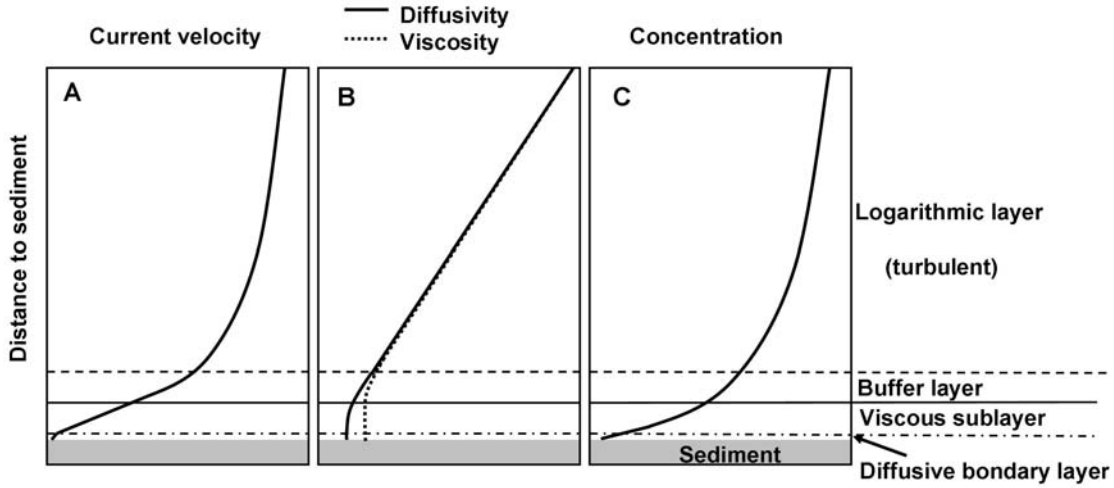

Figure 3: Schematic drawing of the benthic boundary layer comprising the turbulent logarithmic layer at the top, the buffer layer as the transition from turbulent to viscous flow, the viscous sublayer and the diffusive boundary layer. The turbulent diffusion and the turbulent viscosity in the logarithmic layer decrease linearly towards the sediment (B). In the buffer layer, turbulent viscosity becomes insignificant compared to the kinematic viscosity. There, the velocity profile changes from logarithmic to linear shape (A). In the viscous sublayer below, turbulent diffusivity becomes insignificant compared to the molecular diffusivity. There, the concentration profile changes from logarithmic to linear shape (C). Please note that the drawing is not to scale.

The benthic boundary layer itself consists of layers with different flow properties (Figure 3), (see also Dade et al. 2001). Distant from the seabed, the flow is turbulent. There, the velocity gradient is a function of Reynolds stress and turbulent viscosity (see E4). In this region, the eddy size that is most effective for mixing momentum and solutes is approximately equal to the height above the sediment (Boudreau 2001). Approaching the seafloor we find a proportional decrease of the effective eddy size and thus a decrease of the turbulent Reynolds number (Re_T, see above). Close to the seafloor, Re_T approaches unity so that the viscous contribution to the shear stress is significant. This layer is denoted as the buffer layer (Pope 2000). Even closer to the seafloor, the Reynolds stress is negligible and the

velocity gradient is a function of the viscous stress only. This layer is denoted as the viscous sublayer (Pope 2000). Within the viscous sublayer, turbulence can be disregarded in momentum transfer. However, turbulence is still affecting the mixing of solutes. In other words, we find in the viscous sublayer that $\nu_T << \nu$, but $D_T \approx D$, where D is the molecular diffusivity. It is only in the lower 10% of the viscous sublayer that molecular diffusion dominates the solute transport (Boudreau 2001). This layer is denoted as the diffusive boundary layer.

The transitions between these layers are of continuous nature and variable by the flow. However, we may impose an upper boundary for each layer for a specified flow. Assuming a current velocity of 10 cm s^{-1} measured at 1 m above the seafloor, upper boundaries of the buffer layer, the viscous sublayer and the diffusive boundary layer are approximately at 1 cm, 1 mm and 100 µm, respectively (Pope 2000). The boundaries shift to 10 cm, 1 cm and 1 mm, respectively, as the current velocity decreases to 1 cm s^{-1}.

In boundary layer flow it is assumed that the sum of viscous shear stress and Reynolds stress stays constant in the lower 1/3 of the boundary layer (Pope 2000). From equations E3 and E4 it becomes apparent that the mean velocity profiles in the viscous sublayer and in the turbulent layer must be fundamentally different. Within the viscous sublayer, the viscosity is constant and hence the velocity gradient stays constant. Within the turbulent layer, the turbulent viscosity scales with the distance to the boundary (i.e. the sediment) and hence the velocity gradient scales with this distance, too. Theodore von Karman (1930) was the first to publish a function that scales the velocity gradient in the turbulent layer to the boundary distance:

$$\frac{\partial U}{\partial z} = \frac{u_*}{\kappa z} \qquad \text{E5}$$

where κ is the von Karmans constant (~0.41), z is the distance to the boundary. The friction velocity u_* is related to the Reynolds stress (τ_R) and the fluid density (ρ) according to $u_* = \sqrt{\tau_R / \rho}$. The integrated form of equation 5 describes the current velocity as a logarithmic function of the boundary distance (Figure 3A). For this reason the function is widely known as ‘logarithmic Law of the Wall’. A fundamental consequence of the logarithmic Law of the Wall is the linear increase of the turbulent diffusivity with distance to the boundary ($D_T = u_* \kappa z$) (Figure 3B). Yet another consequence that is important with regard to sediments is the logarithmic concentration profile of solutes that results from Fick’s law of diffusion and a constant solute flux across the BBL (Figure 3C).

Besides the logarithmic Law of the Wall, several empirical models of turbulent diffusivity have been published that apply in the viscous layer as well as in the buffer layer and the turbulent layer. The most established models are the Van Driest equation and the Reichardt equation (Boudreau 2001). However, all these models were derived from laboratory flume experiments where density effects could be excluded and flow velocities were constant. In contrast, boundary flows in the field are easily affected by density stratification (Lorke 2007) and intermittent flow (Brand et al. 2008). Under these conditions diffusivity models that scale flow properties with boundary distance do not apply (Dade et al. 2001). The study of the benthic boundary layer in the field should, therefore, include accurate flow and density measurements to investigate the consequences of stratification and intermittent flow on the turbulent diffusivity.

Aim and outline of the thesis

The previous sections provided a short outline of the marine carbon and nitrogen cycles emphasizing the role of microbial mineralization and nitrogen loss processes in marine sediments and waters. The importance of mass transfer between sediments and water column was pointed out. The different physical and chemical environments of the sediments and the water column were described. It was explained how the interaction of sediment and water column at the sediment-water interface form a specific transition zone – the benthic boundary layer. Different strategies to investigate the mass transfer across the sediment-water interface were introduced and the difficulties in sampling the benthic boundary layer were explained. Finally, the complex physical environment of the benthic boundary layer was described in detail to provide the basis for a better understanding of mass transfer and transformation processes in the benthic boundary layer.

The following 4 chapters are the result of 3.5 years of work that included several expeditions to the Baltic Sea, North Sea and Arabian Sea. Both, field measurements as well as model studies on nutrient and oxygen transport in the BBL were used in these investigations. The studies include rate measurements of denitrification, anammox and aerobic respiration in the BBL, sediment and water column. In the following, objectives and outline of the individual chapters are briefly described.

There are only a few studies that show solute concentration profiles across the benthic boundary layer. Reported profiles have, so far, a poor resolution consisting of 4-6 measurements over a range of 1-2 m, which is often not enough to draw conclusions about the solute flux across the BBL. The aim of the study described in Chapter 2 was to increase the

depth resolution of the concentration profiles and to evaluate sediment-water fluxes from solute gradient measurements in the BBL. To resolve the concentration gradients close to the sediment a new sampling device, the so called 'BBL-Profiler', was build. Chapter 2 describes the successful deployment of the BBL-Profiler and presents nutrient and oxygen concentration gradients measured in the BBL of the Baltic Sea. Chapter 2 shows for nutrient and oxygen gradients that the mere direction of the gradients can reveal the sediment as a net sink for oxygen and as a net source for nutrients including nitrate. From the efflux of nitrate from the sediment it is readily deduced that nitrification at the sediment surface is the sole nitrate source for sedimentary denitrification in the Baltic Sea. Furthermore, Chapter 2 presents a method to calculate the ratio of nutrient flux to oxygen flux from concentration profiles in the BBL. On the basis of nutrient-oxygen flux ratios and sedimentary C/N ratios a nitrogen balance for the sediment is established that describes the relative fraction of nitrogen that is nitrified, denitrified or transported to the water column. The new method is non-invasive and considers diffusive as well as advective transport across the sediment surface. The results from the non-invasive approach are compared with the results from sediment incubation experiments.

As pointed out above, the BBL is largely characterized by turbulent flow in which solutes are dispersed by turbulent diffusion. Most studies of turbulent flow in benthic boundary layers apply the logarithmic Law of the Wall from which the turbulent diffusivity can be estimated from average current velocities. The turbulent diffusivity in the benthic boundary layer was seldom measured directly in the field, because of the increased measuring effort. However, the logarithmic Law of the Wall is applicable only for unstratified waters and for flows with high Reynolds numbers. There is little to no field data available on the effects of decreased flow velocities and stratified boundary layers on the turbulent diffusivity. The aim of the study described in Chapter 3 was to develop an approach to measure turbulent diffusivity independently from the logarithmic Law of the Wall and to measure turbulent diffusivity at variable flow conditions. Chapter 3 describes a simple approach to measure turbulent diffusivity from acoustic Doppler velocimeter (ADV) data. The approach is found applicable also in boundary flows that exhibit density stratification or intermittent flow. The results in Chapter 3 confirm the limited applicability of the logarithmic Law of the Wall under these flow conditions. Chapter 3 shows that turbulent diffusivities can decrease much more than predicted from the logarithmic Law of the Wall. The potential effects that such decreased turbulent diffusivities may have on the solute flux are not known. For that reason, Chapter 3 provides a simple oxygen flux model describing the oxygen concentration and the oxygen

flux at the sediment surface as a function of turbulent diffusivity in the BBL. The model results indicate that decreased turbulent diffusivities can control the oxygen flux across the sediment water interface.

Microbial activity is assumed to be enhanced in the BBL but studies that measure microbial activity in the BBL are scarce. Virtually no study exists that measures aerobic respiration rates or nitrogen loss processes in the BBL. The contribution of the BBL to benthic mineralization and nitrogen loss is, therefore, not known. The aim of the study presented in Chapter 4 was to compare the nitrogen loss due to anammox and denitrification from sediments, benthic boundary layer and suboxic waters of the Arabian Sea. Massive nitrogen loss has previously been reported from the oxygen minimum zone of the Arabian Sea but the contribution of the sedimentary nitrogen loss is largely unknown. Results from incubation experiments show that denitrification is the dominant nitrogen loss process in the sediment. The contribution of anammox to the total sedimentary N-loss increases with water depth. The areal rates of nitrogen loss from the sediment exceeded those from the overlying suboxic waters. Anammox rates were low in the Arabian Sea waters and were detected exclusively in the benthic boundary layer and in the oxycline of the upper water column.

The aim of the study presented in Chapter 5 was to compare aerobic respiration rates with the concentration and quality of suspended particulate organic matter in the BBL. It was previously proposed that increased particle concentrations may enhance the mineralization rates in the BBL. Applying oxygen optodes, oxygen respiration rates were measured in samples from various settings in the North Sea and the Baltic Sea that contain different amounts of particulate organic matter. The results in Chapter 5 show that quantity and quality of particulate organic matter only partly explain the oxygen respiration rates in the BBL. Instead, the results indicate considerable aerobic respiration related to dissolved organic matter mineralization rates.

References

Alldredge, A. L., and C. Gotschalk. 1988. In situ settling behavior of marine snow. Limnology and Oceanography **33:** 339-351.

Banse, K. 1992. p. 409-440. *In* P. Falkowski and A. D. Woodhead [eds.], Primary Productivity and Biogeochemical Cycles in the Sea. Plenum.

Berg, P., N. Risgaard-Petersen, and S. Rysgaard. 1998. Interpretation of measured concentration profiles in sediment pore water. Limnology and Oceanography **43:** 1500-1510.

Berg, P. and others 2003. Oxygen uptake by aquatic sediments measured with a novel non-invasive eddy-correlation technique. Marine Ecology-Progress Series **261:** 75-83.

Berg, P., H. Røy, and P. L. Wiberg. 2007. Eddy correlation flux measurements: The sediment surface area that contributes to the flux. Limnology and Oceanography **52:** 1672-1684.

Boudreau, B. P. 2001. Solute transport above the sediment-water interface, p. 104-126. *In* B. P. Boudreau and B. B. Jørgensen [eds.], The Benthic Boundary Layer: Transport Processes and Biogeochemistry. Oxford University Press.

Brand, A., D. F. Mcginnis, B. Wehrli, and A. Wüest. 2008. Intermittent oxygen flux from the interior into the bottom boundary of lakes as observed by eddy correlation Limnology and Oceanography **53:** 1997-2006.

Canfield, D., B. Thamdrup, and E. Kristensen [eds.]. 2005. Aquatic Geomicrobiology. Elsevier.

Capone, D. G., and E. J. Carpenter. 1982. Nitrogen fixation in the marine environment. Science **217:** 1140-1142.

Codispoti, L. A. 2007. An oceanic fixed nitrogen sink exceeding 400 Tg N a vs the concept of homeostasis in the fixed-nitrogen inventory. Biogeosciences **4:** 233-253.

Codispoti, L. A. and others 2001. The oceanic fixed nitrogen and nitrous oxide budgets: Moving targets as we enter the anthropocene? Scientia Marina **65:** 85-105.

Cook, P. L. M. and others 2006. Quantification of denitrification in permeable sediments: Insights from a two-dimensional simulation analysis and experimental data Limnology and Oceanography-Methods **4:** 294-307.

Dade, B. D., A. Hogg, and B. P. Boudreau. 2001. Physics of Flow above the Sediment-Water Interface, p. 4-43. *In* B. P. Boudreau and B. B. Jørgensen [eds.], The Benthic Boundary Layer: Transport Processes and Biogeochemistry. Oxford University Press.

Dalsgaard, T., and B. Thamdrup. 2002. Factors controlling anaerobic ammonium oxidation with nitrite in marine sediments. Applied and Environmental Microbiology **68:** 3802-3808.

Dalsgaard, T., B. Thamdrup, and D. E. Canfield. 2005. Anaerobic ammonium oxidation (anammox) in the marine environment. Research in Microbiology **156:** 457-464.

Duce, R. A. and others 2008. Impacts of atmospheric anthropogenic nitrogen on the open ocean. Science **320:** 893-897.

Eppley, R. W., and B. J. Peterson. 1979. Particulate organic matter flux and planktonic new production in the deep ocean. Nature **282:** 667-680.

Falkowski, P. G., R. T. Barber, and V. Smetacek. 1998. Biogeochemical controls and feedbacks on ocean primary production. Science **281:** 200-206.

Fanning, K. A. 1992. Nutrient Provinces in the Sea - Concentration Ratios, Reaction-Rate Ratios, and Ideal Co-variation. Journal of Geophysical Research-Oceans **97:** 5693-5712.

Froelich, P. N. and others 1979. Early oxidation of organic matter in pelagic sediments of the eastern equatorial Atlantic: suboxic diagenesis. Geochimica et Cosmochimica Acta **43:** 1075-1090.

Glud, R. N. 2008. Oxygen dynamics of marine sediments. Marine Biology Research **4:** 243-289.

Glud, R. N., J. K. Gundersen, B. B. Jørgensen, N. P. Revsbech, and H. D. Schulz. 1994. Diffusive and Total Oxygen-Uptake of Deep-Sea Sediments in the Eastern South-Atlantic Ocean - in-Situ and Laboratory Measurements. Deep-Sea Research Part I-Oceanographic Research Papers **41:** 1767-1788.

Glud, R. N., J. K. Gundersen, N. P. Revsbech, B. B. Jørgensen, and M. Hüttel. 1995. Calibration and Performance of the Stirred Flux Chamber from the Benthic Lander Elinor. Deep-Sea Research Part I-Oceanographic Research Papers **42:** 1029-1042.

Glud, R. N. and others 2009. Nitrogen cycling in a deep ocean margin sediment (Sagami Bay, Japan). Limnology and Oceanography **54:** 723-734.

Gross, M. G., and E. Gross. 1996. Oceanography, a view of earth. Prentice Hall.

Gruber, N. 2004. The dynamics of the marine nitrogen cycle and its influence on atmospheric CO2 variations, p. 97-148. *In* M. Follows and T. Oguz [eds.], The ocean carbon cycle and climate. NATO ASI Series. Kluwer Academic.

Gruber, N., and J. L. Sarmiento. 1997. Global patterns of marine nitrogen fixation and denitrification. Global Biogeochemical Cycles **11:** 235-266.

Hamersley, M. R. and others 2007. Anaerobic ammonium oxidation in the Peruvian oxygen minimum zone. Limnology and Oceanography **52:** 923-933.

Hartnett, H. E., R. G. Keil, J. I. Hedges, and A. H. Devol. 1998. Influence of oxygen exposure time on organic carbon preservation in continental margin sediments. Nature **391:** 572-575.

Herbert, R. A. 1999. Nitrogen cycling in coastal marine ecosystems. Fems Microbiology Reviews **23:** 563-590.

Hill, P. S., and I. N. Mccave. 2001. Suspended particle transport in benthic boundary layers, p. 78-103. *In* B. P. Boudreau and B. B. Jørgensen [eds.], The Benthic Boundary Layer: Transport Processes and Biogeochemistry. Oxford University Press.

Inthorn, M., M. R. Van Der Loeff, and M. Zabel. 2006. A study of particle exchange at the sediment-water interface in the Benguela upwelling area based on Th-234/U-238 disequilibrium. Deep-Sea Research Part I-Oceanographic Research Papers **53:** 1742-1761.

Jørgensen, B. B. 1982. Mineralization of Organic-Matter in the Sea Bed - the Role of Sulfate Reduction. Nature **296:** 643-645.

---. 2001. Life in the diffusive Boundary Layer, p. 348-373. *In* B. P. Boudreau and B. B. Jørgensen [eds.], The Benthic Boundary Layer: Transport Processes and Biogeochemistry. Oxford University Press.

Jørgensen, B. B., and B. P. Boudreau. 2001. Diagenesis and Sediment-Water Exchange, p. 211-244. *In* B. P. Boudreau and B. B. Jørgensen [eds.], The Benthic Boundary Layer: Transport Processes and Biogeochemistry. Oxford University Press.

Jørgensen, B. B., and V. A. Gallardo. 1999. *Thioploca spp*: filamentous sulfur bacteria with nitrate vacuoles. Fems Microbiology Ecology **28:** 301-313.

Jørgensen, B. B., and N. P. Revsbech. 1985. Diffusive boundary layers and the oxygen uptake of sediments and detritus. Limnology and Oceanography **30:** 111-122.

Kolmogorov, A. N. 1962. A refinement of previous hypotheses concerning the local structure of turbulence in a viscous incompressible fluid at high Reynolds numbers. Journal of Fluid Mechanics **13:** 82-85.

Kuypers, M. M. M. and others 2005. Massive nitrogen loss from the Benguela upwelling system through anaerobic ammonium oxidation. Proceedings of the National Academy of Sciences of the United States of America **102:** 6478-6483.

Lam, P. and others 2009. Revising the nitrogen cycle in the Peruvian oxygen minimum zone. Proceedings of the National Academy of Sciences of the United States of America **106:** 4752-4757.

Lorke, A. 2007. Boundary mixing in the thermocline of a large lake. Journal of Geophysical Research-Oceans **112**.

McPhee-Shaw, E. 2006. Boundary-interior exchange: Reviewing the idea that internal-wave mixing enhances lateral dispersal near continental margins. Deep Sea Research Part II: Topical Studies in Oceanography **53:** 42-59.

Middelburg, J. J., K. Soetaert, P. M. J. Herman, and C. H. R. Heip. 1996. Denitrification in marine sediments: A model study. Global Biogeochemical Cycles **10:** 661-673.

Mulder, A., A. A. Vandegraaf, L. A. Robertson, and J. G. Kuenen. 1995. Anaerobic Ammonium Oxidation Discovered in a Denitrifying Fluidized-Bed Reactor. FEMS Microbiology Ecology **16:** 177-183.

Nielsen, L. P., and R. N. Glud. 1996. Denitrification in a coastal sediment measured in situ by the nitrogen isotope pairing technique applied to a benthic flux chamber. Marine Ecology-Progress Series **137:** 181-186.

Pope, S. B. 2000. Turbulent Flows. Cambridge University Press.

Redfield, A. C., B. H. Ketchum, and F. A. Richards. 1963. p. 26-77. *In* M. N. Hill [ed.], The Sea. Interscience.

Reimers, C. E., R. A. Jahnke, and L. Thomsen. 2001. In Situ Sampling in the Benthic Boundary Layer, p. 245-268. *In* B. P. Boudreau and B. B. Jørgensen [eds.], The Benthic Boundary Layer: Transport Processes and Biogeochemistry. Oxford University Press.

Revsbech, N. P., and T. H. Blackburn. 1980. Oxygen in the sea bottom measured with a microelectrode Science **207:** 1355-1356.

Ritzrau, W. 1996. Microbial activity in the benthic boundary layer: Small-scale distribution and its relationship to the hydrodynamic regime. Journal of Sea Research **36:** 171-180.

Ritzrau, W., and L. Thomsen. 1997. Spatial distribution of particle composition and microbial activity in benthic boundary layer (BBL) of the Northeast Water Polynya. Journal of Marine Systems **10:** 415-428.

Rysgaard, S., N. Risgaard-Petersen, N. P. Sloth, K. Jensen, and L. P. Nielsen. 1994. Oxygen Regulation of Nitrification and Denitrification in Sediments. Limnology and Oceanography **39:** 1643-1652.

Sarmiento, J. L., and E. T. Sundquist. 1992. Revised budget for the oceanic uptake of anthropogenic carbon dioxide. Nature **356:** 589-593.

Sauter, E. J., M. Schluter, J. Wegner, and E. Labahn. 2005. A routine device for high resolution bottom water sampling. Journal of Sea Research **54:** 204-210.

Schulz, H. D. 2000. Quantification of early Diagenisis: Dissolved Constituents in Marine Pore Water, p. 85-128. *In* H. D. Schulz and M. Zabel [eds.], Marine Geochemistry. Springer.

Seitzinger, S. and others 2006. Denitrification across landscapes and waterscapes: A synthesis. Ecological Applications **16:** 2064-2090.

Seitzinger, S., J. A. Harrison, E. Dumont, and A. F. Bouwman. 2005. Sources and delivery of carbon, nitrogen, and phosphorus to the coastal zone: An overview of Global Nutrient Export from Watersheds (NEWS) models and their application. Global Biogeochem. Cycles **19:** GB4S01.

Seitzinger, S. P., W. S. Gardner, and A. K. Spratt. 1991. The Effect of Salinity on Ammonium Sorption in Aquatic Sediments - Implications for Benthic Nutrient Recycling. Estuaries **14:** 167-174.

Smetacek, V., K. Von Bröckel, and W. Zenk. 1978. Sedimentation of particulate matter during a phytoplankton spring bloom in relation to the hydrographical regime. Marine Biology **47:** 211-226.

Sprent, J. I., and P. Sprent. 1990. Nitrogen Fixing Organisms: Pure and Applied Aspects. Chapmann and Hall.

Strous, M. and others 1999. Missing lithotroph identified as new planctomycete. Nature **400:** 446-449.

Suess, E. 1980. Particulate Organic-Carbon Flux in the Oceans - Surface Productivity and Oxygen Utilization. Nature **288:** 260-263.

Sundby, B., L. G. Anderson, P. O. J. Hall, Å. Iverfeldt, M. M. R. van der Loeff, and S. F. G. Westerlund. 1986. The effect of oxygen on release and uptake of cobalt, manganese, iron and phosphate at the sediment-water interface. Geochimica et Cosmochimica Acta **50:** 1281-1288.

Sundby, B., C. Gobeil, S. N., and A. Mucci. 1992. The phosphorus cycle in coastal marine sediments. Limnology and Oceanography **37**.

Taylor, G. I. 1921. Diffusion by continuous movements. Proceedings of the London Mathematical Society **20**.

Tengberg, A. and others 2005. Intercalibration of benthic flux chambers II. Hydrodynamic characterization and flux comparisons of 14 different designs. Marine Chemistry **94:** 147-173.

Tennekes, H., and J. L. Lumley. 1972. A First Course in Turbulence. MIT Press.

Thamdrup, B., and T. Dalsgaard. 2002. Production of N-2 through anaerobic ammonium oxidation coupled to nitrate reduction in marine sediments. Applied and Environmental Microbiology **68:** 1312-1318.

Thamdrup, B., T. Dalsgaard, M. M. Jensen, O. Ulloa, L. Farias, and R. Escribano. 2006. Anaerobic ammonium oxidation in the oxygen-deficient waters off northern Chile. Limnology and Oceanography **51:** 2145-2156.

Thomsen, L., and G. Graf. 1994. Boundary-Layer Characteristics of the Continental-Margin of the Western Barents Sea. Oceanologica Acta **17:** 597-607.

Thomsen, L., G. Graf, V. Martens, and E. Steen. 1994. An Instrument for Sampling Water from the Benthic Boundary-Layer. Continental Shelf Research **14:** 871-&.

Thomsen, L., T. van Weering, and G. Gust. 2002. Processes in the benthic boundary layer at the Iberian continental margin and their implication for carbon mineralization. Progress in Oceanography **52:** 315-329.

van Weering, T. C. E. and others 2001. Benthic dynamics and carbon fluxes on the NW European continental margin. Deep Sea Research Part II: Topical Studies in Oceanography **48:** 3191-3221.

Volk, T., and M. I. Hoffert. 1985. p. 99-110. *In* E. T. Sunquist and W. S. Broeker [eds.], The Carbon Cycle and Atmospheric CO2: Natural Variations Archean to Present. American Geophysical Union.

von Karman, T. 1930. Mechanische Ähnlichkeit und Turbulenz, p. 85-105. Proceedings of the Third International Congress of Applied Mechanics.

Wenzhoefer, F., O. Holby, and O. Kohls. 2001. Deep penetrating benthic oxygen profiles measured in situ by oxygen optodes. Deep Sea Research Part I **48:** 1741-1755.

Woebken, D., B. A. Fuchs, M. A. A. Kuypers, and R. Amann. 2007. Potential interactions of particle-associated anammox bacteria with bacterial and archaeal partners in the Namibian upwelling system. Applied and Environmental Microbiology **73:** 4648-4657.

Wollast, R. 1991. The coastal organic carbon cycle: fluxes, sources and sinks, p. 365-381. *In* J.-M. M. R.-F.-C. Mantoura, R. Wollast [ed.], Ocean Margin Processes in Global Change. John Wiley & Sons.

Wunsch, C., and R. Ferrari. 2004. Vertical mixing, energy and the general circulation of the oceans. Annual Review of Fluid Mechanics **36:** 281-314.

Zabel, M. 2000. Benthic Fluxes and their distribution patterns, p. 373-392. *In* H. D. Schulz and M. Zabel [eds.], Marine Geochemistry. Springer.

Zumft, W. G. 1997. Cell biology and molecular basis of denitrification. Microbiology and Molecular Biology Reviews **61:** 533-616.

Overview of Manuscripts

Nutrient fluxes across the benthic boundary layer reveal direct coupling of nitrification-denitrification in Baltic Sea sediments (Chapter 2)

(Moritz Holtappels, Marcel M.M. Kuypers, Michael Schlüter, Volker Brüchert)

(in prep. for *Limnology and Oceanography Methods*)

Estimating turbulent diffusivity from velocity measurements in a benthic boundary layer – the relevance of boundary layer mixing for the mass transfer across the sediment water interface (Chapter 3)

(Moritz Holtappels and Andreas Lorke)

(in prep. for *Limnology and Oceanography Methods*)

Water column versus sedimentary nitrogen loss in the Arabian Sea off Pakistan (Chapter 4)

(Moritz Holtappels, Gavin Collins, Sarah Sokoll, Michael Schlüter, Volker Brüchert, Gaute Lavik, Marcel M.M. Kuypers)

(in prep. for *Limnology and Oceanography)*

Aerobic respiration rates in the benthic boundary layer of the Baltic and North Sea (Chapter 5)

(Moritz Holtappels, Volker Brüchert and Marcel M.M. Kuypers)

(in prep. for *Limnology and Oceanography)*

Nutrient fluxes across the benthic boundary layer reveal direct coupling of nitrification-denitrification in Baltic Sea sediments

Moritz Holtappels[1], Marcel M.M. Kuypers[1], Michael Schlüter[2], Volker Brüchert[1,3]

1) Max Planck Institute for Marine Microbiology, Celsiusstrasse 1, 28359 Bremen

2) Alfred Wegener Institute for Polar and Marine Research, Am Handelshafen 12, 27570 Bremerhaven

3) Present address Department of Geology and Geochemistry, Stockholm University, 10691 Stockholm, Sweden

Acknowledgement

We thank Bernd Schneider and Anne Loeffler (Leibniz Institute for Baltic Sea Research, Warnemünde) who provided ship time on *RV Professor Albrecht Penck*; Gaute Lavik for assistance in mass spectrometry and data analysis, G. Klockgether, M. Meyer and J. Schmidt for analytical assistance, F. Wenzhoefer, H. Røy and P. Faerber for technical assistance and the crews of *RV Heinke* and *RV Professor Albrecht Penck* for excellent collaboration. This study was funded through DFG-Research Center / Excellence Cluster „The Ocean in the Earth System" and the Max Planck Society.

Abstract

Concentration gradients of nutrients and oxygen were measured across the benthic boundary layer (BBL) at two stations in the center and at the periphery of the Arkona Basin, Baltic Sea. The profiles reveal an uptake of oxygen and a release of ammonium, nitrate, nitrite and phosphate from the sediment. Concentration gradients were used to calculate exchange rates of nutrients and oxygen across the sediment water interface. The derived O_2:N flux ratios of 13 and 16 (center and peripheral station, respectively) were significantly higher than those inferred from the molar C:N ratios of surface sediment and particles. This deviation was attributed to the loss of inorganic nitrogen as N_2-gas by sedimentary denitrification. The N-loss (0.22 mmol m^{-2} d^{-1}) was comparable to denitrification rates determined by the isotope pairing technique (IPT). Calculations show that denitrification accounted for 1.7 % and 5.7 % of the total carbon oxidation and for the loss of 22 % and 51 % (center and peripheral station, respectively) of the total mineralized nitrogen (N_{tot}). Mass balance calculations indicated that nitrification at the sediment surface accounted for 40 % and 68 % of N_{tot} inventory, whereas nitrate released from the sediment contributed 18 % and 16 % to N_{tot} (center and peripheral station, respectively). These observations imply that sedimentary denitrification was fully coupled to nitrification in the sediment. The non-invasive approach described here can also be used to evaluate benthic fluxes from sandy sediments and shell beds, which are extremely difficult to obtain with benthic chamber and sediment coring techniques.

Introduction

Coastal marine sediments are important for the regeneration of nutrients necessary to sustain primary production. Coastal and shelf sediments receive 25 – 50 % of the primary production from the photic zone (Wollast 1991). Over 90 % of the particulate carbon, nitrogen and phosphorus that reaches the sediment surface is mineralized and released to the overlying water column to fuel new primary production (Berner 1982). This leads to a tight temporal and spatial coupling of sedimentary and water column processes (Graf 1992; Graf et al. 1995; Soetaert et al. 2000). Hence, a qualitative and quantitative knowledge of organic matter and nutrient exchange across the sediment water interface is required to understand the carbon and nutrient cycling in the ocean.

Nitrogen is an essential nutrient for all living organisms and has the potential to control the marine primary production and thus the biological carbon pump (Falkowski et al. 1998). Moreover, redox cycling of nitrogen compounds is the basis of a variety of microbial metabolisms. Of those, aerobic nitrification produces the most oxidized compounds nitrite and nitrate (here summarized as NO_x), which in turn are required as electron acceptors for anaerobic N-loss processes, i.e. denitrification and anaerobic ammonium oxidation (anammox). Denitrification and anammox convert biologically available (fixed) nitrogen into inert N_2 gas which cannot be utilized by most organisms. As such, denitrification and anammox are the main sinks for oceanic fixed nitrogen (Codispoti et al. 2001; Dalsgaard et al. 2005; Kuypers et al. 2006). Denitrification and anammox rely on a NO_x source. The spatial distance from locations of nitrification to locations of N-loss processes and N-assimilation determines the fraction of NO_x that is either recycled or lost from the system. A spatial coupling of nitrification and N-loss processes was shown for the oxic-anoxic interface at the sediment surface (Rysgaard et al. 1994) and for suboxic waters (Lam et al. 2007).

For many sedimentary environments, however, it remains unresolved to what extent N-loss processes are fueled by NO_3^- coming from sedimentary nitrification or NO_3^- diffusing into the sediment from the overlying water. Many studies assume that sedimentary denitrification was fueled by NO_3^- diffusing into the sediment from the overlying water (Nielsen and Glud 1996; Rysgaard et al. 1996; Rysgaard et al. 1994; Tuominen et al. 1998; Tuominen et al. 1999). The methods used to estimate nutrient fluxes across the sediment water interface so far were porewater profiles, chamber incubations and incubations with stable isotopes. In contrast, Middelburg et al. (1996) modeled denitrification and NO_3^- fluxes for variable carbon fluxes and bottom water concentrations of NO_3^- and O_2 and concluded that

sediments generally act as a source of NO_3^-. The exceptions are sediments underlying high-nitrate-low-oxygen waters (i.e. upwelling areas). Sediments that are a net source of NO_3^- cannot take up NO_3^- from the overlying water. This implies that sedimentary nitrification is the sole NO_3^- source for sedimentary denitrification and, therefore, denitrification is fully coupled to nitrification in the sediment.

In this study we present a new approach which uses the concentration gradients across the benthic boundary layer (BBL) to quantify fluxes of nutrients and oxygen. The BBL is the water layer overlying the sediment, which is affected by the friction between the moving water column and the sediment (Dade et al. 2001). The shear stress in the BBL causes turbulent mixing with enhanced but variable eddy diffusion coefficients. The diffusion coefficients in sediments are low and a function of sediment and solute properties. In contrast, the eddy diffusion coefficients in the BBL are large (10^3-10^5 times the sediment diffusion coefficients) and a function of the fluid flow only. Diffusive fluxes in sediments and waters depend on the presence of a concentration gradient. Although a few studies report concentration gradients of solutes and particles in the BBL (Sauter et al. 2005; Thomsen and Graf 1994; Thomsen and Ritzrau 1996; van Weering et al. 2001) these gradients have so far not been used to calculate fluxes across the BBL.

We determined nutrient and oxygen concentration gradients in the BBL at two stations in the Baltic Sea. These gradients were used to calculate nutrient fluxes across the sediment water interface and benthic nitrification and N-loss rates. Our results indicate that nitrification at the sediment water interface was the sole source of nitrate consumed by benthic denitrification.

Methods

Study site and sampling procedure

Sediment and water samples were collected in September 2006 at station A1, close to the center of the Arkona Basin (N 54° 46.50', E 13° 49.00', depth 42.4 m) and in June 2007 at station A2 at the periphery of the Arkona Basin (N 54° 39.18', E 13° 28.21', depth 20.0 m). The sediment at station A1 was organic rich and muddy while the sediment at A2 was dominated by fine sand. At station A1 the water column was sampled for temperature and salinity using a Sea-Bird CTD (SBE 19-04). Samples for oxygen, nutrients and particles were collected with regular Niskin bottles from the surface down to 2 m above the sediment. The BBL was sampled with a Bottom Water Sampler (BWS) previously described by Sauter et al. (2005). The BWS consisted of 6 horizontally aligned free flow bottles (volume: 6 L) that collected water samples over a range of 2 m above the sediment surface. Due to technical problems only 4 of the 6 bottles were used for sampling. Subsamples were taken for oxygen and nutrient analysis as well as for particle filtration and oxygen consumption measurements. The salinity of the BWS samples was measured with a conductivity meter (WTW, LF 197).

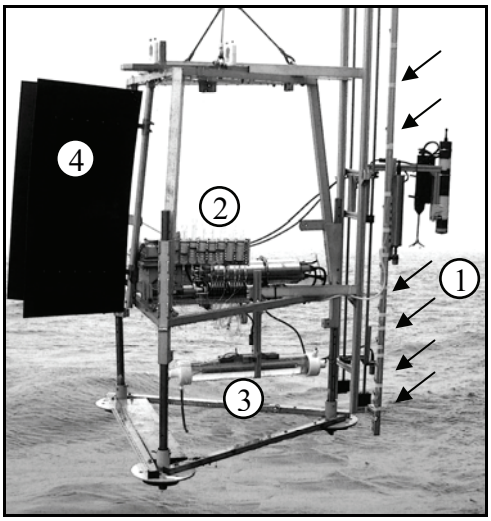

Figure 1. BBL-Profiler, deployed at station A2. The numbers mark: (1) The slider, carrying O_2-Optodes, ADV and CTD; (2) Electronics, syringes and a 12 channel peristaltic pump; (3) The BWS free flow bottle; (4) A vane is attached to the frame to direct the Profiler towards the water current. The arrows mark inlets from where water samples were drawn.

At station A2 the BBL was sampled at high spatial resolution with a newly built instrument named BBL-Profiler (Fig. 1). The profiler consists of a slider that moves vertically along the first meter above the sediment surface. The slider carries an oxygen optode (Model 3830, Aanderaa), a CTD (YSI, 600XLM-M) and an acoustic doppler velocimeter (Vectrino, Nortek AS). A 12-channel peristaltic pump (KC, Denmark) was used to draw water samples (60 ml) for nutrient analysis from 0.07 to 1.8 m above the sediment surface. In addition, a BWS free flow bottle was mounted 35 cm above the sediment surface to take samples for particle filtration and oxygen consumption measurements. The BBL-Profiler was deployed to the sea floor for 2.5 hours while connected to a surface marker buoy. The sampling procedure started with a delay of 30 min to allow the drift of artificially resuspended sediment from the BBL-Profiler deployment.

Sediment was sampled at station A1 by using a multicorer equipped with acrylic liners of 10 cm diameter. Subsamples of Ø 3.6 cm cores were taken for oxygen uptake and denitrification experiments. Porewater from a Ø 10 cm core was sampled on board by inserting Rhizon Soil Solution Samplers (Seeberg-Elverfeldt et al. 2005) with a vertical resolution of 1 cm (between 0 and 5 cm depth) and 2 cm (between 5 and 22 cm depth).

Chemical analysis

Oxygen and ammonium concentrations in the water column at station A1 were measured immediately on board by Winkler titration and fluorometric analysis (Holmes et al. 1999), respectively. At station A2 oxygen concentration was measured in situ by oxygen optodes. Water column samples for nutrient analysis were stored in centrifuge tubes at –20°C until measured in the laboratory for NH_4^+, NO_3^-, NO_2^- and PO_4^{3-} concentrations (autoanalyzer, TRAACS 800, Bran & Luebbe, Germany). Porewater samples for NO_3^- and NO_2^- were stored frozen in eppendorf vials until measured with a chemoluminescence NOx analyzer (Thermo Environmental Instruments Inc, USA) after Braman and Hendrix (1989). Samples for NH_4^+ were amended with 100 µl saturated $HgCl_2$ and stored without headspace at 4 °C and measured by flow injection according to Hall and Aller (1992).

Water column samples for particle analysis (1 liter) were filtered on board onto precombusted and weighted Whatman glass fiber filters (GF/F) and stored frozen at –20 °C. In the laboratory, filters were dried at 60 °C and weighed to determine particulate matter (PM). C/N analysis was conducted using an Elemental Analyzer (Fisons NA 1500 Series 2, Fison Instruments). Inorganic carbon was removed prior to the analysis by HCl-vapor

treatment for 24 h in an exsiccator. At station A1, sedimentary organic carbon and nitrogen concentrations of surface sediment samples were analyzed using the same methods as above.

Oxygen consumption

Oxygen consumption rates in the BBL were measured on board. At station A1 two BWS samples, derived from 35 cm and 205 cm above the sediment, were carefully transferred into 600 ml glass incubation chambers which were then sealed with rubber stoppers leaving no gas phase inside. The contents were gently mixed by stirring magnets. Oxygen concentrations were measured with needle optodes (PreSens, Precision Sensing GmbH, Germany) that were pushed through the rubber stoppers. The incubation chambers were kept in a water bath at in situ temperatures. Measurements were performed in the dark. At station A2, a sample was obtained from 35 cm above the sediment. The setup used at station A1 was modified by increasing the sample volume to 3000 ml and by using a more sensitive optode (Oxygen Optode, Model 3830, Aanderaa Data Instruments, Norway) for the oxygen measurement.

Oxygen uptake of the sediment (only station A1) was determined on board for two subsamples (Ø 3.6 cm cores) by measuring the oxygen decrease in the overlying water. To mix the overlying water we placed small magnetic stirrers inside the cores that were driven by a large external magnet. The cores were then sealed with rubber stoppers, leaving no gas phase inside. Oxygen concentration was measured with needle optodes (see above) that were pushed through the rubber stoppers. Measurements were performed in the dark at in situ temperatures.

15N labeling experiments

Sedimentary denitrification rates (only station A1) were determined using the isotope pairing technique (IPT) described in detail by Nielsen (1992). Experiments were carried out on board. 15 sediment subcores were taken from the multicorer using Ø 3.6 cm plastic tubes. Sediment height in the cores was adjusted to 13 cm. In each core, the overlying water column of 12.5 cm height was amended with $^{15}NO_3^-$ to a final concentration of 50 µmol L^{-1}. The overlying water was mixed with small magnetic stirrers as described previously for the oxygen uptake experiments. After preincubation of the open cores for 12 h all cores were sealed with rubber stoppers and incubated without a gas phase. Time points were taken at 0:00, 1:15, 2:20, 4:45 and 9:00 h. Subsequently, 3 cores for each time point were sacrificed by first taking of the rubber stopper and injecting 1 ml of 50 % $ZnCl_2$ on to the sediment surface to precipitate dissolved sulfide. Then, the top 3 cm of the sediment were thoroughly mixed

with the overlying water and a slurry sample was drawn of into 12 ml gas tight vials (Exetainers, Labco) and fixed with 100 µl saturated $HgCl_2$ solution. Measurements were performed in the dark at in situ temperatures. In the laboratory, a 2 ml Helium headspace was introduced into the exetainer. The exetainer were shaken vigorously to allow N_2 to equilibrate between the headspace and the water phase. The isotope ratio ($^{28}N_2$, $^{29}N_2$, and $^{30}N_2$) of the headspace was determined by gas chromatography-isotopic ratio mass spectrometry by direct injections from the headspace according to Kuypers et al. (2005). Concentrations of $^{30}N_2$ and $^{29}N_2$ were normalized to $^{28}N_2$ and calculated as excess relative to air. N_2 production rates were calculated from the slope of $^{29}N_2$ and $^{30}N_2$ increase over time and denitrification of $^{15}NO_3^-$ (D_{15}) and $^{14}NO_3^-$ (D_{14}) was calculated after (Nielsen 1992) from the production of $^{30}N_2$ and $^{29}N_2$ according to: $D_{15} = {}^{29}N_2 + 2\ {}^{30}N_2$ and $D_{14} = D_{15}\frac{{}^{29}N_2}{2\ {}^{30}N_2}$.

Results

Station A1

At station A1, the density structure of the water column was characterized by a halocline which extended into the BBL (Fig.2). The salinity gradient changed little from 8 m to 1 m above sediment but decreased rapidly close to the sediment. Current velocities at 30 cm above the sediment were between 8 and 9 cm s^{-1}. In the BBL, the concentrations of the combined fixed nitrogen N_{fix} (i.e. $NH_4^+ + NO_2^- + NO_3^-$) as well as the concentration of PO_4^{3-} increased towards the sediment whereas oxygen concentration decreased. All gradients, with the exception of phosphate, slightly increased between 2 m and 60 cm above the sediment before they decreased again toward the sediment surface.

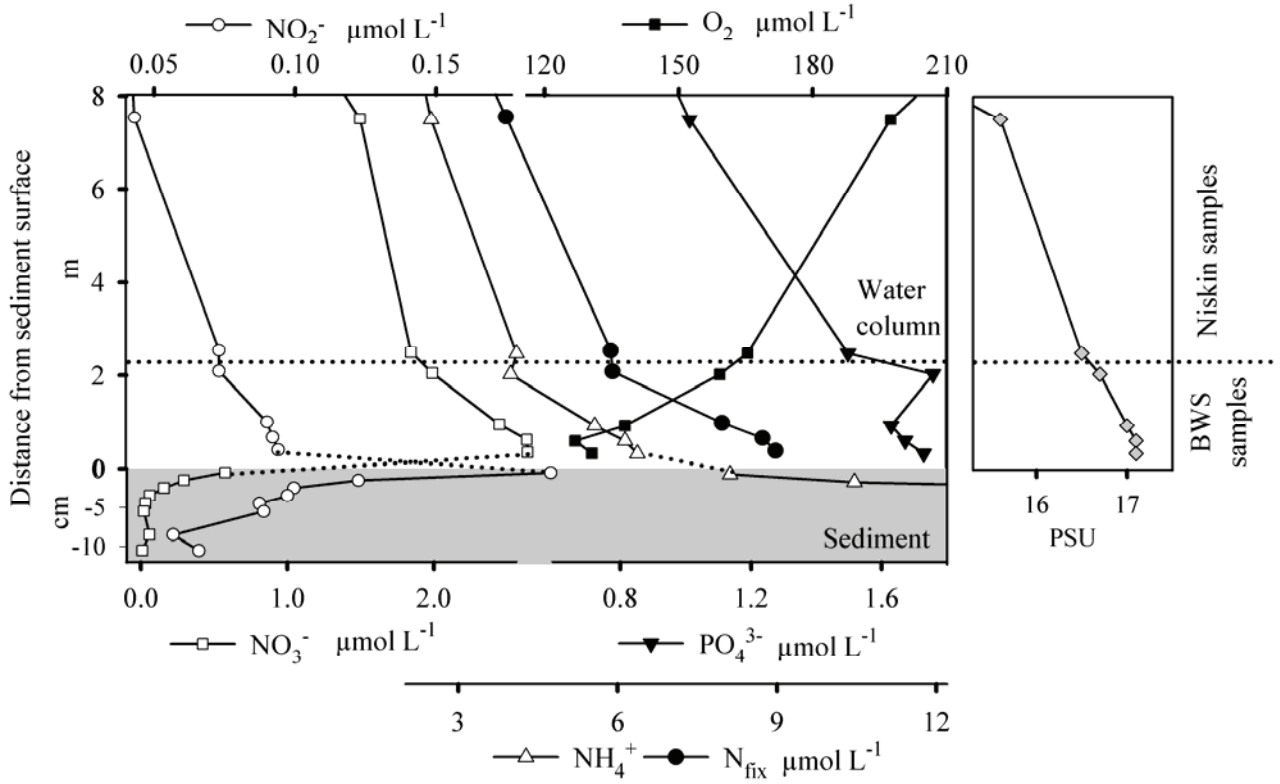

Figure 2. Station A1. Left side: Nutrient and oxygen concentrations across the BBL and in the porewater. The grey area marks the sediment and the dotted horizontal line separates the sampling range of the BWS from the sampling range of the Niskin bottles. N_{fix} was calculated as the sum of NH_4^+, NO_2^- and NO_3^-. Right side: Salinity concentrations across the BBL.

Particle concentrations (data not shown) were constant (0.6 +/- 0.17 mg L^{-1}) from the surface down to 8 m above the sediment but increased rapidly in the lower 2 m with a maximum concentration gradient between 1 m and 0.6 m above the sediment and a maximum concentration of 8.2 mg L^{-1} 0.35 m above the sediment. Molar C/N ratio of the particles were 10.1 and 10.3 at the lower most depth of 0.35 m and 0.62 m above the sediment, respectively. Concentrations of porewater NO_2^- and NO_3^- decreased exponentially with depth while NH_4^+ concentrations increased linearly (total profile not shown in Fig. 2). The combined porewater and BBL profile showed the highest concentrations of NO_2^- and NO_3^- close to the sediment surface.

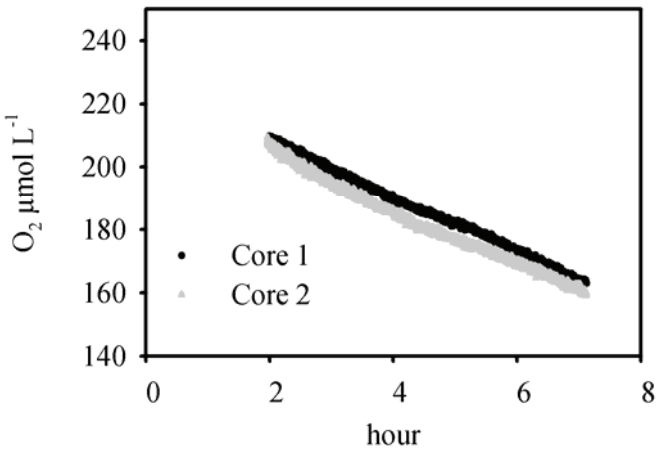

Figure 3. Station A1. Decrease of oxygen concentrations in the overlying water of two sediment cores. The calculated oxygen fluxes into the sediment were 10.5 and 10.4 mmol m^{-2} d^{-1} (R^2 = 0.989 and R^2 = 0.996, respectively).

During the incubation of the bottom water samples changes in oxygen concentration were within the analytical noise of the oxygen measurements and prevented calculation of oxygen consumption rates in the BBL. A linear regression of the measured oxygen concentration over 5 h showed no significant change over time. Considering the experimental setup and the scattering of the optode signal we conclude that the oxygen consumption in the BBL was < 2 µmol L^{-1} d^{-1}. Oxygen uptake of the sediment was determined from the sediment core incubation experiments. In the overlying water of the sediment cores, oxygen concentrations decreased with time (Fig. 3). The slope of a linear regression was used to calculate oxygen fluxes of 10.5 and 10.4 mmol m^{-2} d^{-1} (R^2 = 0.989 and R^2 = 0.996, respectively). The $^{15}NO_3^-$ uptake experiments indicated denitrification in the sediment based on the increase of $^{29}N_2$ and $^{30}N_2$ concentrations over time (R^2=0.90, $p < 0.001$ and R^2 = 0.82,

$p < 0.01$, respectively). Assuming denitrification as the sole N-loss process (see discussion) the calculated loss of $^{14}NO_3^-$ due to denitrification was 0.33 mmol m^{-2} d^{-1}. The organic carbon content was 3.3 wt% and the molar C/N ratio of the surface sediment was 10.0 +/- 0.3.

Station A2

At station A2, temperature and salinity did not change throughout the BBL (Fig.4). In contrast, the concentrations of NH_4^+, NO_2^- and NO_3^- increased and the O_2 concentration decreased towards the sediment. The highest concentrations of NH_4^+, NO_2^- and NO_3^- (0.88, 0.08 and 0.66 µmol L^{-1}, respectively) and the lowest O_2 concentrations of 261 µmol L^{-1} were found close to the sediment surface. PO_4^{3-} concentrations did not show a clear trend. Current velocities were 3 - 4 cm s^{-1} at 2 m above the sediment. Using the more sensitive Aanderaa optode, oxygen consumption in the BBL was detected. Oxygen concentration in the incubation chamber decreased linear over time (Fig. 5). Oxygen consumption of 5 µmol L^{-1} d^{-1} was calculated using the slope of the linear regression ($R^2 = 0.993$). Particle concentration 35 cm above the sediment was 4 mg/l. The atomic C/N ratio of the particles was 7.1.

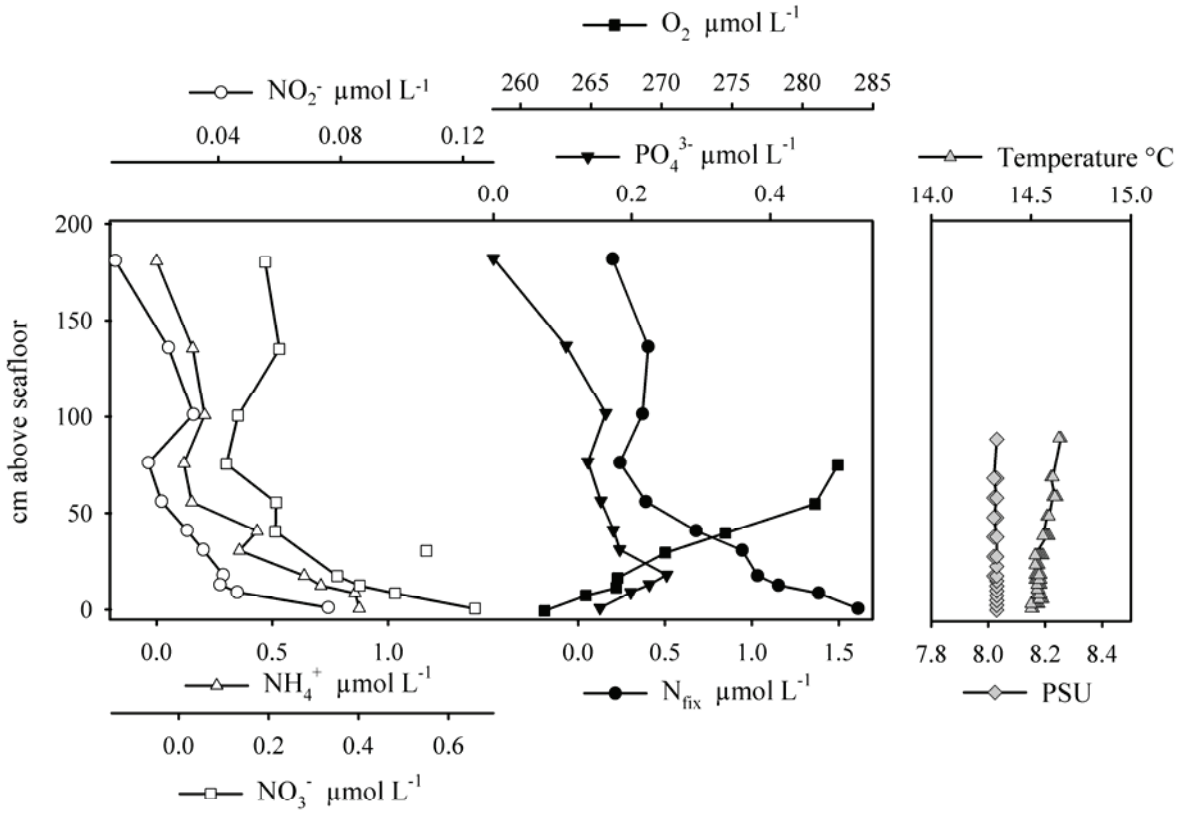

Figure 4. Station A2. The left side shows nutrient and oxygen concentrations across the BBL. The NO_3^- concentration at 30 cm above the sediment was discarded as outlier and not used for further calculations. The right side shows salinity and temperature across the BBL. The sensors for oxygen concentration, temperature and salinity were mounted on the slider that operated only in the lowermost meter above the sediment.

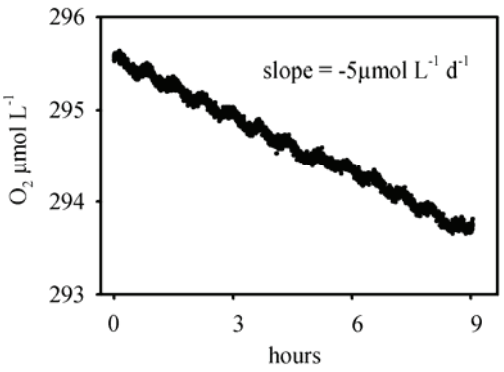

Figure 5. Respiration experiment at Station A2. Oxygen concentration over time of BBL water sampled from 35 cm above the sediment. The undulating pattern in the oxygen signal resulted from the cooling cycles of the cooling device. The calculated oxygen uptake of the BBL water was 5 µmol L^{-1} d^{-1} (R^2 = 0.993).

Discussion

Concentration profiles

In the Arkona Basin, the halocline is a permanent feature caused by periodically injected saline North Sea water that accumulates in the deeper parts of the basin and separates from the overlying brackish waters. At station A1, the halocline extended from 25 m water depth down to about 60 cm above the sediment (Fig. 2). Further down, the gradient decreased rapidly, most probably due to increased turbulent mixing caused by the boundary friction between the sediment and the moving water column. The density stratification caused by the salinity gradient reduces vertical mixing and, therefore, increases the vertical concentration gradient for a given solute flux across the BBL. For this reason concentration gradients of nutrients and oxygen could be measured up to several meters above the sediment. In general, the range of the observed salinity, oxygen and nutrient concentration in the bottom water were in good agreement with reported values from a nearby monitoring station (Nausch et al. 2007). In contrast to station A1, the water column at station A2 was thoroughly mixed and did not show any salinity or temperature gradients (Fig. 4). Accordingly, concentration gradients were only found between 0-1 m above the sediment. Above this height, increased mixing resulted in undetectable concentration gradients for the various nutrient species.

For the following analysis of the BBL concentration profiles, we assume a steady state situation with negligible horizontal concentration gradients. At both stations, minimum O_2 concentrations at the sediment surface identified the sediment as a net O_2 sink. At both stations, maximum nutrient concentrations at the sediment surface indicate that the sediment was a net source of PO_4^{3-}, NH_4^+, NO_2^- and NO_3^-. Hence, there was no NO_2^- and NO_3^- flux from the overlying water into the sediment, which in turn implies that all NO_2^- and NO_3^- reducing processes in the sediment were fully coupled to nitrification at the sediment surface. At station A1, the combined BBL and porewater profiles suggest that NH_4^+ was released due to mineralization processes deeper in the sediment from where it diffused up towards the sediment surface and into the water column. The maximum concentrations of NO_2^- and NO_3^- at the sediment surface indicate that NH_4^+ was nitrified at the sediment surface. In turn, NO_2^- and NO_3^- were transported from the sediment surface into the upper water column as well as deeper into the sediment where they were converted to N_2 gas via denitrification. In the BBL at station A2, the PO_4^{3-} profile showed no clear trend, which we attribute to the fact that PO_4^{3-} concentrations were at the detection limit and the values are uncertain.

Nutrient fluxes across the sediment surface and nutrient turnover in the BBL

As a first estimate, we assume that the concentration profiles reflect the nutrient flux across the sediment surface. However, it can not be excluded that these profiles were biased by net nutrient turnover rates within the BBL. Particulate organic matter (POM) often accumulates in bottom waters (Christiansen et al. 2002; Inthorn et al. 2006; Ritzrau 1996; van Weering et al. 2001) and may support enhanced mineralization in the BBL. Although POM accumulates in the lower BBL at station A1, the measured respiration rates of < 2 mmol m^{-3} d^{-1} were low compared to the oxygen uptake of the sediment (10.4 mmol m^{-2} d^{-1}). These low respiration rates in the BBL can be attributed to the low reactivity of the POM as indicated by the high molar C/N ratios (10.5 and 13.4) that were well above the Redfield ratio of 6.6. Emeis et al. (2002) observed similar C/N ratios and suggested that part of the particulate matter originates from the Oder estuary. During transport, the labile POM fraction is consumed leaving the refractory POM fraction behind. The contributions of both, the flux across the sediment surface (F_{Sed}) and the rate within the BBL (R_{BBL}) to the overall flux (F_{tot}) at a given depth (z) can be summed up as follows:

$$F_{tot} = F_{Sed} + z\, R_{BBL} \qquad (1)$$

For simplicity we assumed a constant R_{BBL} throughout the BBL. Equation 1 states that the contribution of R_{BBL} to F_{tot} increases with increasing distances from the sediment surface. For F_{Sed} = 10.4 mmol m^{-2} d^{-1} and R_{BBL} = 2 mmol m^{-3} d^{-1} at station A1, we calculate that R_{BBL} can contribute no more than 50 % to F_{tot} in the lower 5 meters of the BBL. We assumed, therefore, that the BBL profiles reflected basically the solute fluxes across the sediment surface.

This can be assumed for the profiles at station A2 as well. Given the thoroughly mixed bottom water, the measured oxygen consumption rate of 5 mmol m^{-3} d^{-1} would have been too low to build up the steep oxygen gradient (25 mmol m^{-4}) in the lower 75 cm of the BBL. This becomes apparent if one assumes a F_{Sed} similar to station A1 (10.4 mmol m^{-2} d^{-1}) and uses the measured R_{BBL} value of 5 mmol m^{-3} d^{-1} throughout the BBL. Under these conditions, a 50 % contribution of R_{BBL} to the total flux is reached at a distance of 2 m. However, the steepest gradients were measured within 50 cm above the sediment suggesting a minor contribution of R_{BBL} to the total flux.

In contrast to station A1, the BBL at station A2 was thoroughly mixed allowing a direct comparison of measured concentration profiles with profiles predicted by the theory for

turbulent boundary layers, the so-called law-of-the-wall (Boudreau 2001; Dade et al. 2001; Faber 1995; Tennekes and Lumley 1972). At a given depth z the concentration gradient $\partial C / \partial z$ of a solute is proportional to the total flux (Fick's first law of diffusion):

$$F_{tot} = Ez\ \partial C / \partial z \tag{2}$$

with the turbulent diffusion coefficient Ez. The lower part of a fully mixed, turbulent boundary layer is characterized by a linear increase of Ez with distance z to the sediment:

$$Ez = k\ u^*\ z \tag{3}$$

with the Karman's constant k and the friction velocity u^*. By inserting Eq. 1 and 3 into Eq. 2 and by rearranging the combined equation we obtain an expression for the concentration gradient:

$$\frac{\partial C}{\partial z} = \frac{F_{Sed}}{k\ u^*\ z} + \frac{R_{BBL}}{k\ u^*} \tag{4}$$

The shape of the concentration gradient profile depends on the contribution of F_{Sed} and R_{BBL} to the total flux. We discuss two scenarios: i) only F_{Sed} contributes to the total flux. In this case, the second term on the right hand side of Eq. 4 is zero and $\partial C / \partial z$ decreases with distance z to the sediment ii) only R_{BBL} contributes to the total flux. In this case, the first term on the right hand side of Eq. 4 is zero and $\partial C / \partial z$ is constant. Integration of Eq. 4 gives the concentration profile:

$$C(z) = \frac{F_{Sed}}{k\ u^*} \ln\left(\frac{z}{z_0}\right) + \frac{R_{BBL}}{k\ u^*}(z - z_0) + C_0 \tag{5}$$

with the boundary condition $C(z) = C_0$ at the sediment surface $z = z_0$. The first scenario yields a logarithmic shaped concentration profile, similar to the measured ones, while the second scenario yields a linear concentration profile. Equation 5 can be fitted to the measured concentration profiles at station A2 to estimate unknown variables like u^* or F_{Sed}. For now we only want to highlight the logarithmic shape of the concentration profiles and the low oxygen consumption rate in the BBL at A2 suggesting that the BBL profiles at station A2 basically reflect the solute fluxes across the sediment surface. In the following analysis we therefore neglect the mineralization rates in the BBL.

Calculation of fluxes at station A1 and A2

In the following we describe a method that allows a semi-quantitative analysis of nutrient fluxes from BBL concentration profiles without the need for determining the turbulent

diffusivity Ez . If turnover rates in the BBL are negligible, the concentration gradients $\partial C / \partial z$ in the BBL reflect the flux of the respective solute across the sediment surface $F_{Sed} = Ez\ \partial C / \partial z$. We compared the oxygen flux, $\vec{O}_2$ and the ammonium flux, $\vec{NH}_4$ by expressing the flux ratio:

$$\frac{\vec{NH}_4}{\vec{O}_2} = \frac{Ez\ \partial C_{NH4}\ \partial z}{Ez\ \partial C_{O2}\ \partial z} \tag{6}$$

Here, the overbar arrow indicates the flux magnitude of a specific solute. The turbulent diffusion coefficient Ez is a function of the flow field and, therefore, is the same for every solute. The sampling interval was the same for every solute and we can, therefore, simplify equation 6:

$$\frac{\vec{NH}_4}{\vec{O}_2} = \frac{\partial C_{NH4}}{\partial C_{O2}} \tag{7}$$

The term $\partial C_{NH4} / \partial C_{O2}$ can be expressed graphically by plotting NH_4^+ over O_2 concentrations. (Figs. 6A+B). A significant linear correlation between NH_4^+ and O_2 concentrations was observed at both stations. Here, the slope of the linear regression is $\partial C_{NH4} / \partial C_{O2}$, which equals the flux ratio $\vec{NH}_4 / \vec{O}_2$. The negative slope of the regression indicates that O_2 and NH_4^+ were transported in opposite directions. By using the regression we calculated that for each mole of O_2 transported towards the sediment an equivalent of 56 mmol (station A1) and 37 mmol of NH_4^+ (station A2) was released from the sediment. Flux ratios were calculated for all nutrients with respect to $\vec{O}_2$ and summarized in Table 1. All correlations are significant ($p < 0.05$ for $\vec{PO}_4^{3-}$ at station A1, all others at least $p < 0.01$) except $\vec{PO}_4^{3-}$ at station A2, which was not used for further calculations. The concentration of fixed nitrogen

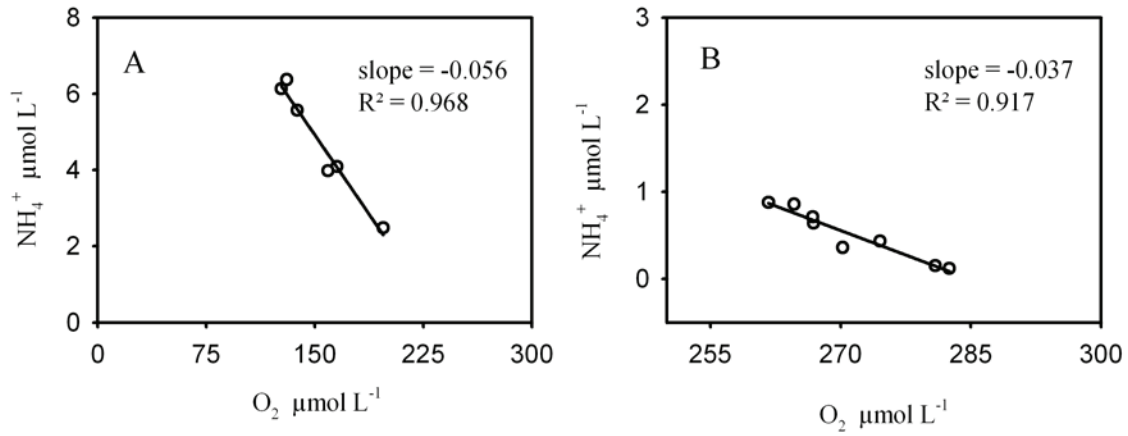

Figure 6: Ammonium concentrations in the BBL plotted over oxygen concentrations at corresponding depths at Stations A1 (A) and station A2 (B).

($N_{fix} = NH_4^+ + NO_3^- + NO_2^-$) was calculated for each sampling depth and plotted over O_2 to calculate the $\vec{N}_{fix} / \vec{O}_2$ flux ratio. At both stations NH_4^+ was the major constituent of the nutrient efflux followed by NO_3^-, PO_4^{3-} (only station A1) and NO_2^-.

Table 1: Nutrient fluxes relative to oxygen flux derived from the slope of a linear regression between the oxygen and the respective nutrient concentrations in the BBL. R^2 gives the coefficient of determination.

(Fluxes relative to $\vec{O}_2$)		$\vec{O}_2$	$\vec{PO}_4^{3-}$	$\vec{N}_{fix}$	$\vec{NH}_4^+$	$\vec{NO}_3^-$	$\vec{NO}_2^-$
Station A1	flux	1	0.0089	0.074	0.056	0.017	0.0007
	R^2	1	0.722	0.972	0.968	0.969	0.975
Station A2	flux	1	0.0028	0.061	0.037	0.021	0.0021
	R^2	1	0.302	0.970	0.917	0.856	0.793

Calculation of the nitrogen balance

To determine the flux ratio $\vec{O}_2 / \vec{N}$, the amount of oxygen that is used for nitrification at the sediment surface needs to be subtracted from the oxygen flux since the oxygen bound as nitrate and nitrite is carried back into the water column. The complete nitrification reaction can be expressed as two separate processes:

$$NH_4^+ + 1.5\,O_2^- \rightarrow NO_2^- + H_2O + 2H^+ \quad (8)$$

$$NO_2^- + 0.5\,O_2^- \rightarrow NO_3^- \quad (9)$$

Thus, the flux ratio $\vec{O}_2 / \vec{N}$ is expressed as:

$$\vec{O}_2 / \vec{N} = \frac{\vec{O}_2 - \left(2\,\vec{NO}_3^- + 1.5\,\vec{NO}_2^- \right)}{\vec{N}_{fix}} \quad (10)$$

In sediments underlying well oxygenated bottom waters, oxygen is the ultimate electron acceptor of almost all electron equivalents released during the oxidation of organic matter (Canfield et al. 2005; Thamdrup and Canfield 2000). Thus, the oxygen uptake of the sediment can be used as a proxy for the total carbon mineralization:

$$C\ mineralization = O_2\ respiration + inorganic\ reoxidation = O_2\ consumption$$

Furthermore, we assume as first approximation that the C:N:P ratio of the mineralized organic matter in the sediment reflects the C:N:P ratio of the particulate organic matter. Thus, using oxygen as a proxy for total carbon mineralization we assume particulate C:N:P ratios equals the $\vec{O}_2 : \vec{N} : \vec{P}$ flux ratios across the sediment surface. Table 2 compares the $\vec{O}_2 / \vec{N}$ and $\vec{O}_2 / \vec{P}$ flux ratios with the Redfield ratios and with the C/N ratios of organic matter from the two stations. The $\vec{O}_2 / \vec{P}$ flux ratio of 109 at station A1 was consistent with the Redfield ratio

Table 2: BBL flux ratios of $\vec{O}_2 : \vec{N} : \vec{P}$ compared to the Redfield ratio and the C:N ratio of POM. At station A2, $\vec{P}$ was not determined

	$\vec{O}_2 / \vec{P}$	$\vec{N} / \vec{P}$	$\vec{O}_2 / \vec{N}$	C / N_{POM}
Station A1	108.9	8.3	13.1	10.0
Station A2	-	-	15.6	7.1
Redfield	106.0	16.0	6.6	

of 106, while the $\vec{O}_2 / \vec{N}$ flux ratios of 13.1 (station A1) and 15.6 (station A2) were significantly higher compared to the Redfield ratio (C/N: 6.6) and the C/N ratios at station A1 (C/N: 10.0) and station A2 (C/N: 7.1). This deviation suggests a substantial loss of mineralized nitrogen from the sediment. The N-loss can be attributed to denitrification in the sediment. The contribution of anammox to the total N-loss in near shore sediments is usually considered to be of minor importance (< 15 %) (Dalsgaard et al. 2005; Engström et al. 2005; Kuypers et al. 2006) and was, therefore, neglected. Denitrification was measured at station A1 and was very likely active at station A2 as well. At both stations, the sole NO_3^- source for denitrification was nitrification in the sediment surface. The particulate C/N ratio deviates from the $\vec{O}_2 / \vec{N}$ flux ratio, because denitrification was not considered in Eq. 10. We therefore expanded Eq. 10 for a nitrate flux ($\vec{NO}_{3\,Den}^-$) used for denitrification and considered the stoichiometry of carbon oxidation via denitrification to derive the following equation:

$$C/N = \frac{\vec{O}_2 - \left(2\,\vec{NO}_3^- + 1.5\,\vec{NO}_2^- + 2\,\vec{NO}_{3\,Den}^- \right) + 4/5\,\vec{NO}_{3\,Den}^-}{\vec{N}_{fix} + \vec{NO}_{3\,Den}^-} \qquad (11)$$

The term inside brackets corrects the oxygen flux for the oxygen consumed by nitrification, whereas 4/5 NO_3^- are required to oxidize organic carbon to CO_2 via denitrification (Canfield et al. 1993). The nitrogen flux in the denominator of equation 11 is corrected by the amount of nitrogen lost due to denitrification. Equation 11 can be solved for $\vec{NO}_{3\,Den}^-$ and simplified:

$$\vec{NO}_{3\,Den}^{-} = \frac{\vec{O}_2/\vec{N} - C/N}{C/N + 6/5}\vec{N}_{fix} \qquad (12)$$

Here, the flux ratio $\vec{O}_2/\vec{N}$ is taken from equation 10. The nitrate used for denitrification $\vec{NO}_{3\,Den}^{-}$ and the flux of fixed nitrogen $\vec{N}_{fix}$ into the water column gave the total mineralized nitrogen $N_{tot} = \vec{N}_{fix} + \vec{NO}_{3\,Den}^{-}$, whereas the amount of nitrified ammonium N_{nit} was the sum of $\vec{NO}_{3\,Den}^{-}$ and $\vec{NO}_3^{-}$ released into the water column: $N_{nit} = \vec{NO}_3^{-} + \vec{NO}_{3\,Den}^{-}$. Table 3 summarizes the fluxes of fixed nitrogen, released nitrate, nitrate used for denitrification, and nitrified ammonium with respect to the total mineralized nitrogen. Of the total mineralized

Table 3: The nitrogen balance. Nitrogen fluxes, nitrification and denitrification rates relative to the total mineralized nitrogen. Right column: Contribution of denitrification to the total carbon mineralization.

(relative to N_{tot})	$\vec{N}_{fix}$	$\vec{NO}_3^{-}$	$\vec{NO}_{3\,Den}^{-}$	N_{nit}	$\vec{CO}_{2\,Den}/\vec{CO}_{2\,tot}$
Station A1	0.78	0.18	0.22	0.40	0.017
Station A2	0.49	0.17	0.51	0.68	0.057

nitrogen 78 % (station A1) and 49 % (station A2) were released to the water column, whereas 22 % (station A1) and 51 % (station A2) were lost due to denitrification. Of the total mineralized nitrogen 40 % (station A1) and 68 % (station A2) was oxidized to nitrate, with nitrification accounting for 8 % (station A1) and 18 % (station A2) of the total oxygen demand of the sediment. Carbon oxidation via denitrification relative to the total carbon oxidation was calculated according to:

$$\frac{\vec{CO}_{2\,Den}}{\vec{CO}_{2\,tot}} = \frac{4/5\,\vec{NO}_{3\,Den}^{-}}{\vec{O}_2 - \left(2\,\vec{NO}_3^{-} + 1.5\,\vec{NO}_2^{-} + 2\,\vec{NO}_{3\,Den}^{-}\right) + 4/5\,\vec{NO}_{3\,Den}^{-}} \qquad (13)$$

The relative contribution of carbon oxidation via denitrification to the total carbon oxidation varied from 1.7 % at station A1 to 5.7 % at station A2. This agrees well with reported values of 1-8 % in the Kattegat (Rysgaard et al. 2001), 2 % in Aarhus Bay (Jørgensen 1996) and 3-6 % in the Skagerrak (Canfield et al. 1993).

Calculation of absolute fluxes:

So far, the ratio of nutrient flux to oxygen flux was determined to calculate the contribution of the specific nitrogen pathways at each station. Nevertheless, the quantification of 'absolute'

fluxes is of interest to investigate the impact that processes such as denitrification may have on the entire ecosystem. For the approach presented in this study, a single estimate of an absolute nutrient or oxygen flux is sufficient to determine the absolute fluxes of all other solutes from their flux ratios. At station A1, the absolute oxygen flux into the sediment was measured in two cores with very similar results (10.4 and 10.5 mmol m^{-2} d^{-1}). We used the averaged oxygen flux of 10.45 mmol m^{-2} d^{-1} and the previous determined flux ratios (Table 1) to calculate the absolute flux of every nutrient species (Table 4). Of the total mineralized nitrogen (0.98 mmol m^{-2} d^{-1}), denitrification removes 0.22 mmol m^{-2} d^{-1} from the Baltic Sea sediments. This is comparable to our experimentally determined denitrification rate of 0.33 mmol m^{-2} d^{-1} and those (0.15 – 0.65 mmol m^{-2} d^{-1}) measured by Tuominen (1998). Middelburg (1996) predicted similar rates (~0.4 mmol m^{-2} d^{-1}) for shallow water depths with bottom water oxygen and nitrate concentrations of about 100 and 2.5 µmol L^{-1}, respectively.

In contrast to the results presented in Table 4, fluxes derived from porewater profiles are 1-2 orders of magnitude lower. At station A1, we used the diffusion coefficients of NH_4^+ and NO_3^- in seawater at 15°C (1.68 x 10^{-9} and 1.44 x 10^{-9} m^2 s^{-1}, respectively) and a porosity of 0.85 to calculate a NO_3^- flux into the sediment of 2.3 µmol m^{-2} d^{-1} and a NH_4^+ flux into the water column of 54 µmol m^{-2} d^{-1}. Several publications discuss the importance of bioirrigation

Table 4: Absolute fluxes of oxygen and nutrients at station A1. Right columns: total mineralized nitrogen and rates of nitrification and denitrification.

mmol m^{-2} d^{-1}	$\vec{O}_2$	$\vec{PO_4}^{3-}$	$\vec{N}_{fix}$	$\vec{NH_4}^+$	$\vec{NO_3}^-$	$\vec{NO_2}^-$	N_{tot}	$\vec{NO_3}^-_{Den}$	N_{nit}
Station A1	10.45	0.093	0.77	0.58	0.18	0.008	0.98	0.22	0.38

on the solute transport in the sediment (Forster et al. 1999; Schlueter et al. 2000; Wenzhoefer and Glud 2002; 2004). They suggest that fluxes derived from porewater profiles heavily underestimate the true fluxes if macrofauna is present. In addition, we suggest that the resolution of porewater profiles is too coarse to resolve the thin but very active surface layer that is typical for organic-rich sediments.

Concluding remarks

Flux estimates obtained from BBL profiles have clear advantages. The measurements are distant from the sediment surface and, therefore, vertically integrate the surface layer, which is advantageous especially for sediments that are covered with fluff. For the same reason the measurements horizontally integrate a large surface area that contributes to the flux, considering bioirrigation and the spatial variability of sediment structure and macrofauna distribution. The so called footprint that contributes to the flux can be estimated according to Berg et al. (2007). Finally, our approach is non-invasive and can also be used to determine benthic fluxes from sandy sediments and shell beds, which are extremely difficult to obtain with benthic chamber and sediment coring techniques.

In our study we used ex situ core incubations to determine the oxygen flux and, subsequently, the nutrient flux. The use of ex situ core incubations is known to underestimate bio-irrigation and, thus, counteracts any non-invasive approach. Nevertheless, since we measured both, oxygen uptake as well as denitrification from ex situ core incubations the bias that these experiments produce with respect to bio-irrigation accounts for both flux measurements. The ratio of oxygen flux to denitrification flux in the core experiments agreed with the ratio of oxygen to denitrification flux calculated from the BBL concentration profiles (Table 4). In this context, we feel confident that the ex situ core incubations can be used to verify our approach. Nonetheless, our approach can be highly improved by using the eddy correlation technique for the determination of oxygen fluxes in the BBL (Berg et al. 2003; McGinnis et al. 2008). Eddy correlation flux measurements are performed in the BBL and therefore feature the same advantages as mentioned above for the BBL profiles.

Detecting concentration gradients is a prerequisite for the BBL approach presented here. The magnitude of concentration gradients depends on both, the eddy diffusivity and the respective solute flux. Given a moderate flux, increased current velocities lead to increased turbulent mixing, which may result in undetectable concentration gradients. This limits the applicability of the BBL approach to moderate current velocities. However, the method could be improved by increasing the vertical sampling resolution and by measuring closer to the sediment surface where turbulent diffusion is reduced.

BBL profiles allow direct identification of solute sinks and sources, visualizing the direction of their flux. In this study the sediment surface was identified as a net source of NO_3^- and NO_2^-, whereas the water column and the deeper sediment were net sinks. NO_3^- and NO_2^- fluxes from the overlying water (i.e. low concentrations) towards the sediment surface (i.e. high concentrations) could be excluded since this would contradict Fick's law of

diffusion. As a consequence, sedimentary denitrification must be fully coupled to nitrification at the sediment surface. Our findings have implications for the isotope pairing technique (IPT) for whole core incubations, commonly used to determine denitrification rates. The IPT approach separates the nitrate source for denitrification into the $^{14}NO_3^-$ flux from the overlying water (D_{14W}) and the $^{14}NO_3^-$ flux from nitrification in the surface sediment (D_{14N}). It is common practice to determine the ratios of $^{14}NO_3^-$ over $^{15}NO_3^-$ in the overlying water and distinguish D_{14W} from D_{14N} according to Nielsen (1992; 1996):

$$D_{14W} = D_{15} \frac{^{14}NO_3^-}{^{15}NO_3^-} \quad (14)$$

$$D_{14N} = D_{14} - D_{14W} \quad (15)$$

D_{14} and D_{15} are the rates of denitrification due to $^{14}NO_3^-$ and $^{15}NO_3^-$, respectively (see method section). In our study, D_{14W} must be zero and D_{14N} must be 100 %. However, applying these equations to our denitrification experiment, results in a D_{14W} of 18 %. This deviation results from the fact that D_{14W} is proportional to the $^{14}NO_3^-/^{15}NO_3^-$ ratio in the overlying water (Eq. 14). Any measurable $^{14}NO_3^-$ in the water column will, therefore, lead to a positive D_{14W}. Equation 14 can be written as $D_{14W} / D_{15} = {}^{14}NO_3^- / {}^{15}NO_3^-$ which implies that the ratio of denitrification fueled by $^{14}NO_3^-$ and $^{15}NO_3^-$ from the overlying water equals the ratio of the $^{14}NO_3^-$ and $^{15}NO_3^-$ concentrations in the overlying water. This assumption neglects the fact that diffusive transport from the water into the sediment is a function of the respective $^{14}NO_3^-$ and $^{15}NO_3^-$ concentration gradient and, therefore, is different for each solute. For that reason $^{15}NO_3^-$ diffuses into the sediment and is not affected by the $^{14}NO_3^-$ production in the nitrification layer, while a net transport of $^{14}NO_3^-$ against a positive $^{14}NO_3^-$ concentration gradient is not possible. We, therefore, consider equations 14 and 15 as problematic when used to determine NO_3^- fluxes across the water sediment interface in whole core incubations.

References

Berg, P. and others 2003. Oxygen uptake by aquatic sediments measured with a novel non-invasive eddy-correlation technique. Marine Ecology-Progress Series **261:** 75-83.

Berg, P., H. Roy, and P. L. Wiberg. 2007. Eddy correlation flux measurements: The sediment surface area that contributes to the flux. Limnology and Oceanography **52:** 1672-1684.

Berner, R. A. 1982. Burial of Organic-Carbon and Pyrite Sulfur in the Modern Ocean - Its Geochemical and Environmental Significance. American Journal of Science **282:** 451-473.

Boudreau, B. P. 2001. Solute transport above the sediment-water interface, p. 104-126. *In* B. P. Boudreau and B. B. Jørgensen [eds.], The Benthic Boundary Layer: Transport Processes and Biogeochemistry. Oxford University Press.

Braman, R. S., and S. A. Hendrix. 1989. Nanogram Nitrite and Nitrate Determination in Environmental and Biological-Materials by Vanadium(Iii) Reduction with Chemi-Luminescence Detection. Analytical Chemistry **61:** 2715-2718.

Canfield, D., B. Thamdrup, and E. Kristensen [eds.]. 2005. Aquatic Geomicrobiology. Elsevier.

Canfield, D. E. and others 1993. Pathways of Organic-Carbon Oxidation in 3 Continental-Margin Sediments. Marine Geology **113:** 27-40.

Christiansen, C. and others 2002. Material transport from the nearshore to the basinal environment in the southern Baltic Sea - I. Processes and mass estimates. Journal of Marine Systems **35:** 133-150.

Codispoti, L. A. and others 2001. The oceanic fixed nitrogen and nitrous oxide budgets: Moving targets as we enter the anthropocene? Scientia Marina **65:** 85-105.

Dade, B. D., A. Hogg, and B. P. Boudreau. 2001. Physics of Flow above the Sediment-Water Interface, p. 4-43. *In* B. P. Boudreau and B. B. Jørgensen [eds.], The Benthic Boundary Layer: Transport Processes and Biogeochemistry. Oxford University Press.

Dalsgaard, T., B. Thamdrup, and D. E. Canfield. 2005. Anaerobic ammonium oxidation (anammox) in the marine environment. Research in Microbiology **156:** 457-464.

Emeis, K. and others 2002. Material transport from the near shore to the basinal environment in the southern Baltic Sea - II: Synthesis of data on origin and properties of material. Journal of Marine Systems **35:** 151-168.

Engstrom, P., T. Dalsgaard, S. Hulth, and R. C. Aller. 2005. Anaerobic ammonium oxidation by nitrite (anammox): Implications for N-2 production in coastal marine sediments. Geochimica Et Cosmochimica Acta **69:** 2057-2065.

Faber, T. E. 1995. Fluid Dynamics for Physicists. Cambridge University Press.

Falkowski, P. G., R. T. Barber, and V. Smetacek. 1998. Biogeochemical controls and feedbacks on ocean primary production. Science **281:** 200-206.

Forster, S., R. N. Glud, J. K. Gundersen, and M. Huettel. 1999. In situ study of bromide tracer and oxygen flux in coastal sediments. Estuarine Coastal and Shelf Science **49:** 813-827.

Graf, G. 1992. Benthic-Pelagic Coupling - a Benthic View. Oceanography and Marine Biology **30:** 149-190.

Graf, G. and others 1995. Benthic-Pelagic Coupling in the Greenland Norwegian Sea and Its Effect on the Geological Record. Geologische Rundschau **84:** 49-58.

Hall, P. O., and R. C. Aller. 1992. Rapid, Small-Volume, Flow-Injection Analysis for Sigma-Co2 and Nh4+ in Marine and Fresh-Waters. Limnology and Oceanography **37:** 1113-1119.

Holmes, R. M., A. Aminot, R. Kerouel, B. A. Hooker, and B. J. Peterson. 1999. A simple and precise method for measuring ammonium in marine and freshwater ecosystems. Canadian Journal of Fisheries and Aquatic Sciences **56:** 1801-1808.

Inthorn, M., M. R. Van Der Loeff, and M. Zabel. 2006. A study of particle exchange at the sediment-water interface in the Benguela upwelling area based on Th-234/U-238 disequilibrium. Deep-Sea Research Part I-Oceanographic Research Papers **53:** 1742-1761.

Jørgensen, B. B. 1996. Case Study - Aarhus Bay, p. 137-154. *In* B. B. Jørgensen and K. Richardson [eds.], Eutrophication in Coastal Marine Ecosystems. American Geophysical Union.

Kuypers, M. M. M., G. Lavik, and B. Thamdrup. 2006. Anaerobic ammonium oxidation in the marine environment, p. 311-335. *In* L. N. Neretin [ed.], Past and Present Water Column Anoxia. Springer.

Kuypers, M. M. M. and others 2005. Massive nitrogen loss from the Benguela upwelling system through anaerobic ammonium oxidation. Proceedings of the National Academy of Sciences of the United States of America **102:** 6478-6483.

Lam, P. and others 2007. Linking crenarchaeal and bacterial nitrification to anammox in the Black Sea. Proceedings of the National Academy of Sciences of the United States of America **104:** 7104-7109.

Mcginnis, D. F., P. Berg, A. Brand, C. Lorrai, T. J. Edmonds, and A. Wuest. 2008. Measurements of eddy correlation oxygen fluxes in shallow freshwaters: Towards routine applications and analysis. Geophysical Research Letters **35**.

Middelburg, J. J., K. Soetaert, P. M. J. Herman, and C. H. R. Heip. 1996. Denitrification in marine sediments: A model study. Global Biogeochemical Cycles **10:** 661-673.

Nausch, G., R. Feistel, H. Lass, K. Nagel, and H. Siegel. 2007. Hydrographisch-chemische Zustandseinschätzung der Ostsee 2006.

Nielsen, L. P. 1992. Denitrification in Sediment Determined from Nitrogen Isotope Pairing. Fems Microbiology Ecology **86:** 357-362.

Nielsen, L. P., and R. N. Glud. 1996. Denitrification in a coastal sediment measured in situ by the nitrogen isotope pairing technique applied to a benthic flux chamber. Marine Ecology-Progress Series **137:** 181-186.

Ritzrau, W. 1996. Microbial activity in the benthic boundary layer: Small-scale distribution and its relationship to the hydrodynamic regime. Journal of Sea Research **36:** 171-180.

Rysgaard, S., H. Fossing, and M. M. Jensen. 2001. Organic matter degradation through oxygen respiration, denitrification, and manganese, iron, and sulfate reduction in marine sediments (the Kattegat and the Skagerrak). Ophelia **55:** 77-91.

Rysgaard, S., N. Risgaard-Petersen, and N. P. Sloth. 1996. Nitrification, denitrification, and nitrate ammonification in sediments of two coastal lagoons in Southern France. Hydrobiologia **329:** 133-141.

Rysgaard, S., N. Risgaardpetersen, N. P. Sloth, K. Jensen, and L. P. Nielsen. 1994. Oxygen Regulation of Nitrification and Denitrification in Sediments. Limnology and Oceanography **39:** 1643-1652.

Sauter, E. J., M. Schluter, J. Wegner, and E. Labahn. 2005. A routine device for high resolution bottom water sampling. Journal of Sea Research **54:** 204-210.

Schlueter, M., E. Sauter, H. P. Hansen, and E. Suess. 2000. Seasonal variations of bioirrigation in coastal sediments: Modeling of field data. Geochimica Et Cosmochimica Acta **64:** 821-834.

Seeberg-Elverfeldt, J., M. Schluter, T. Feseker, and M. Kolling. 2005. Rhizon sampling of porewaters near the sediment-water interface of aquatic systems. Limnology and Oceanography-Methods **3:** 361-371.

Soetaert, K., J. J. Middelburg, P. M. J. Herman, and K. Buis. 2000. On the coupling of benthic and pelagic biogeochemical models. Earth-Science Reviews **51:** 173-201.

Tennekes, H., and J. L. Lumley. 1972. A first course in turbulence. MIT Press.

Thamdrup, B., and D. Canfield. 2000. Benthic respiration in aquatic sediments, p. 86-103. *In* O. Sala, H. Mooney, R. Jackson and R. Howarth [eds.], Methods in Ecosystem Science. Springer.

Thomsen, L., and G. Graf. 1994. Boundary-Layer Characteristics of the Continental-Margin of the Western Barents Sea. Oceanologica Acta **17:** 597-607.

Thomsen, L., and W. Ritzrau. 1996. Aggregate studies in the benthic boundary layer at a continental margin. Journal of Sea Research **36:** 143-146.

Tuominen, L., A. Heinanen, J. Kuparinen, and L. P. Nielsen. 1998. Spatial and temporal variability of denitrification in the sediments of the northern Baltic Proper. Marine Ecology-Progress Series **172:** 13-24.

Tuominen, L., K. Makela, K. K. Lehtonen, H. Haahti, S. Hietanen, and J. Kuparinen. 1999. Nutrient fluxes, porewater profiles and denitrification in sediment influenced by algal sedimentation and bioturbation by *Monoporeia affinis*. Estuarine Coastal and Shelf Science **49:** 83-97.

van Weering, T. C. E. and others 2001. Benthic dynamics and carbon fluxes on the NW European continental margin. Deep-Sea Research Part Ii-Topical Studies in Oceanography **48:** 3191-3221.

Wenzhoefer, F., and R. N. Glud. 2002. Benthic carbon mineralization in the Atlantic: a synthesis based on in situ data from the last decade. Deep-Sea Research Part I-Oceanographic Research Papers **49:** 1255-1279.

---. 2004. Small-scale spatial and temporal variability in coastal benthic O-2 dynamics: Effects of fauna activity. Limnology and Oceanography **49:** 1471-1481.

Wollast, R. 1991. The coastal organic carbon cycle: fluxes, sources and sinks, p. 365-381. *In* J.-M. M. R.-F.-C. Mantoura, R. Wollast [ed.], Ocean Margin Processes in Global Change. John Wiley & Sons.

Estimating turbulent diffusivity in a benthic boundary layer: the relevance of boundary layer mixing for the mass transfer across the sediment water interface

Moritz Holtappels and Andreas Lorke

1) Max Planck Institute for Marine Microbiology, Celsiusstrasse 1, 28359 Bremen

2) Institute of Environmental Sciences, University of Koblenz-Landau, Fortstrasse 7, 76829 Landau

Acknowledgement

We thank Lars Umlauf and Volker Mohrholz for ideas and preparation of the measurement campaign as well as Christian Noss for advice and fruitful discussions. We gratefully acknowledge the help of the crew of the *RV Robert Lauterborn* during field work at Lake Constance. This study was financially supported by the German Research Foundation (grants Lo1150/3-1 and Um 79/3-1).

Abstract

In aquatic environments, the benthic boundary layer (BBL) is the transition zone for dissolved solutes that are released or consumed from the sediments. The exchange of solutes between the sediment and the overlying water column depends on the quasi diffusive turbulent transport in the benthic boundary layer. In situ measurements of turbulent diffusion in natural benthic boundary layers are scarce and estimates are usually derived from the logarithmic law of the wall (log-law). Based on G. I. Taylor's turbulent diffusion theory, we derived a simple approach to estimate turbulent diffusivity from acoustic Doppler velocimeter (ADV) data. The approach was applied to ADV data collected over a period of 155 hours in the BBL of Lake Constance, Germany. The calculated turbulent diffusivities agreed well with those derived in parallel from gradient-flux measurements. In addition, turbulent diffusivities were calculated from the logarithmic law of the wall. The log-law failed to predict plausible diffusivities whenever the boundary flow exhibited decreased current velocities or stable density stratification. Under these conditions, the turbulent diffusivities calculated from the gradient-flux measurement and from Taylor's theory were as low as 10^{-6} m^2 s^{-1}. To discuss the potential control that low turbulent diffusivities in the BBL have on the solute flux between sediments and water column, we present a simple oxygen flux model that included the turbulent as well as the diffusive boundary layer. Model results indicate that decreased turbulent diffusivities such as measured in this study can control the oxygen flux across the sediment water interface.

Introduction

In the shallow waters of lakes and the coastal ocean, primary productivity is strongly linked to the mineralization of organic matter in the sediments and thus to the exchange of organic matter, nutrients and metabolites between sediments and water column (Wollast 1991). The benthic boundary layer (BBL) is the interface between the sediments and the water column. By definition, it is the water layer that is influenced by the friction between the sediment and the moving water column (Dade et al. 2001). The vertical transport of solutes and particulate matter across the BBL is of turbulent nature. Assuming stationary conditions and neglecting the reactivity of the solute in the BBL (see chapter 2), the turbulent transport of solutes can be described as quasi diffusive transport according to Fick's law of diffusion:

$$J = -D_T \frac{\partial C}{\partial z} \qquad \text{E1}$$

where J denotes the flux, D_T is the turbulent diffusivity and $\partial C / \partial z$ is the vertical concentration gradient. Turbulent transport in the BBL is believed to be several orders of magnitude faster compared to molecular diffusion in the sediments. In contrast to molecular diffusion, turbulent diffusion is a function of the flow field and, therefore, varies with the flow velocity in the BBL. There are numerous models in which turbulent diffusivity scales as a function of boundary distance and mean current velocity (Dade et al. 2001). The most common model is the logarithmic law of the wall (i.e. log-law) (von Karman 1930), verified in various laboratory flume experiments (Pope 2000).

However, measurements of turbulent diffusivity in natural boundary flows are scarce. Theoretical constraints from the log-law suggest that the turbulent transport in the BBL is too fast to limit the oxygen and nutrient fluxes across the sediment-water interface (Boudreau 2001) and, in this respect, turbulent diffusivity may be seen as a parameter of minor interest. We give two reasons why the measurement of turbulent diffusivity in the BBL is of interest. First, Holtappels et al. (see chapter 2) and Sauter et al. (2005) recently demonstrated that nutrient and oxygen gradients in the BBL are measureable. With the knowledge of the turbulent diffusivity, it becomes possible to calculate the respective solute flux according to Fick's law. This approach would provide a new non-invasive method to determine the solute fluxes across the sediment-water interface. Second, there is evidence that the log-law does not apply for conditions of low current velocities and stratified boundary layers (Brand et al. 2008; Lorke et al. 2002), which commonly occur in natural aquatic systems. Under these conditions turbulent diffusivities as low as 10^{-7} m^2 s^{-1} (Lorke 2007) have been measured that

potentially control the solute flux between the sediment and the water column. It is, therefore, imperative to (i) derive a convenient method that measures the turbulent diffusivity independent from the log law and (ii) measure the turbulent diffusivity at critical conditions such as low current velocities and stratification.

In this study, we present a new approach for measuring turbulent diffusivity. The approach is based on Taylor (1921) who described the quasi diffusive transport by continuous movements from statistical measures. We applied this theory to measure turbulent diffusivities in the benthic boundary layer of Lake Constance, Germany. We compared the turbulent diffusivities with those derived from density gradient and density flux measurements according to Fick's law. Furthermore, we tested three approaches based on the log-law as well as turbulent diffusivities derived from the concept of turbulent viscosity and from Osborn's equation for turbulence in stratified flows (Osborn 1980). We discuss the results in the context of the measured current velocity and density stratification in the BBL. Finally, we discuss the potential control of low turbulent diffusivities on the solute flux between sediments and water column by means of a simple oxygen flux model.

Theory

Turbulent diffusivity derived from Taylor's theory

In stationary, homogenous turbulence, the mean square displacement $\langle X^2 \rangle$ of a fluid parcel at elapsed time *t* due to its fluctuation velocities u_L is expressed according to Taylor (1921) as:

$$\langle X^2 \rangle = 2 \cdot \langle {u_L}^2 \rangle \cdot t \cdot \int_0^\infty R_L(\tau)\, d\tau \qquad \text{E2}$$

Here and in the following, the instantaneous velocity U_L is decomposed into a mean velocity $\overline{U_L}$ and a fluctuating velocity u_L according to $U_L = \overline{U_L} + u_L$. Lagrangian and Eulerian velocities are denoted as U_L and U, respectively. The normalized Lagrangian autocorrelation coefficient R_L is defined as

$$R_L = \frac{\langle u_L(t) \cdot u_L(t+\tau) \rangle}{\langle {u_L}^2 \rangle} \qquad \text{E3}$$

with the time difference $\tau = t' - t$. For $\tau = 0$, R_L equals 1 and for $\tau \to \infty$, R_L approaches 0. The integral of R_L is called the Lagrangian integral time scale $\mathrm{T}_L = \int_0^\infty R_L(\tau)\, d\tau$ which approaches a constant value for $\tau \to \infty$ (Taylor 1921). T_L represents the characteristic time interval over which the instantaneous velocity of the fluid parcel is correlated with its previous velocities. For $t >> \mathrm{T}_L$, the mean square displacement $\langle X^2 \rangle$ in E2 is a linear function of *t*, thus characterizing a diffusive process. The turbulent diffusion coefficient is defined as $D_T = \langle X_2 \rangle / 2t$ and from E2 we obtain:

$$D_T = \langle {u_L}^2 \rangle \cdot \mathrm{T}_L \qquad \text{E4}$$

The Lagrangian integral length scale L_L is defined by (Tennekes and Lumley 1972)

$$L_L = u_L' \cdot \mathrm{T}_L \qquad \text{E5}$$

where u_L' denotes the standard deviation of u_L. We can write E4 as

$$D_T = u_L' \cdot L_L \qquad \text{E6}$$

Equation 4 was verified experimentally for the Lagrangian velocities of fluid particles (Sato and Yamamoto 1987). However, in the BBL, velocities are usually measured in the Eulerian reference frame at a fixed position above the sediment. Turbulent flow is measured as it floats

past the velocity sensor with the mean flow. A velocity sensor would have to move with the mean flow to derive a time series of turbulent velocities within an eddy. A fixed senor, therefore, measures a mixture of a spatial transect through the flow and a time series. According to Taylor's hypothesis (1938), the rate of change of a turbulent eddy is small compared to the velocity of the mean flow $\overline{U}$, so that the turbulence can be considered as 'frozen', as it passes by the sensor. Therefore, the time interval τ between two consecutive velocity measurements of the sensor can be translated into the spatial distance $r = \tau \cdot \overline{U}$ and the autocorrelation coefficient of the Eulerian velocity *u* translates into the Eulerian spatial correlation coefficient

$$E_E = \frac{\langle u(x) \cdot u(x+r) \rangle}{\langle u^2 \rangle} \qquad \text{E7}$$

The integral of E_E is called the Eulerian integral length scale (Tennekes and Lumley 1972)

$$L_E = \int_0^\infty E_E(r)\, dr \qquad \text{E8}$$

A common assumption is that $L_L \approx L_E$ and furthermore it was shown that $u' = u_L'$ (Tennekes and Lumley 1972) so that the turbulent diffusion coefficient can be calculated from Eulerian velocities according to:

$$D_T = u' \cdot L_E \qquad \text{E9}$$

In the benthic boundary layer, we assume a stationary boundary flow in which flow characteristics vary in the vertical scale but are homogeneous in the horizontal plane. In the following we denote *u*, *v*, *w* as the *x*, *y*, *z* component of the fluctuating velocity with the mean flow pointing towards *x* and the transversal and vertical flow towards *y* and *z* (positive z in upward direction), respectively. Since we are interested in the vertical diffusive transport across the turbulent boundary layer the vertical turbulent diffusion coefficient was calculated according to E9 as:

$$D_T = w' L_E \qquad \text{E10}$$

In the following, the turbulent diffusion coefficient derived from Taylor's theory is denoted as D_{T_T}. D_{T_T} can be estimated from single point velocity measurements with a sampling frequency that is high enough to resolve turbulent motion.

Turbulent diffusivity derived from the concept of turbulent viscosity.

In turbulent fluid flow, the shear stress due to turbulent fluctuations of fluid momentum is called Reynolds stress. A definition of the Reynolds stress (τ_{ij}) is derived from Reynolds averaging of the Navier-Stokes equations (Tennekes and Lumley 1972) which, in case of a boundary flow, results in:

$$\tau_{xz} = -\rho\langle u\, w\rangle \qquad \text{E11}$$

where ρ is the fluid density and $\langle u\, w\rangle$ is the time averaged covariance of the velocity fluctuations in the mean flow direction (u) and vertical direction (w). In analogy to the shear stress in laminar flow, the Reynolds stress in turbulent shear flow is assumed to be proportional to the mean velocity gradient (Tennekes and Lumley 1972):

$$\langle u\, w\rangle = -\nu_T \frac{\partial \overline{U}}{\partial z} \qquad \text{E12}$$

where the constant of proportionality (ν_T) is denoted as turbulent viscosity or momentum diffusion coefficient. It is assumed that ν_T equals the turbulent diffusion coefficient for heat and solutes (D_T) (Tennekes and Lumley 1972), so that:

$$D_T = -\frac{\langle u\, w\rangle}{\partial \overline{U} / \partial z} \qquad \text{E13}$$

In the following, the turbulent diffusion coefficient derived from turbulent viscosity is denoted as D_{T_V}. To estimate D_{T_V} it needs a high frequency single point velocity measurement together with a mean velocity profile. It should be mentioned that D_{T_T} and D_{T_V} are determined without any assumption regarding the structure of the boundary layer and are valid also for free shear flows.

Turbulent diffusivity derived from the logarithmic law of the wall.

Expressions of D_T that include the boundary dimensions are derived from the logarithmic law of the wall. In fully developed turbulent boundary flows the average current velocity profile $\overline{U}(z)$ is described by the logarithmic law of the wall (von Karman 1930):

$$\overline{U}(z) = \frac{u_*}{\kappa} \ln\left(\frac{z}{z_0}\right) \qquad \text{E14}$$

where κ is the Karmans constant (~0.41), z is the height above the bottom and z_0 is the hydraulic roughness, a constant of integration found to increase with bottom roughness. The

friction velocity u_* is related to the Reynolds stress (τ_{xz}) and the fluid density (ρ) according to $u_* = \sqrt{\tau_{xz}/\rho}$. Considering E11 it follows that:

$$u_*^{\,2} = -\langle u\, w \rangle . \qquad \text{E15}$$

The logarithmic law of the wall applies to a specific range in the BBL defined by upper and lower boundaries. However, the boundaries themselves depend on the flow field. The lower boundary is set where direct effects of viscosity (ν) on the velocity gradient are negligible. Expressed in terms of viscosity and friction velocity, the lower boundary is set where $z > 30\nu/u_*$ (Pope 2000). The log-law applies to about 30 % of the total boundary layer thickness, which is defined as the value of z where $\overline{U}$ equals 99% of the free flow velocity (Pope 2000). In lakes and oceans with moderate current velocities of ~0.1 m s^{-1} the log-layer extends from a few centimeters to a few meters above the sediment (Wüest and Lorke 2003).

A fundamental assumption of the log-law is a constant Reynolds stress throughout the layer and a velocity gradient that is a reciprocal function of z:

$$\frac{\partial \overline{U}}{\partial z} = \frac{u_*}{\kappa z} \qquad \text{E16}$$

For the log-layer we derive a specific solution for D_T by substituting E15 and E16 into E13:

$$D_T(z) = u_*\, \kappa\, z \qquad \text{E17}$$

Hence in the log-layer, D_T increases linearly with the distance to the sediment. A value for u_* is derived either from the Reynolds stress (E15) leading to:

$$D_T(z) = \sqrt{-\langle u\, w \rangle}\, \kappa\, z \qquad \text{E18}$$

or from the mean velocity $\overline{U}$ (E14) which leads to:

$$D_T(z) = \frac{\overline{U}(z)\, \kappa^2\, z}{\ln(z/z_0)} \qquad \text{E19}$$

Yet another assumption that applies for the log-layer is the balance between the production rate of turbulent kinetic energy from shear stress (P) and the rate of energy dissipation (ε) by viscous shear (Kim et al. 2000; Tennekes and Lumley 1972):

$$-P + \varepsilon = -\langle u\, w \rangle \frac{\partial \overline{U}}{\partial z} + \varepsilon = 0 \qquad \text{E20}$$

Assuming the energy balance we estimate D_T from ε by combining equation E15, E16, E17 and E20:

$$D_T(z) = (\varepsilon\, \kappa\, z)^{1/3}\, \kappa\, z \qquad \text{E21}$$

In the following, the turbulent diffusion coefficients in the log-layer that were derived from Reynolds stress (E18), mean velocity (E19) and energy dissipation (E21) are denoted as D_{T_LR}, D_{T_LU} and D_{T_LD}, respectively. A high frequency single point velocity measurement and the precise knowledge of z are sufficient to determine D_{T_LR} and D_{T_LD}, whereas D_{T_LU} is tied to the flow field only by the average flow velocity $\overline{U}$. However, for D_{T_LU} the hydraulic roughness z_0 needs to be estimated.

The assumed balance between production and dissipation of turbulent energy (see E20) no longer holds true for boundary layers exhibiting density stratification. In this case, the energy balance needs to be reconsidered, because some energy is required for the buoyancy flux (Osborn 1980).

Turbulent diffusivity in stratified flows.

In turbulent and stratified flows the turbulent diffusion coefficient can be estimated from the buoyancy flux and the density gradient according to (Osborn 1980):

$$D_T = \frac{J_b}{N^2} \qquad \text{E22}$$

with the buoyancy flux:

$$J_b = \frac{g}{\rho}\langle w\rho \rangle \qquad \text{E23}$$

and the Brunt-Väisälä frequency N, defined as:

$$N^2 = -\frac{g}{\rho}\frac{\partial \rho}{\partial z} \qquad \text{E24}$$

where g is the gravitational acceleration and $\langle w\rho \rangle$ is the covariance between the vertical velocity and the fluctuating density. E22 can be simplified to:

$$D_T = -\frac{\langle w\rho \rangle}{\partial \rho / \partial z} \qquad \text{E25}$$

Here, $\langle w\rho \rangle$ expresses the instantaneous density flux averaged over a long time period. The flux is assumed proportional to the respective gradient, therewith defining the constant of proportionality as the turbulent diffusion coefficient (i.e. Fick's law of diffusion). In the following, D_T derived from combined flux and gradient measurements (E25) is denoted as D_{T_F}. Similar to D_{T_T} and D_{T_V}, D_{T_F} is not restricted to log-law conditions.

As mentioned before, energy is required for the buoyancy flux in stratified flows. Hence, the energy balance becomes $P = \varepsilon + J_b$. The flux Richardson number R_f is defined as the ratio of buoyancy flux to turbulent production ($R_f = J_b / P$) leading to:

$$J_b = \left(\frac{R_f}{1 - R_f} \right) \varepsilon \qquad \text{E26}$$

which is substituted into E22 to derive:

$$D_T = \frac{\gamma \varepsilon}{N^2} \qquad \text{E27}$$

with the mixing coefficient $\gamma = R_f / (1 - R_f)$. Osborn (1980) found $\gamma \approx 0.2$ which was subsequently applied in various studies. In the following D_T derived from Osborn's relation is denoted as D_{T_O}. D_{T_O} is only applicable in shear flows with stable stratification where buoyancy flux is at the expense of shear production. In contrast, D_{T_F} is also applicable in shear flow with density anomalies (i.e. unstable stratification), because both, the density flux and the density gradient would change sign. Please note that the negative sign in E24 and E25 is due to the upward pointing positive *z*-coordinate which leads to a negative density gradient for a stable stratification. When the stratification is unstable the density gradient is positive and N^2 becomes negative. In this case, N can not be interpreted as frequency anymore but can still be understood as stratification parameter.

In this section, we introduced several approaches to determine D_T from various measurable quantities. Table 1 summarizes all approaches that were used for the following comparison. The *in situ* measurement and the specific data processing are described in the next section.

Table 1: A summary of approaches determining D_T in the BBL, grouped by their field of application.

Approach	Equation		Field of application
Taylor's	$D_{T\_T} = w' L_E$	E10	Free shear flow
Fick's law	$D_{T\_F} = -\frac{\langle w \rho' \rangle}{\partial \rho / \partial z}$	E25	Free shear flow
Turbulent viscosity	$D_{T\_V} = -\frac{\langle u w \rangle}{\partial \overline{U} / \partial z}$	E13	Free shear flow
Osborn's	$D_{T\_O} = \frac{\gamma \varepsilon}{N^2}$	E27	Stably, stratified free shear flow
Log-law Reynolds stress	$D_{T\_LR}(z) = \sqrt{-\langle u w \rangle}\, \kappa z$	E18	Shear flow in log-layer
Log-law mean flow	$D_{T\_LU}(z) = \frac{\overline{U}(z) \kappa^2 z}{\ln(z / z_0)}$	E19	Shear flow in log-layer
Log-law dissipation	$D_{T\_LD}(z) = (\varepsilon \kappa z)^{1/3} \kappa z$	E21	Shear flow in log-layer

Methods

Study site and sampling procedure

The measurements were conducted in Lake Constance, Germany (47°83'99 N, 9°81'89 E) in June 2007 (Fig. 1A). Lake Constance is a large (536 km^2) monomictic lake that experiences a deep convective mixing during winter (December-March) and is thermally stratified during summer (June-October). The oscillatory current regime of Lake Constance is well described by Appt et al. (2004) and Lorke (2007). A mooring was deployed in the north-western sub-basin (Lake Überlingen) at 100 m depth. The bottom slope within this depth is about 0.7°. As described in detail by Lorke et al. (2008), the mooring was equipped with a chain of 13 temperature loggers (TR-1050, RBR Ltd.), evenly distributed between 0.5 and 12.5 m above the bottom. Temperature was recorded every 10 s with a resolution of $5x10^{-5}$ °C. An acoustic Doppler velocimeter (ADV, Vector, Nortek AS) was mounted to the mooring with its sampling volume located 1 m above the bottom (Fig. 1B). A fast response thermistor (PME Inc.) was placed in the direct vicinity of the sampling volume. The ADV was operated in burst mode, sampling temperature and current velocities for 256 s every 15 minutes with a sampling rate of 8 Hz. In addition, the mooring was equipped with an acoustic Doppler current profiler (ADCP, WH-600, RDI) operating in pulse coherent mode (RDI mode 5). The ADCP (Fig. 1B) resolved the near-bottom current velocity profile within 0.89 and 8.79 m above the sediment with a vertical resolution of 0.1 m and a sampling interval of 2.5 s. For further analysis, data from the ADCP and the temperature loggers were averaged over the

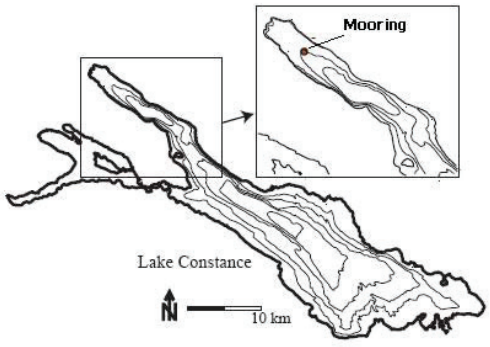

Figure 1A: Map of Lake Constance. The mooring was deployed in the north-western sub basin (Lake Überlingen) at 100 m water depth.

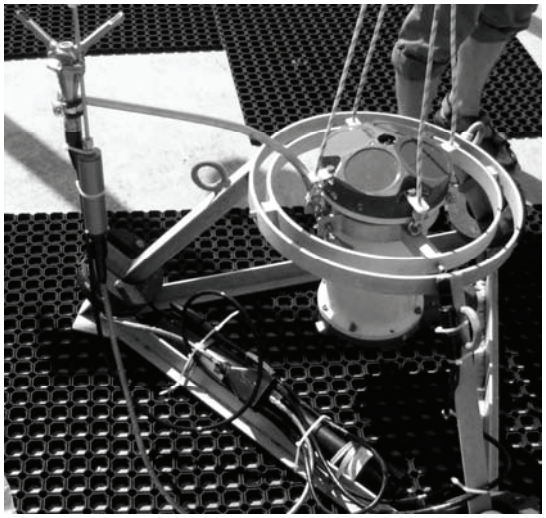

Figure 1B: A small tripod with upward looking ADV and ADCP

burst interval of the ADV. The data set used in this study consisted of 620 bursts covering a time period of 155 hours.

Data processing

For each burst, current velocities measured by the ADV and by the ADCP were rotated horizontally such that the mean flow vector was pointing along the x-axis. Subsequently, mean velocity $\overline{U}$ and standard deviations *u'*, *v'*, *w'* were calculated as well as the covariance $\langle u\,w \rangle$. From the fluctuating vertical velocity (*w)* we derived the Eulerian spatial correlation function and its integral, the Eulerian integral length scale (L_L), according to E7 and E8. The energy dissipation rate (ε) was determined from frequency spectra of the vertical velocity *w* as described by Lorke (2005). Briefly, the velocity frequency spectrum is transferred into a wave number spectrum assuming Taylor's frozen turbulence hypothesis und subsequently fitted to the universal Kolmogorov spectrum: $\Phi = \alpha\, \varepsilon^{2/3}\, k^{-5/3}$ with the wavenumber k and the Kolmogorov constant for the vertical velocity $\alpha = 0.68$. The mean velocity gradient ($\partial\overline{U} / \partial z$) was calculated from velocities measured by the ADCP at 0.89 and 1.09 m above the sediment. In Lake Constance, variations in density are mainly caused by temperature variations. Therefore, the buoyancy flux was calculated from the covariance of temperature and vertical velocity, using the eddy correlation technique (Berg et al. 2003). Beforehand, temperatures were detrended by linear regression over the full burst period. The temperature gradient was calculated from the difference of mean temperature at 0.5 and 1.5 m above the sediment. The mixing coefficient γ (E27) was assumed to be 0.2 (Osborn 1980). The hydraulic roughness z_0 was estimated according to (Imboden and Wüest 1995):

$$z_0 = 0.1\,\nu / u_* \qquad \text{E28}$$

with $u_* = (\varepsilon\,\kappa\,z)^{1/3}$ (see E21) averaged over all bursts and the kinematic viscosity (ν) of 1.52 x 10^{-6} m^2 s^{-1}. From the measured quantities all D_T's presented in Table 1 were calculated for each burst. To compare the different approaches we chose the Fickian approach (D_{T_F}) as reference (the reasons are discussed below). From a total of 620 bursts we had to discard 140 bursts that showed temperature gradients below the accuracy of the thermistors (1 x 10^{-3} °C) and another 125 bursts with negative (i.e. not defined) D_{T_F} . In the following we present the results of 353 bursts.

Results

Current regime and density structure in the BBL

Current velocities at 1 m above the sediment varied from a few millimeters per second up to 7 cm s^{-1} with an average of 2 cm s^{-1} (Fig. 2A). Current flow was predominantly in upslope (260-350°) and downslope (90-180°) direction (Fig. 2B, compare with Fig. 1A). The associated up- and downwelling caused significant changes of the mean temperature (Fig. 2C) and stratification (Fig. 2D). Temperatures decreased during upwelling and increased during downwelling over a range of 0.4 °C. The temperature gradients at 1 m above the sediment varied from -10^{-2} to 10^{-1} °C m^{-1} (Fig. 2D). Negative temperature gradients imply that the

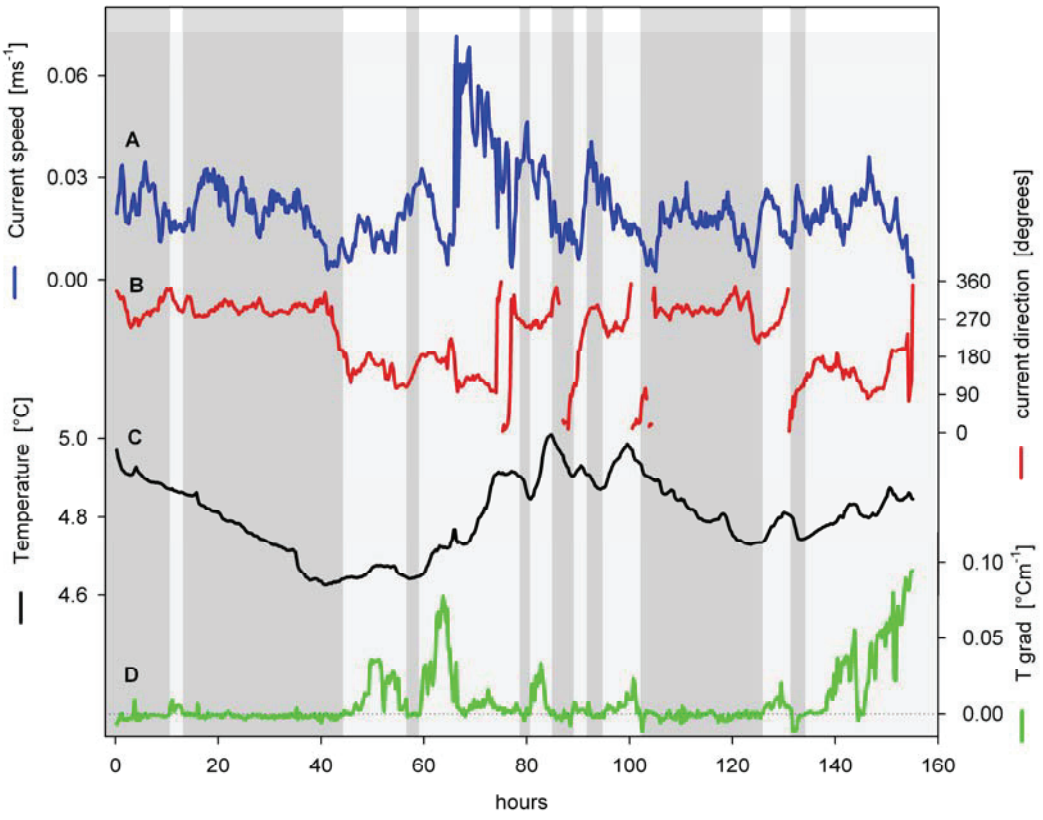

Figure 2: (A+B) Current speed and direction measured 1 m above the sediment. Current directions were derived from north and east components of the current velocities measured by the ADCP. Upslope and downslope directions were north-west (260-350°) and south-east (9-180°), respectively. (C+D) Temperature at 0.5 m above the sediment and temperature gradient between 0.5 and 1.5 m above the sediment. The dotted line denotes zero temperature gradient. Time periods with gravitational unstable stratification (negative temperature gradients) are marked by grey bars.

water column was gravitational unstable (grey bars in Fig. 2), whereas positive temperature gradients denote stabile stratification. Positive and negative temperature gradients were associated with downwelling and upwelling, respectively. Increased positive temperature gradients were found at low current velocities (see Lorke et al. 2008 for details).

Turbulent diffusivity in the BBL

The turbulent diffusion coefficients derived from heat flux and temperature gradient (Fick's first law, D_{T_F}) varied from 1 x 10^{-6} to 5 x 10^{-4} m^2 s^{-1} (Fig. 3A) after smoothing with a 1 hour running average (4 bursts). At time periods of unstable stratification and high current velocities (grey bars in Fig. 3) D_{T_F} maximized (>10^{-4} m^2 s^{-1}), whereas low current velocities and stable stratification led to reduced D_{T_F} (10^{-4} to 10^{-6} m^2 s^{-1}). Turbulent diffusivity derived from Taylor's hypothesis (D_{T_T} in Fig. 3A) agreed well with D_{T_F} and followed the trend of low diffusivities at stable stratification and high diffusivities at unstable stratification. The overall arithmetic mean of D_{T_F} (1.5 x10^{-4} m^2 s^{-1}) and D_{T_T} (1.6 x 10^{-4} m^2 s^{-1}) were in good agreement.

A hydraulic roughness (z_0) of 4 x 10^{-4} m was derived from E28 and used to calculate D_{T_LU}. All diffusivities derived from the logarithmic law of the wall (D_{T_LD}, D_{T_LU} and D_{T_LR} in Fig. 3B) were persistently at the upper boundary of D_{T_F} and did not reproduce the decrease of D_{T_F} during time periods of stable stratification and low current velocities (light grey bars in Fig. 3). Consequently, the temporal variability of D_{T_LD}, D_{T_LU} and D_{T_LR} was decreased (10^{-3} to 10^{-4} m^2 s^{-1}) and the arithmetic mean was increased (3.9 x 10^{-4} to 4.8 x 10^{-4} m^2 s^{-1}) when compared to D_{T_F} and D_{T_T}. According to E18, D_{T_LR} was defined only for negative $\langle u\,w \rangle$. Bursts with positive $\langle u\,w \rangle$ were discarded reducing the fraction of usable bursts to 65 %. D_{T_LR} was similar to D_{T_LD} and D_{T_LU} except for increased D_{T_LR} at hour 42.

Diffusivity that was derived from turbulent viscosity (D_{T_V}) is defined for a negative ratio of $\langle u\,w \rangle$ to $\partial \overline{U} / \partial z$ only (see E13). D_{T_V} was defined for 64 % of all bursts showing a high variability from 4 x 10^{-7} to 4 x 10^{-2} m^2 s^{-1} with considerable deviations from D_{T_F} (Fig. 3C). Maximized D_{T_V} was found at low current velocities e.g. at hour 42, 125 and 153. Diffusivity that was derived from Osborn's equation (D_{T_O}) is defined for a positive temperature gradient only (E27 et seq.). D_{T_O} was calculated for 50 % of all bursts and varied from 1 x 10^{-6} to 3 x 10^{-2} m^2 s^{-1} (Fig. 3C). D_{T_O} strongly deviated from D_{T_F} at decreased temperature gradients (hours 70-80, 100 and 130), whereas D_{T_O} agreed well with D_{T_F} when a stable stratification of the BBL was measured (hours 50, 63 and 140-150).

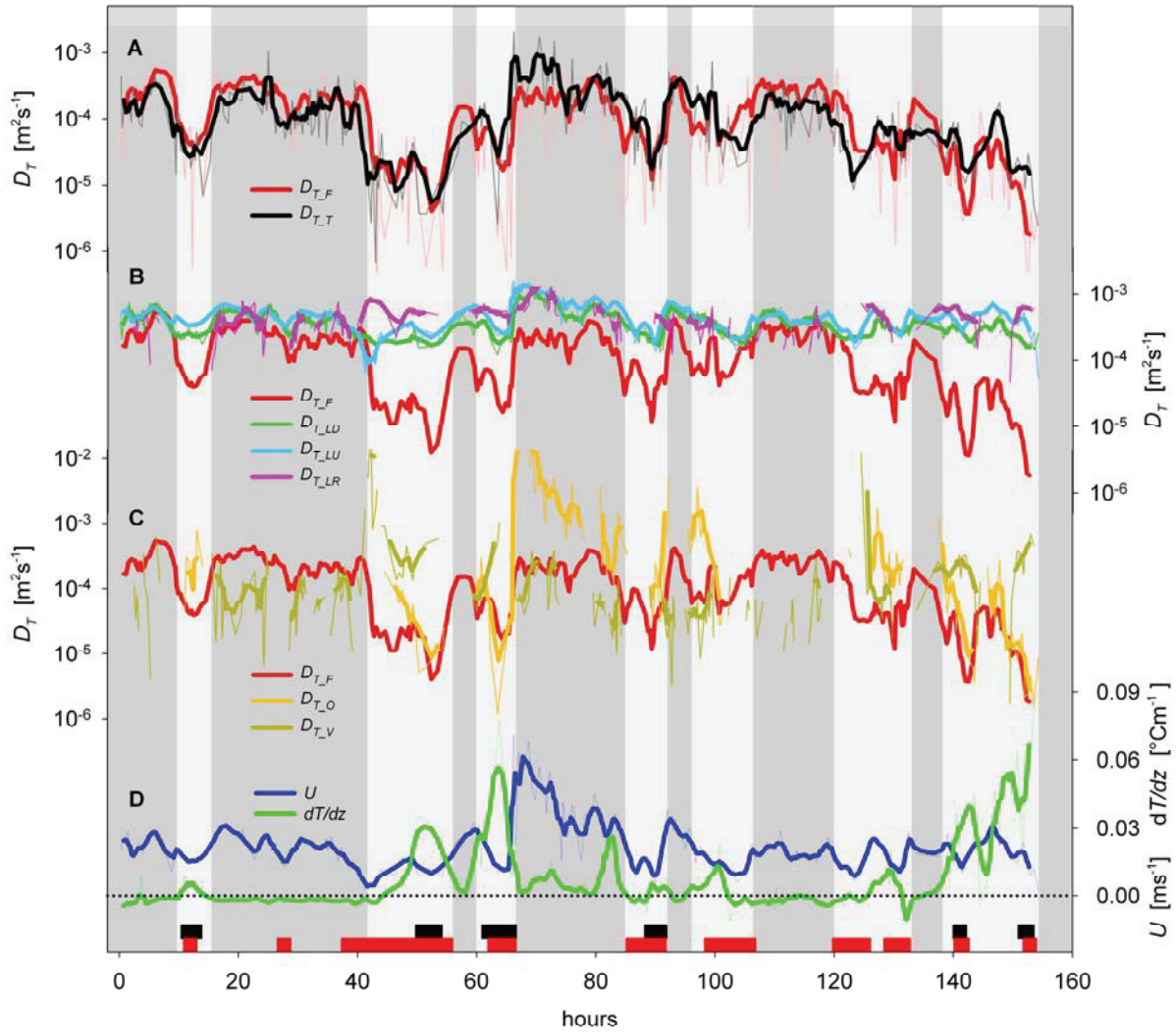

Figure 3: Comparing turbulent diffusion coefficients derived from Fick's law (D_{T_F}) with estimates derived from (A): Taylor's hypothesis (D_{T_T}), from (B): the log-law and energy dissipation (D_{T_LD}), mean current velocities (D_{T_LU}), and Reynolds stress (D_{T_LR}), from (C): Osborn's equation (D_{T_O}) and turbulent viscosity (D_{T_V}). The lower panel (D) presents mean current velocity (U) and the temperature gradient (dT/dz) at 0.5 to 1.5 m above the sediment. dT/dz above and below the dotted line (zero gradient) indicate stable and unstable stratification, respectively. Thin lines represent raw data and thick lines show a running average of four Bursts. The light grey areas mark episodes where D_{T_LD}, D_{T_LU} and D_{T_LR} strongly deviate from D_{T_F} and D_{T_T}. The red and black bars on the time axis denote periods with a Reynolds number below 10,000 and a gradient Richardson number (R_i) above 0.25, respectively (see discussion).

Factors determining turbulent diffusion:

The contributions of L_E and w' to D_{T_T} as well as the contributions of J_b and N^2 to D_{T_F} are shown in Figure 4. The fluctuation of the vertical velocity, expressed by w' varied little between 1 x 10^{-3} and 4 x 10^{-3} m s^{-1}, whereas the integrated length scale L_E varied by a factor of 30 from 1 to 30 cm. Consequently, the variability of D_{T_T} was mainly determined by L_E. The Brunt-Väisälä frequency ($|N^2|$) and the buoyancy flux ($|J_b|$) in Figure 4 were expressed in absolute values. $|N^2|$ varied over two orders of magnitude from 10^{-7} to 10^{-5} s^{-2}. The buoyancy flux varied from 5 x 10^{-12} to 10^{-9} W kg^{-1}. The oscillation of $|N^2|$ and $|J_b|$ were predominantly in phase causing little variations of D_{T_F}. The out of phase events at hour 10, 52, 90 and 142 resulted in rapid decrease of D_{T_F}. The energy dissipation rate (ε) ranged from 1 x 10^{-10} to 4 x 10^{-8} W kg^{-1} and was well correlated with the current velocity and the vertical velocity gradient. Time periods of increased ε, $\overline{U}$ and $\partial\overline{U}/\partial z$ correspond with time periods of increased L_E, D_{T_T} and D_{T_F}.

Figure 5 shows three bursts (marked by the arrows in Figure 4) that were analyzed in detail. Burst 97 and 167 were characterized by low but negative temperature gradient of -2 x 10^{-3} and -3 x 10^{-3} °C m^{-1}, respectively (Fig. 5A). The current velocity was increased during burst 97 (2.6 cm s^{-1}) and decreased during burst 167 (0.5 cm s^{-1}). Burst 249 was characterized by moderate velocities (1.7 cm s^{-1}) and a strong positive temperature gradient of 4 x 10^{-2} °C m^{-1}.

Comparing burst 97 and 167 we observed a decrease of standard deviations of both, vertical velocity and temperature fluctuations from 1.9 x 10^{-3} to 1.3 x 10^{-3} m s^{-1} and from 2.5 x 10^{-5} to 1.8 x 10^{-5} °C (Fig. 5B+C), which corresponded to a decrease in current velocity. The temperature gradients during burst 97 and 167 were negative, which implies that the density gradients were positive and the resulting density fluxes again negative. Comparing burst 97 and 167, the absolute density flux decreased by a factor of 7 from 2.1 x 10^{-10} to 3.0 x 10^{-11} W kg^{-1} and the resulting D_{T_F} decreased by a factor of ~10 from 4 x 10^{-4} to 4 x 10^{-5} m^2 s^{-1}. Although the density flux was very low during burst 167, it was consistent throughout the burst period as shown by the steady decrease of the integrated density flux (Fig. 5D small plot). The length scale L_E is presented in Figure 5E in form of the integral of E_E plotted over the spatial distance r (see E8). With increasing r, the integral of E_E approached the value L_E. The decrease of L_E from 14 cm (burst 97) to 1 cm (burst 167) resulted in a significant decrease of D_{T_T}.

During burst 249, the strong positive temperature gradient stabilized the BBL causing strong temperature fluctuations (standard deviation: 2 x 10^{-4} °C, Fig. 5C) and a pronounced positive density flux (6.5 x 10^{-10} W kg^{-1}, Fig. 5D). D_{T_F} during burst 249 was decreased by a factor of 5 compared to burst 97, when the BBL was not stably stratified. Furthermore, L_E decreased significantly to 5 cm during burst 249 which resulted in D_{T_T} that was comparable to of D_{T_F} (6 x 10^{-5} and 8 x 10^{-5} m^2 s^{-1}, respectively).

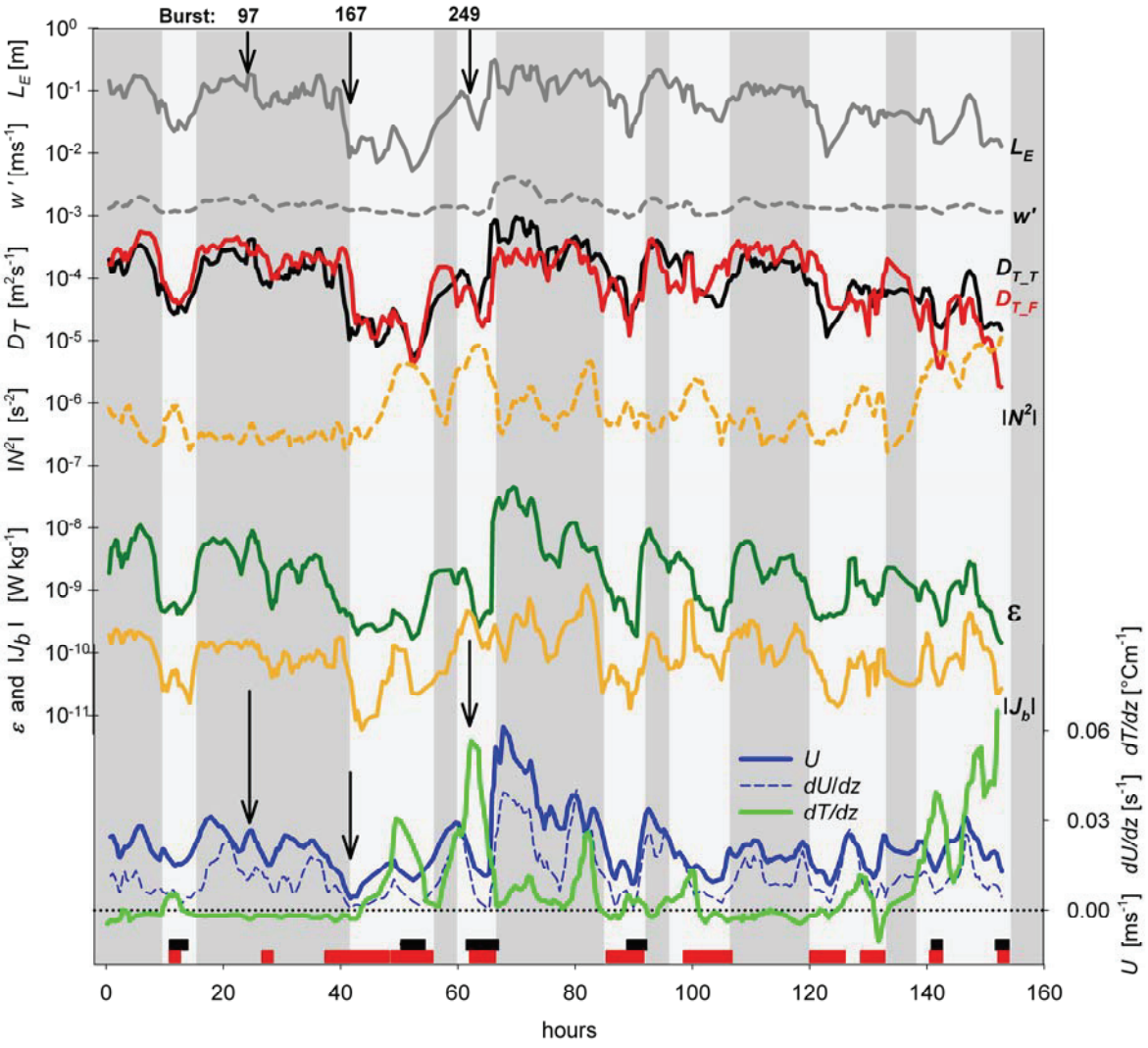

Figure 4: Black and grey lines: time series of the Eulerian Lengthscale (L_E) and the standard deviation of the vertical velocity (w') contributing to D_{T_T}. In red and orange: time series of the buoyancy flux (|J_b|) and the Brunt-Väisälä frequency (|N^2|) contributing to D_{T_F}. For comparison, the mean current velocity (U), the velocity gradient (dU/dz) and the temperature gradient (dT/dz) are shown. The light grey areas mark episodes where the log-law based estimates of D_T strongly deviate from D_{T_F} and D_{T_T}. The red and black bars on the time axis denote periods with a Reynolds number below 10,000 and a gradient Richardson number (R_i) above 0.25, respectively (see discussion). Details of three individual bursts (arrows) are presented in Figure 5.

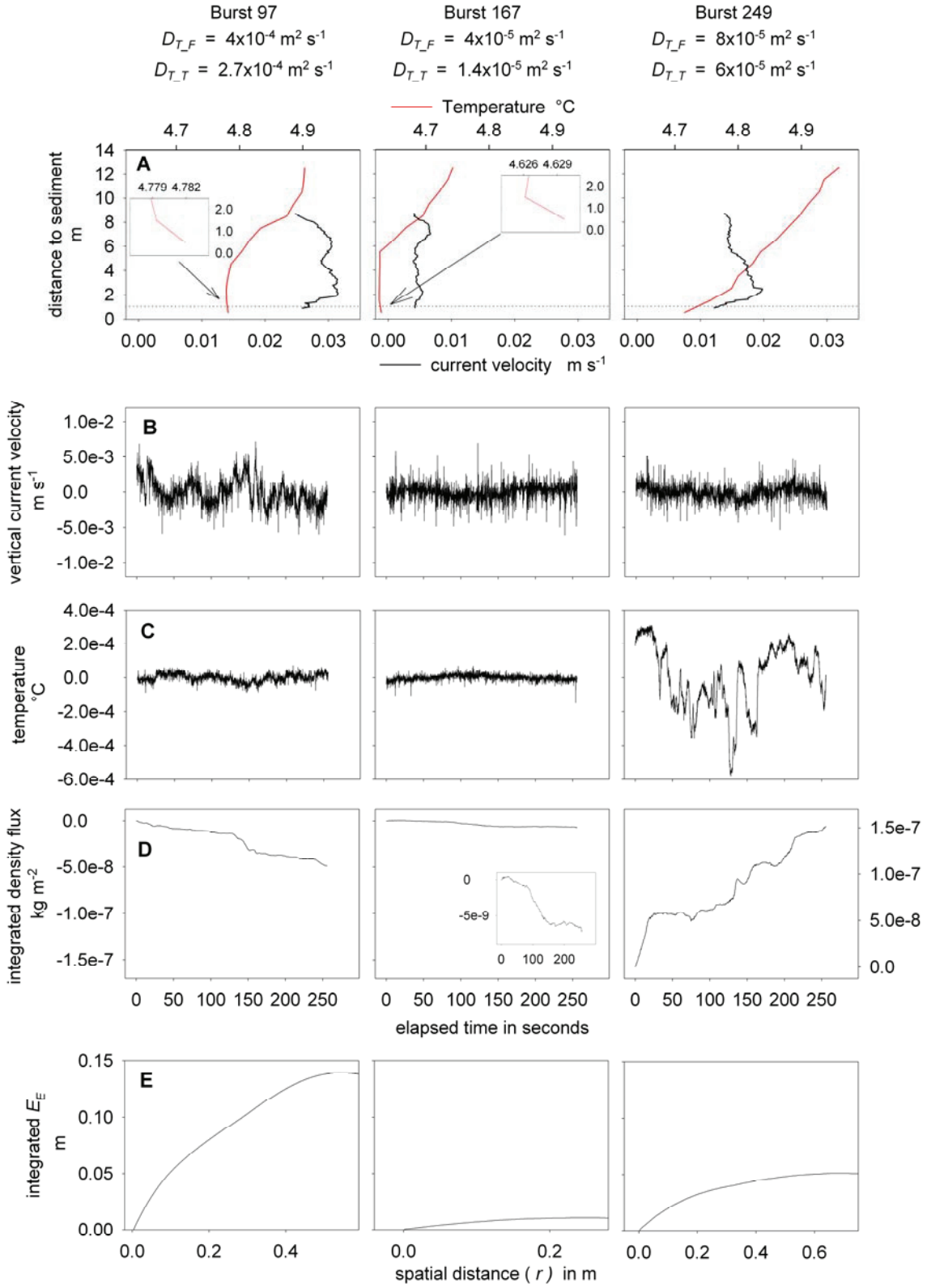

Figure 5: From 3 bursts with distinct vertical gradients of temperature and current velocity (A), the velocity (B) and temperature (C) fluctuations as well as the integrated density flux, J_b, (D) and L_E (E) in the form of the integrated spatial correlation coefficient, E_E, are presented. The dotted line in (A) marks the height of the ADV sampling volume. The position of the bursts in the time series are marked by arrows in Figure 4.

Discussion

The dynamics of upwelling and downwelling bottom currents in Lake Constance and the resulting oscillation of unstable and stable stratification were discussed in detail by Lorke et al. (2008). The oscillatory motion of the bottom water (Fig. 2) is mainly caused by a Kelvin wave of a period of approximately 4 days. This basin-scale vertical mode-one Kelvin wave is a well known feature during the stratified season in Lake Constance (Appt et al. 2004). Furthermore, the oscillation of flow magnitude and energy dissipation with a period of approximately 12 hours (Fig. 4) corresponded with a first-mode Poincare-type wave suggested by Appt et al. (2004). The oscillatory motions questioned the assumption of a stationary boundary layer – a precondition for all diffusivity calculations. It has been shown for oscillating flows that the readjustment of the mean velocity profile can cause distinct local velocity maxima that disagree with the log-law (Foster et al. 2000; Soulsby and Dyer 1981). Lorke et al. (2002) described the dynamics of turbulence in a boundary layer oscillating with a period of 24 hours. They found that friction velocities (u_*) derived from the log-law (E14) were significantly elevated compared to those derived from measured dissipation rates or a $k-\varepsilon$ turbulence model, suggesting that the boundary flow was not readjusted to the logarithmic profile. In this study, we frequently observed a velocity maximum at 2-3 m above the sediment (see Fig. 5A) indicating that the boundary flow did not readjust to a logarithmic profile. While the readjustment of the mean velocity profile violates the stationarity assumption of the log-law, the local flow field can be seen as quasi stationary for a measurement interval of 254 seconds during which the change of mean current velocity and shear stress is small compared to their absolute values (see Fig. 5B).

It is useful to divide the diffusivity models in our study into two categories (Table 1). Models that describe diffusivity independently from boundary dimensions include the equations for D_{T_F}, D_{T_T}, D_{T_O} and D_{T_V}. These so called free-shear-flow models are basically applicable in all shear flows that produce stationary and homogeneous turbulence. Well established is the Osborn model (D_{T_O}) for open ocean settings (Fennel 1995; Gregg et al. 1986; Lam et al. 2007) as well as in lakes (Lorke 2007), which involves the measurement of density gradients and kinetic energy dissipation. The second category of diffusivity models is only applicable for boundary flow, because these models depend on boundary dimensions. The model equations for D_{T_LU}, D_{T_LD} and D_{T_LR} were all derived from the logarithmic law of the wall and can be summarized as log-law models. They offer different solutions for obtaining the shear velocity (u_*) according to E17, but they all scale with distance (z) to the

sediment. The log-law is well established for high Reynold number flows from numerous laboratory flume experiments and direct numerical simulations (Pope 2000).

Log-law models of turbulent diffusion

In our study, the different log-law models yielded similar diffusivities (Fig. 3) of which D_{T_LU} and D_{T_LD} showed the best agreement. The agreement between D_{T_LU} and D_{T_LD} can be explained by the high correlation of current velocity ($\overline{U}$) and dissipation rate (ε) (Fig. 4) which were used to determine D_{T_LU} and D_{T_LD}, respectively (E19+E21). Estimates from log-law models agreed well with D_{T_F} at periods of no or unstable stratification. However, the log-law models could not account for a stable stratification. At transitions from unstable to stable stratification D_{T_LU}, D_{T_LD} and D_{T_LR} stayed constant (Fig. 3), although a stable stratification should considerably decrease the diffusivity. In contrast, D_{T_F} was strongly affected by a stable stratification and decreased more than one order of magnitude. As a result, low D_{T_F}, correlated well with high temperature gradients (Fig. 3). For this reason, and because Fick's law provides the most direct approach to determine diffusivity we assumed that the estimates of D_{T_F} were correct and can be used as reference for the other approaches.

Independent from a stable stratification, low current velocities strongly affected the diffusivity. D_{T_F} decreased rapidly when current velocities fell below ~1.5 cm s^{-1} (see D_{T_F} at hour 42, 85 and 125 in Figure 3). For the critical velocity of 1.5 cm s^{-1} a corresponding critical Reynolds number (Re_c) of ~10,000 was calculated according to $Re = z\overline{U}/\nu$, where z is the characteristic length scale that corresponds to the measurement height above the sediment (i.e. 1 m). For flows with Re_c < 10,000 (red bars in Figure 3+4), results from the log-law models strongly deviated from D_{T_F} and failed to give plausible diffusivities. As can be seen from E19, the log-law models predict diffusivities that decrease linearly with $\overline{U}$ (see E19). However, the decrease of D_{T_F} at current velocities below 1.5 cm s^{-1} was strongly non-linear with respect to $\overline{U}$ (e.g. hour 42). In summary, the oscillatory mean flow, the occasionally low current velocities as well as the stable stratification caused the failure of the log-law models to predict plausible diffusivities.

Common free-shear-flow models of turbulent diffusion

Of the diffusivities from the free-shear-flow models, both, D_{T_O} and D_{T_V} deviated up to two orders of magnitude from D_{T_F} (Fig. 3). D_{T_V} was significantly higher than D_{T_F} at flow velocities with Reynolds numbers below Re_c. At 42, 125 and 153 hours, high D_{T_V} coincided with the change of current direction between upwelling and downwelling (Fig. 2). As a result,

velocity gradients were close to zero and, therefore, below the resolution of the ADCP. At periods of unstable stratification D_{T_V} was well below D_{T_F}, whereas at periods of moderate stable stratification and increased current velocity D_{T_V} agreed with D_{T_F}. In summary, D_{T_V} was not suitable to determine diffusivities under the present flow conditions, which in part was due to the problematic measurements of current velocity gradients. From the D_{T_O} model, reasonable estimates were calculated only for a stably stratified BBL. A useful criterion for the applicability of D_{T_O} was the dimensionless gradient Richardson number $Ri = N^2/(\partial\overline{U}/dz)^2$, which describes the dynamic stability of a stratified shear flow. From theoretical considerations Miles (1961) deduced a critical value of Ri = 0.25, above which a stratified shear flow is sufficiently stable. We found that D_{T_O} was comparable to D_{T_F} whenever Ri was above 0.25 (black bars in Fig. 3). However, the requirement of a stable stratification for the D_{T_O} model certainly limits its applicability in boundary flows.

Taylor's model of turbulent diffusion

Of all applied models, diffusivities derived from Taylor's model (D_{T_T}) agreed best with diffusivities from Fick's law of diffusion (D_{T_F}). At flow regimes above as well as below Re_c, D_{T_T} was comparable with D_{T_F} (Fig. 3). D_{T_T} was calculated as the product of the length scale L_E and the velocity w'. L_E may be interpreted as the characteristic eddy size that contains most of the turbulent kinetic energy. L_E varied from 1 to 30 cm and correlated with the current velocity (Fig. 4). At high current velocities, larger eddies were formed that contained more kinetic energy. As eddies fell apart, their energy cascaded down to smaller eddies until viscosity affected the flow and the energy dissipated into viscous shear. Large L_E therefore corresponded with increased dissipation rates (Fig. 4).

The characteristic size (L_E) of an eddy is associated with its characteristic velocity (w'). We defined the Reynolds number for energy containing eddies as $Re_T = w'L_E/\nu$, which is eventually the ratio of turbulent diffusivity to viscosity $Re_T = D_T/\nu$. At stable stratification and decreased current velocity (e.g. hour 50, Fig. 4) Re_T was around 10, a range where viscosity affects the flow. At such decreased flow it is questionable if diffusivities on the basis of density flux measurements (D_{T_F}) were reliable. However, a consistent density flux throughout the burst period was observed for density fluxes as low as 10^{-11} W kg^{-1} (see also Burst 167 in Fig. 5D). Comparing D_{T_T} for high and low current velocities at negligible stratification (Burst 97 and burst 167 in Fig. 5), we observed a significant increase of L_E and a moderate increase of *w'* with increasing current velocities. However, when the BBL was stably stratified (Burst 249 in Fig. 5) L_E and *w'* were reduced.

The variability of diffusivities

In this study, the diffusivities derived from Taylor's model and from Fick's law varied over approximately three orders of magnitude from 1 x 10^{-3} to less than 1 x 10^{-6} m^2 s^{-1} with logarithmic means of 6.7 x 10^{-5} and 8 x 10^{-5} m^2 s^{-1} for D_{T_F} and D_{T_T}, respectively (Fig. 6). In contrast, diffusivities derived from the log-law varied over not more than one order of magnitude with logarithmic means of 4.3 x 10^{-4} and 3.4 x 10^{-4} m^2 s^{-1} for D_{T_LD} and D_{T_LU}, respectively. This is because the log-law diffusivities depend linearly on the mean current velocity, which also varied over approximately one order of magnitude (0.5-6 cm s^{-1}). D_{T_F} and D_{T_T} compared well with the highly variable diffusivities reported previously by Lorke (2007) for a shallow and stably stratified station in Lake Constance using Osborn's approach (D_{T_O}). However, most hydrodynamic studies in the BBL focus on estimating bottom stress (Dewey and Crawford 1988; Howarth and Souza 2005; Kim et al. 2000; Trowbridge et al. 1999) from which diffusivities may be derived using the log-law. Diffusivity measurements in the BBL that are not based on the log-law (i.e. free-shear-flow models) are scarce, in lakes as

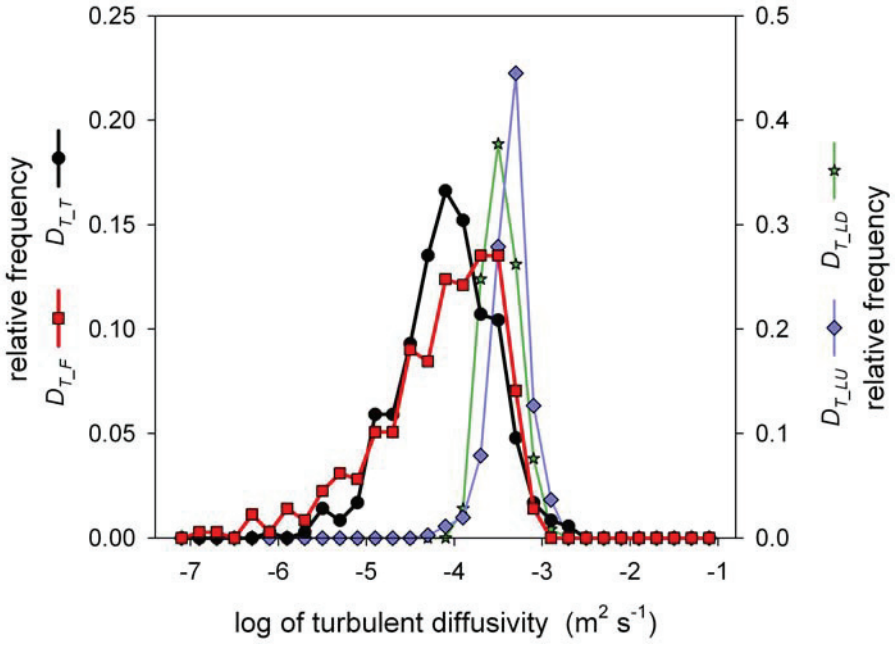

Figure 6: Normalized frequency distribution of log10 turbulent diffusivities derived from different approaches.

well as in the ocean. Since the log-law does not apply for low current velocities and stratified shear flow, the low diffusivities that occur under these conditions are poorly described. It is therefore of interest, to investigate the potential effects that low diffusivities in the BBL may

have on the solute transport across the sediment water interface. For this reason, we discuss in the following section the effects of low diffusivities on the benthic oxygen flux by means of a simple flux model.

A simple flux model

In the sediment, the oxygen concentration (C) at depth (z) can be described by the following equation (Bouldin 1968):

$$D_S \cdot \frac{\partial^2 C}{\partial z^2} = -R \qquad \text{E 29}$$

where R is a constant, zero order oxygen consumption rate and D_S is a constant sedimentary diffusion coefficient. E 29 is solved for the following boundary conditions: (i) the oxygen concentration at the sediment surface is $C(z = 0) = C_0$ and (ii) the oxygen concentration and the concentration gradient are zero at an unknown oxygen penetration depth ($-L$) (i.e. $C(z = -L) = 0$ and $\partial C / \partial z\ (z = -L) = 0$). Subsequently, the oxygen flux at the sediment surface (J_S) is expressed according to Jørgensen and Boudreau (2001):

$$J_S = -\sqrt{-2 D_S C_0 R} \qquad \text{E30}$$

In the overlying BBL, oxygen consumption rates are usually low compared to sedimentary oxygen uptake (see Chapter 2 of the thesis). To simplify matters, we assume negligible rates in the BBL ($R = 0$) so that the flux in the BBL is equal to the flux at the sediment surface. At depth z_1 above the sediment we define the concentration C_1. For a concentration C_0 at the sediment surface z_0, the flux (J_S) is expressed as:

$$J_S = -D_{BE} \frac{C_1 - C_0}{z_1 - z_0} \qquad \text{E31}$$

where D_{BE} is the effective diffusion coefficient along the depth interval z_1 - z_0. The meaning of D_{BE} is discussed below. By substituting E31 into E30 we derive the expression

$$\sqrt{-2 D_S C_0 R} = D_{BE} \frac{C_1 - C_0}{z_1 - z_0} \qquad \text{E32}$$

which can be solved for C_0. A schematic diagram of the model is presented in Figure 7. With reasonable values for the constants R, D_S and C_1, we can describe C_0 (and furthermore J_S from E30) as a function of D_{BE}.

It should be mentioned that E30 applies only, when oxic respiration is the sole sedimentary oxygen sink. In this case, J_S is a function of both R and the oxygen penetration depth L (a constant R implies that $J_S = R \cdot L$). A decreased C_0 would shift L towards the

sediment surface thereby reducing J_S (Fig. 7). However, in many shallow sediments a considerable fraction of oxygen is consumed by the re-oxidation of reduced metabolites such as sulfide, reduced iron and ammonium (Jørgensen 1977; 1982). We assume that the re-oxidation of the metabolites occurs at the re-oxidation depth *L'* (Fig. 7), at rates *R* that depend only on the upward flux of reduced metabolites. A decreased C_0 would shift *L* towards the sediment surface but would not decrease the oxygen flux J_S. In case of re-oxidation as the sole oxygen sink we assume that J_S stays constant and E31 is sufficient to describe C_0 as a function of D_{BE}.

D_{BE} itself is derived as follows: The differential quotient $C_1 - C_0 / z_1 - z_0$ from E31 relates to the integrated concentration gradients between z_0 and z_1 according to:

$$\frac{C_1 - C_0}{z_1 - z_0} = \frac{1}{z_1 - z_0} \int_{z_0}^{z_1} \frac{\partial C}{\partial z} dz \qquad \text{E33}$$

Substituting E31 and Fick's law ($\partial C / \partial z = J_S / D_B$), the effective diffusivity (D_{BE}) is thus defined as:

$$\frac{1}{D_{BE}} = \frac{1}{z_1 - z_0} \int_{z_0}^{z_1} \frac{1}{D_B(z)} dz \qquad \text{E34}$$

where D_B is the depth dependent diffusivity. With z_0 (z = 0) located at the sediment surface, D_{BE} includes the molecular diffusivity in the diffusive boundary layer (DBL). Although the DBL thickness ($\delta \approx 0.5$ mm) is small compared to z_1-z_0, the low molecular diffusivity ($D_0 \approx 10^{-9}$ m^2 s^{-1}) increases the concentration gradients in the DBL by several orders of magnitude (Jørgensen and Revsbech 1985). D_0, which is readily available from literature, is constant across δ, but in the turbulent layer above, D_B remains an unknown function of z, especially at flow condition where the log-law does not apply. A rough estimate for D_{BE} is therefore derived from a two layer model assuming a molecular diffusivity D_0 in the DBL and a turbulent diffusivity D_T in the BBL above. For a two layer model (Fig. 7) E34 simplifies to:

$$\frac{1}{D_{BE}} = \frac{1}{z_1} \left(\frac{\delta}{D_0} + \frac{z_1 - \delta}{D_T} \right) \qquad \text{E35}$$

Having defined D_{BE}, we calculated C_0 for variable D_T assuming either oxic respiration (E32) or re-oxidation (E31) as sole oxygen sink. We applied a porosity of $\phi = 0.85$ and a molecular diffusivity for oxygen of D_0 = 1.46 x 10^{-9} m^2 s^{-1} (assuming 10 °C) from which a sedimentary diffusivity D_S = 1.1 x 10^{-9} m^2 s^{-1} was calculated according to $D_S = D_0 / (1 - \ln(\phi^2))$ (Boudreau 1997). The oxygen concentration at z_1 = 1 m was set to C_1 = 270 µmol l^{-1} and the thickness of the DBL was assumed to be either $\delta = 0.5$ or 1 mm. We applied three different oxygen

respiration rates of $R = 0.5$, 5 and 50 µmol cm^{-3} d^{-1}. All parameters are reasonable estimates for Lakes and coastal waters as found in Lorke et al. (2003), Maerki et al. (2009), Wenzhöfer and Glud (2004) and Glud (2007).

The Figure 8A-C shows the relative decrease of C_0 and J_S as a function of D_{BE} for three different respiration rates (R). The constant flux for the case of sole re-oxidation, was set

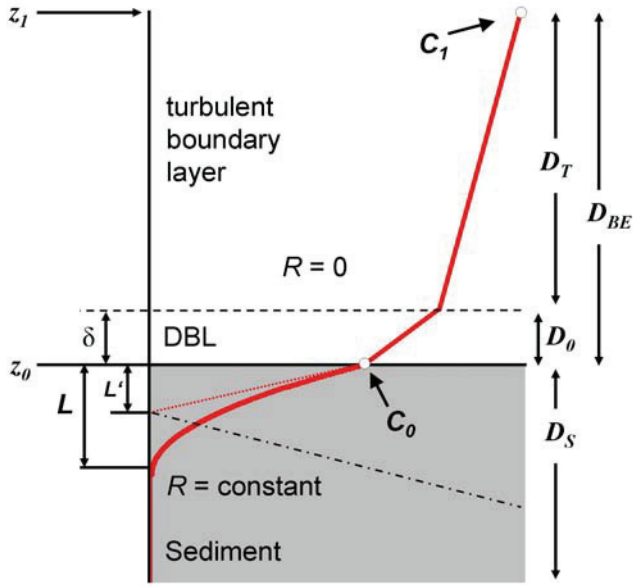

Figure 7: A schematic diagram of the flux model. Oxygen concentrations (red lines) are modeled for constant C_1, R, D_S and variable D_{BE}. D_{BE} itself is a function of constant δ, D_0 and variable D_T. The sole oxygen sink in the sediment is either oxic respiration (solid red line) with a constant rate (R) down to the oxygen penetration depth L, or re-oxidation (dotted red line) of reduced metabolites (black dash-dotted line) at the re-oxidation depth L' with a constant flux. Please note that the drawing is not to scale.

equal to the maximum flux J_{Smax} at $D_{BE} \rightarrow \infty$ in the case of oxic respiration (i.e. J_S from E30 with C_0=C_1). When the effective diffusion coefficient (D_{BE}) is above 10^{-4} m^2 s^{-1}, the effect on the oxygen concentration (C_0) and the oxygen flux (J_S) at the sediment surface is negligible. However, when D_{BE} falls below 10^{-5} m^2 s^{-1}, C_0 and J_S start to decrease, whereby sediments with increased R and J_{Smax} are affected first (Fig. 8C). The decrease of C_0 in the case of re-oxidation is steeper than in the case of oxic respiration because J_S is reduced in the latter case attenuating the decrease of C_0. Since both, re-oxidation and oxic respiration occur simultaneously in natural sediments, a realistic estimate for C_0 should range between the two estimates for C_0.

Figure 8D shows the effective diffusion coefficient (D_{BE}) as a function of the turbulent diffusion coefficient (D_T) for two different DBL thicknesses (δ) according to equation 35. At D_T above 10^{-5} m^2 s^{-1}, the DBL fully controls the effective diffusivity (D_{BE}) and thereby sets the upper limit of D_{BE} to 3 x 10^{-6} m^2 s^{-1} (and 1.5 x 10^{-6} m^2 s^{-1} for δ = 1 mm). The decrease of C_0 and J_S is minor, which agrees well with the results of Glud et al. (2007) who modeled a decrease of J_S by 2-10 % caused by the mere presence of the DBL. When the turbulent diffusivity (D_T) falls below 10^{-5} m^2 s^{-1} it starts influencing the effective diffusivity. For measured D_T's as low as 1 x 10^{-6} m^2 s^{-1} (see Fig. 6), D_{BE} decreases down to 7.4 x 10^{-7} m^2 s^{-1} (and 6.0 x 10^{-7} m^2 s^{-1} for δ = 1 mm). In sediments with low R and J_{Smax} (Fig. 8A), this drop of D_{BE} causes only a minor decrease of C_0 and J_S. However, sediments with moderate to high R and J_{Smax} (Fig. 8B+C) were strongly affected showing a severe reduction of oxygen fluxes and oxygen concentrations at the sediment surface by 45 - 78 % (J_S) and by 70 - 100 % (C_0). The reduction of C_0 by 100 % implies that reduced metabolites diffuse out of the sediment, pushing the re-oxidation front into the water column.

The model clearly indicates that highly variable diffusivities in the BBL have the ability to control the solute exchange between sediment and water column. It should be mentioned that all assumptions made to simplify the model led to a more conservative estimate. The two layer model assumes constant turbulent diffusivity from z_1 down to the DBL. We would rather expect a decrease of D_T close to the sediment that would decrease the effective diffusivity and lower C_0. Furthermore, we neglected the respiration rates in the BBL that would, again, reduce C_0.

Conclusions

From Taylor's theory (1921) we derived a new approach that allows determining the turbulent diffusivity in the BBL from high resolution velocity measurements. The diffusivities derived from the new approach (D_{T_T}) agreed well with those derived from gradient-flux measurements (D_{T_F}) whereas the common log-law models failed at decreased current velocities and stratified flow conditions. Our approach combines the broad applicability in free shear flows with a simple set up. A simple velocity measurement suffices to calculate D_{T_T} whereas the measurement of D_{T_F}, D_{T_V} and D_{T_O} need at least additional gradient measurements.

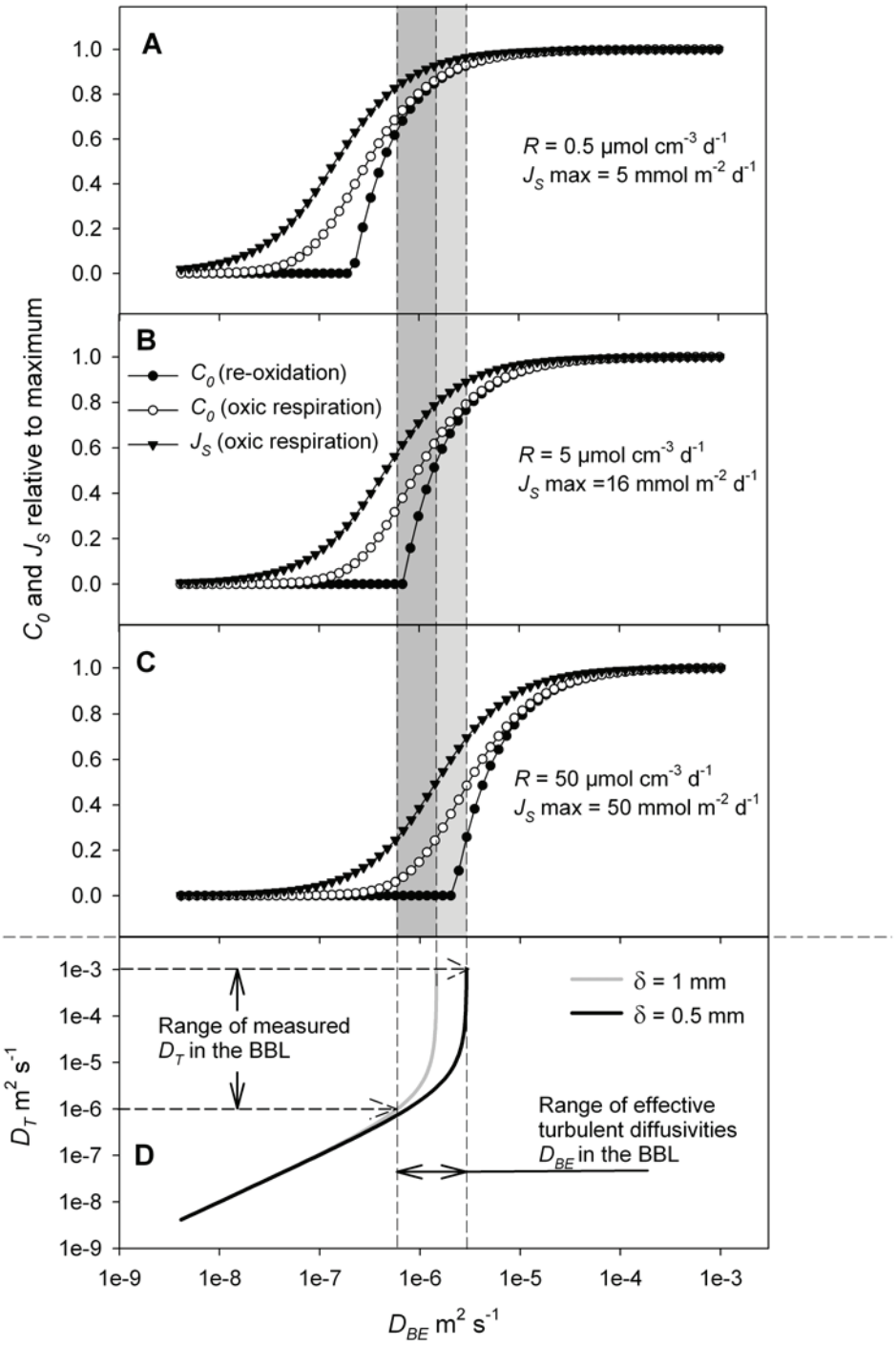

Figure 8: Oxygen flux (J_S) and oxygen concentrations (C_0) at the sediment surface as a function of the effective diffusivity (D_{BE}) for three different settings of low (A), moderate (B) and high (C) oxygen respiration rates (R), calculated according to E32 and normalized by the respective maximum value. C_0 for the case of re-oxidation as oxygen sink, was calculated according E31 for a constant flux of J_{Smax}. (D): D_{BE} as a function of D_T was calculated for two different δ of 0.5 and 1 mm according to E35 and translates the range measured D_T into a range of D_{BE}.

When combined with solute gradient measurements (see Chapter 2), the new approach allows to determine the solute flux across the BBL according to Fick's law. This non-invasive flux measurement provides an alternative to the eddy correlation approach which allows flux measurements only for a very limited number of solutes that are measurable with high temporal and spatial resolution (e.g. oxygen via microsensors). However, solute gradients in the BBL decrease at high current velocities to eventually undetectable values, which limits the application to low and moderate flows.

We showed that the new approach was capable to measure diffusivities at low current velocities as well as in stably stratified boundary layers. Under these conditions, diffusivities were much below the common estimates derived from the log-law. The decreased diffusivities question the common view that turbulent transport in the BBL is not limiting the flux across the sediment-water interface. By means of a simple oxygen flux model we demonstrated that turbulent diffusion in the BBL potentially controls the oxygen flux into the sediment. As a result, turbulent diffusivities may not be seen as a mere quantity to calculate vertical fluxes. In fact, the focus is on the turbulent diffusivity itself and how it evolves during stratified and low flow conditions. Understanding the dynamics of turbulent transport in the BBL may be crucial to predict hypoxia in bottom waters and sulfide efflux from the sediments. The response of oxygen fluxes on variable current velocities and diffusivities, therefore, needs to be studied in more detail in the future.

References

Appt, J., J. Imberger, and H. Kobus. 2004. Basin-scale motion in stratified upper Lake Constance. Limnology and Oceanography **49:** 919-933.

Berg, P. and others 2003. Oxygen uptake by aquatic sediments measured with a novel non-invasive eddy-correlation technique. Marine Ecology-Progress Series **261:** 75-83.

Boudreau, B. P. 1997. Diagenetic Models and their Implementation: Modeling Transport and Reactions in Aquatic Sediments. Springer.

---. 2001. Solute transport above the sediment-water interface, p. 104-126. *In* B. P. Boudreau and B. B. Jørgensen [eds.], The Benthic Boundary Layer: Transport Processes and Biogeochemistry. Oxford University Press.

Bouldin, D. R. 1968. Models for Describing Diffusion of Oxygen and Other Mobile Constituents across Mud-Water Interface. Journal of Ecology **56:** 77-&.

Brand, A., D. F. McGinnis, B. Wehrli, and A. Wüest. 2008. Intermittent oxygen flux from the interior into the bottom boundary of lakes as observed by eddy correlation Limnology and Oceanography **53:** 1997-2006.

Dade, B. D., A. Hogg, and B. P. Boudreau. 2001. Physics of Flow above the Sediment-Water Interface, p. 4-43. *In* B. P. Boudreau and B. B. Jørgensen [eds.], The Benthic Boundary Layer: Transport Processes and Biogeochemistry. Oxford University Press.

Dewey, R. K., and W. R. Crawford. 1988. Bottom Stress Estimates from Vertical Dissipation Rate Profiles on the Continental-Shelf. Journal of Physical Oceanography **18:** 1167-1177.

Fennel, W. 1995. A Model of the Yearly Cycle of Nutrients and Plankton in the Baltic Sea. Journal of Marine Systems **6:** 313-329.

Foster, D. L., R. A. Beach, and R. A. Holman. 2000. Field observations of the wave bottom boundary layer. Journal of Geophysical Research **105:** 19631-19641.

Glud, R. N., P. Berg, H. Fossing, and B. B. Jorgensen. 2007. Effect of the diffusive boundary layer on benthic mineralization and O-2 distribution: A theoretical model analysis. Limnology and Oceanography **52:** 547-557.

Gregg, M. C., E. A. Dasaro, T. J. Shay, and N. Larson. 1986. Observations of Persistent Mixing and near-Inertial Internal Waves. Journal of Physical Oceanography **16:** 856-885.

Howarth, M., and A. Souza. 2005. Reynolds stress observations in continental shelf seas. Deep-Sea Research Part Ii-Topical Studies in Oceanography **52:** 1075-1086.

Imboden, D. M., and A. Wüest. 1995. Mixing mechanisms in lakes, p. 83-138. *In* A. Lerman, D. M. Imboden and J. Gat [eds.], Physics and Chemistry of Lakes. Springer-Verlag.

Jørgensen, B. B. 1977. Sulfur Cycle of a Coastal Marine Sediment (Limfjorden, Denmark). Limnology and Oceanography **22:** 814-832.

---. 1982. Mineralization of Organic-Matter in the Sea Bed - the Role of Sulfate Reduction. Nature **296:** 643-645.

Jørgensen, B. B., and B. P. Boudreau. 2001. Diagenesis and Sediment-Water Exchange, p. 211-244. *In* B. P. Boudreau and B. B. Jørgensen [eds.], The Benthic Boundary Layer: Transport Processes and Biogeochemistry. Oxford University Press.

Jørgensen, B. B., and N. P. Revsbech. 1985. Diffusive boundary layers and the oxygen uptake of sediments and detritus. Limnology and Oceanography **30:** 111-122.

Kim, S. C., C. T. Friedrichs, J. P. Y. Maa, and L. D. Wright. 2000. Estimating bottom stress in tidal boundary layer from Acoustic Doppler Velocimeter data. Journal of Hydraulic Engineering-Asce **126:** 399-406.

Lam, P. and others 2007. Linking crenarchaeal and bacterial nitrification to anammox in the Black Sea. Proceedings of the National Academy of Sciences of the United States of America **104:** 7104-7109.

Lorke, A. 2007. Boundary mixing in the thermocline of a large lake. Journal of Geophysical Research-Oceans **112**.

Lorke, A., B. Muller, M. Maerki, and A. Wuest. 2003. Breathing sediments: The control of diffusive transport across the sediment-water interface by periodic boundary-layer turbulence. Limnology and Oceanography **48:** 2077-2085.

Lorke, A., F. Peeters, and A. Wuest. 2005. Shear-induced convective mixing in bottom boundary layers on slopes. Limnology and Oceanography **50:** 1612-1619.

Lorke, A., L. Umlauf, T. Jonas, and A. Wüest. 2002. Dynamics of Turbulence in Low-Speed Oscillating Bottom-Boundary Layers of Stratified Basins. Environmental Fluid Mechanics **2:** 291-313.

Lorke, A., L. Umlauf, and V. Mohrholz. 2008. Stratification and mixing on sloping boundaries. Geophysical Research Letters **35**.

Maerki, M., B. Muller, C. Dinkel, and B. Wehrli. 2009. Mineralization pathways in lake sediments with different oxygen and organic carbon supply. Limnology and Oceanography **54:** 428-438.

Miles, J. W. 1961. On the stability of heterogeneous shear flows. Journal of Fluid Mechanics Digital Archive **10:** 496-508.

Osborn, T. R. 1980. Estimates of the Local Rate of Vertical Diffusion from Dissipation Measurements, p. 83-89.

Pope, S. B. 2000. Turbulent Flows. Cambridge University Press.

Sato, Y., and K. Yamamoto. 1987. Lagrangian Measurement of Fluid-Particle Motion in an Isotropic Turbulent Field. Journal of Fluid Mechanics **175:** 183-199.

Sauter, E. J., M. Schluter, J. Wegner, and E. Labahn. 2005. A routine device for high resolution bottom water sampling. Journal of Sea Research **54:** 204-210.

Soulsby, R. L., and K. R. Dyer. 1981. The form of the near bed velocity profile in a tidally accelerating flow. Journal of Geophysical Research **86:** 8067-8074.

Taylor, G. I. 1921. Diffusion by continuous movements. Proceedings of the London Mathematical Society **20**.

---. 1938. The Spectrum of Turbulence, p. 476-490.

Tennekes, H., and J. L. Lumley. 1972. A First Course in Turbulence. MIT Press.

Trowbridge, J. H., W. R. Geyer, M. M. Bowen, and A. J. Williams. 1999. Near-bottom turbulence measurements in a partially mixed estuary: Turbulent energy balance, velocity structure, and along-channel momentum balance. Journal of Physical Oceanography **29:** 3056-3072.

von Karman, T. 1930. Mechanische Ähnlichkeit und Turbulenz, p. 85-105. Proceedings of the Third International Congress of Applied Mechanics.

Wenzhoefer, F., and R. N. Glud. 2004. Small-scale spatial and temporal variability in coastal benthic O-2 dynamics: Effects of fauna activity. Limnology and Oceanography **49:** 1471-1481.

Wollast, R. 1991. The coastal organic carbon cycle: fluxes, sources and sinks, p. 365-381. *In* J.-M. M. R.-F.-C. Mantoura, R. Wollast [ed.], Ocean Margin Processes in Global Change. John Wiley & Sons.

Wüest, A., and A. Lorke. 2003. Small-scale hydrodynamics in lakes. Annual Review of Fluid Mechanics **35:** 373-412.

Water column versus sedimentary nitrogen loss in the Arabian Sea

Moritz Holtappels[1*], Gavin Collins[1,2], Sarah Sokoll[1], Michael Schlüter[3], Volker Brüchert[4], Gaute Lavik[1], Marcel M.M. Kuypers[1]

1) Max Planck Institute for Marine Microbiology, Celsiusstrasse 1, 28359 Bremen

2) Present address: National University of Ireland, Galway, University Road, Galway, Ireland

3) Alfred Wegener Institute for Polar and Marine Research, Am Handelshafen 12, 27570 Bremerhaven

4) Department of Geology and Geochemistry, Stockholm University, 10691 Stockholm, Sweden

Acknowledgement

We thank Aurelien Paulmier for support and advice, Karin Zonneveld and Sabine Kasten for sharing equipment, data and information from the Meteor Cruise M-74/3. We especially thank Ireen Vieweg, Martina Meyer and Gabi Klockgether, for their assistance in sampling and sample analysis and the crew of *RV Meteor* for excellent collaboration. This study was funded through DFG-Research Center / Excellence Cluster „The Ocean in the Earth System" and the Max Planck Society.

Abstract

The Arabian Sea exhibits one of the largest and most stable Oxygen Minimum Zones (OMZ) in the Ocean. Reported N-deficits in suboxic waters suggest heavy loss of fixed nitrogen that, so far, is attributed to pelagic denitrification. N-loss from the sediment is thought to be less relevant than from the water column of the Arabian Sea. However, at sites where the OMZ intersects with the sediment it is not known to what extend sedimentary N-loss contributes to the N-deficit in the water column. In the Arabian Sea, measurements of sedimentary N-loss are scarce and the contribution of anammox to the total sedimentary N-loss is unknown. Here, we present data from a cruise to the Pakistan continental margin that was conducted during the inter-monsoon season in October 2007. At sites across the OMZ we determined N-loss rates in the water column and in the sediments using ^{15}N-labeled substrates. Our results indicate that anammox was responsible for the N-loss in the water column. Anammox rates integrated over the water column were low (<200 μmol m^{-2} d^{-1}). Highest anammox rates were found in the oxycline and in the benthic boundary layer. Low N-loss rates agreed well with low oxygen consumption rates (1-4 nM d^{-1}) calculated from salinity and oxygen profiles using a mixing model. Average sedimentary N-loss in the OMZ was 380 μmol m^{-2} d^{-1}. Denitrification was identified as the main sedimentary N-sink but the contribution of anammox increased with depth from 5 % at 360 m (upper OMZ) to 40 % at 1430 m (below the OMZ). Based on these results pelagic N-loss seems to be limited by organic matter availability leaving sedimentary N-loss as the dominant nitrogen sink in this region of the Arabian Sea.

Introduction

Nitrogen is essential for all living organisms. Nitrogen limits primary production in most of the ocean and potentially controls CO_2 sequestration and thus the biological carbon pump (Falkowski et al. 1998; Gruber 2004). The marine nitrogen cycle is mostly mediated by microorganisms. More than 50 % of the biologically available (fixed) nitrogen (i.e. NO_3^-, NO_2^- NH_4^+) in the ocean derives from the microbial assimilation of gaseous N_2, whereas most of the fixed nitrogen (~90 %) is lost from the ocean by the microbial production of N_2 (Codispoti et al. 2001; Gruber and Sarmiento 1997; Middelburg et al. 1996).

Roughly, 55 % to 75 % of the N-loss is attributed to microbial N_2 production in ocean sediments. The remaining part (25-45 %) is lost from oceanic oxygen minimum zones (OMZ) that, altogether, constitute only about 0.1 % of the ocean volume (Codispoti et al. 2001). The most prominent OMZ's can be found in the Eastern Tropical North Pacific (ETNP), the Eastern Tropical South Pacific (ETSP) as well as in the Arabian Sea and off Namibia.

For decades microbial N_2 production was attributed to heterotrophic denitrification only. Denitrification consists of a number of respiratory reduction steps thereby converting NO_3^- to N_2 ($NO_3^- \rightarrow NO_2^- \rightarrow NO \rightarrow N_2O \rightarrow N_2$). Both, the accumulation of intermediates and products (NO_2^-, N_2O and N_2) in the suboxic environment as well as decreased ratios of dissolved fixed nitrogen to phosphorus that are below the expected Redfield ratio were often used as evidence for heterotrophic denitrification. However, this interpretation is challenged by the recent findings of a second microbial N-loss pathway, the anaerobic ammonium oxidation (anammox) (Mulder et al. 1995). Anammox is a chemolithoautotrophic pathway that yields energy from the oxidation of NH_4^+ with NO_2^- to yield N_2 ($NH_4^+ + NO_2^- \rightarrow N_2$). Anammox was found active in ocean sediments (Thamdrup and Dalsgaard 2002), with highly variable contributions (0-80 %) to the total sedimentary N-loss (Dalsgaard et al. 2005). Furthermore, anammox was shown to be the dominant pelagic N-loss pathway in major OMZ's off Namibia (Kuypers et al. 2005), in the ETSP (Thamdrup et al. 2006), (Hamersley et al. 2007) as well as in the Black Sea (Kuypers et al. 2003). However, the role of anammox in the OMZ of the Arabian Sea is not known yet.

The Arabian Sea exhibits the worlds largest and most stable OMZ, which spans an area of roughly 5 million square kilometers. In water depths between ~100 m and ~1000 m, oxygen concentrations below 5 µM are widespread. It is assumed that low oxygen concentrations are maintained by a combination of moderate to high respiration rates and sluggish replacement of oxygenated waters (Olson et al. 1993). However, biological

production and current regimes in the Arabian Sea are variable and depend on the monsoon season (Rixen et al. 2005).

The oxygen-deficient waters in the Arabian Sea permit anaerobic microbial N_2 production. A pronounced and widespread deficit of fixed nitrogen (i.e. a decrease of the ratio of inorganic fixed nitrogen to phosphate) in the OMZ has been attributed to denitrification (Bange et al. 2000; Codispoti et al. 2001; Naqvi 1994). Based on N-deficit measurements, total pelagic N-loss in the Arabian Sea was estimated to range from 21 to 34 Tg N yr^{-1} (Bange et al. 2005; Howell et al. 1997). Interestingly, N_2 production estimated from excess N_2 concentrations in the OMZ (as N_2/Ar ratios) exceed those derived from N-deficit measurements by a factor of 2-4 (Codispoti et al. 2001). Based on these results Codispoti (2001) revised the total pelagic N-loss to 60 Tg N yr^{-1}, therewith attributing 40 % of the global pelagic N-loss to the Arabian Sea.

So far, the discrepancy between N-deficit and N_2/Ar estimates could not be explained, revealing our lack of understanding about the actual N-loss pathway in the Arabian Sea. It is important to note that none of the above mentioned estimates is based on direct measurements of the N-loss rates. Direct rate measurements were presented by Devol et al. (2006) who traced the conversion of isotopically labeled $^{15}NO_3^-$ to $^{29}N_2$. Devol found considerable differences between coastal and open ocean N-loss rates. The spatial and temporal extrapolation of the average rates amounted to an N-loss of 41 Tg N yr^{-1} from the OMZ. However, in his calculations he considered denitrification as the only possible N-loss pathway.

While many studies focused on the pelagic N-loss in the Arabian Sea, estimates of sedimentary N-loss are scarce. Because the Arabian Sea is semi enclosed by land masses, the area of shelf and margin sediments above 1000 m water depth accounts for almost 15 % of the total area. It is uncertain to what extend the N-loss from shelf and ocean margin sediments contribute to the N-deficit in the Arabian Sea. Using a model that links primary production to sedimentary denitrification, Bange et al. (2000) estimated a contribution of ~17 % (i.e. 6.8 Tg N yr^{-1}) to the total N-loss. Sedimentary N-loss was directly measured only by Naik and Naqvi (2002) using the acetylene block technique and by Schwartz (2009) measuring sedimentary N_2 release and NO_3^- uptake. Extrapolated to the Arabian Sea shelf and margin sediments they calculated a sedimentary N-loss in the range of 0.4 to 10.5 Tg N yr^{-1}.

For both, sedimentary as well as pelagic N-loss direct rate measurements are scarce and do not cover the spatial and temporal variability to allow a reasonable extrapolation of the results. Moreover, the processes responsible for the N-loss (i.e. anammox or denitrification)

are unknown. In this study, we present directly measured sedimentary and water column N-loss rates from the continental margin off Pakistan. N-loss rates were based on ^{15}N enrichment experiments that allowed quantifying the respective contributions of anammox and denitrification. Furthermore, O_2 consumption rates in suboxic waters were estimated and discussed along with water column N-loss rates.

Methods

Study site and sampling procedure

During the inter-monsoon season in October 2007, cruise M74/2 of the research vessel *Meteor* was conducted to the continental margin off Pakistan. Sediment and water samples were collected at 5 different stations across the OMZ at depths between 350 m and 1500 m. Table 1 lists the station, positions, water depths and gears that were used in chronological order. Figure 1 shows the bathymetry of the investigated area and the position of the stations.

A CTD-Rosette was used to sample the water column from surface waters down to 10m above the sediment. The CTD (SBE 9plus, Sea-Bird Electronics) was equipped with oxygen (SBE 43, Sea-Bird Electronics) and fluorimetric sensors (Haardt, Germany). Density was calculated using the data processing program SeaSoft (Sea-Bird Electronics). The stability of the water column was expressed using the stability frequency N, also known as Brunt-Väisälä frequency, defined as:

$$N^2 = \frac{g}{\rho}\frac{\partial \rho}{\partial z} \qquad \text{E (1)}$$

where ρ is the water density, g is the gravitational acceleration and z is the water depth. With the Rosette, water samples of 10 L volume were taken in 18 discrete depths, chosen after interpreting the downcast profile of the CTD.

The Benthic Boundary Layer (BBL) was sampled with a Bottom Water Sampler (BWS) and a new built BBL-Profiler (see Chapter 2). The BWS, previously described by Sauter (2005), consisted of 6 horizontally aligned free flow bottles (volume: 6 L) over a vertical range of two meter. The BWS was deployed to the seafloor. After a delay time of 15 min, the bottles closed automatically and the samples were retrieved. The BBL-Profiler consisted of a 12-channel peristaltic pump (KC, Denmark) that was used to draw water samples (30-60 ml) for nutrient analysis from 0.04 to 1.4 m above the sediment surface into 100 ml plastic syringes. After deploying the BBL-Profiler to the sea floor, the sampling procedure started after a delay time of about 20 min. From the BWS and the Niskin bottles of the CTD-Rosette, subsamples were taken for oxygen and nutrient analysis as well as for experiments with ^{15}N-labeled substrate. From the BBL-Profiler, samples were taken for nutrient analysis only.

Sediment was sampled with a multicorer (MUC) equipped with 8 acrylic liners (Ø 10 cm). Subsamples for slurry incubations were taken from Ø 10 cm cores directly by

cutting the core into 2 cm slices between 0 and 8 cm depths. Subsamples for the incubations of intact sediments were taken from the Ø 10 cm cores using smaller Ø 3.6 cm cores. From other Ø 10 cm cores porewater was squeezed out of sediment slices with a vertical resolution of 0.5 cm (between 0 and 1 cm depth), 1 cm (between 2 and 5 cm depth) and 2.5 cm (between 5 and 10 cm depth) using a porewater squeezer. The solid phase was sampled from 0 to 8 cm and stored at -20°C until further treatment in the laboratory.

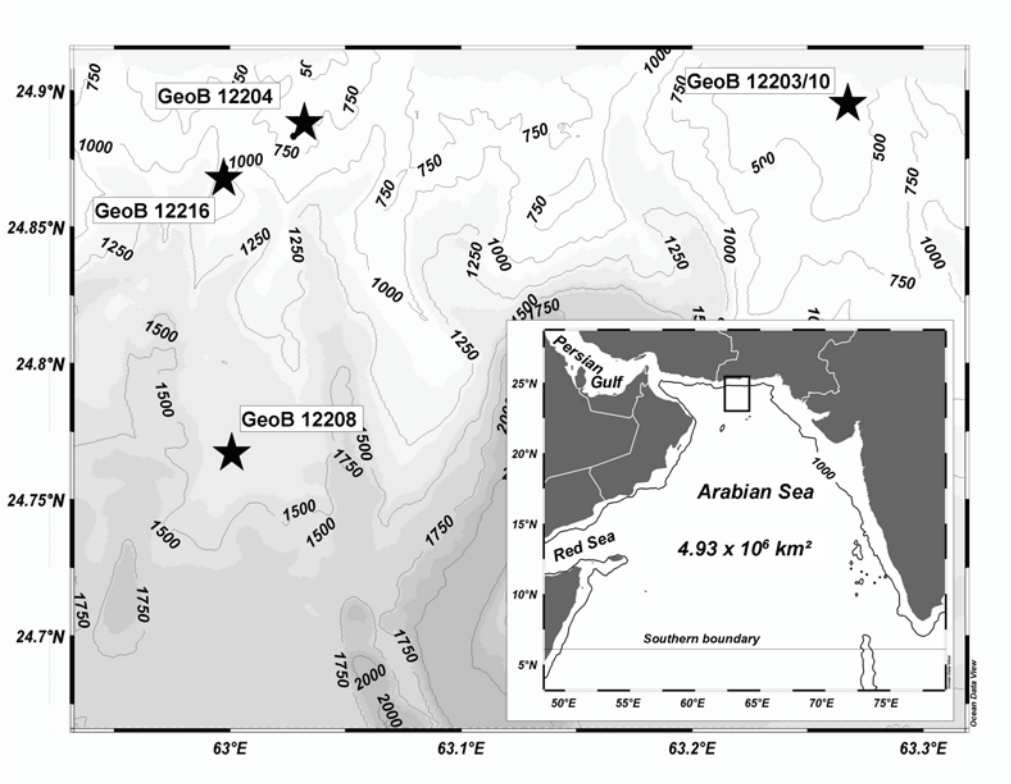

Figure 1: Large map: Bathymetry and stations (stars) in the investigated area. Small map: The Arabian Sea with depth contour at 1000m. The square marks the investigated area off Pakistan.

Table 1: Compilation of station name, position, water depth, sampling date, and deployed gears (Abbreviations are explained in the text).

Station	Date	Latitude (N)	Longitude (E)	Depth (m)	Gear
GeoB12203	09.Oct.2007	24° 53.72'	63° 16.02'	350	CTD, BWS
GeoB12204	13.Oct.2007	24° 53.01'	63° 01.65'	680	CTD, BWS, BBL, MUC
GeoB12208	16.Oct.2007	24° 45.99'	63° 00.01'	1429	CTD, BWS, MUC
GeoB12210	22.Oct.2007	24° 53.76'	63° 16.01'	363	CTD, BBL, MUC
GeoB12216	24.Oct.2007	24° 52.31'	62° 59.87'	970	CTD, BWS, BBL, MUC

Chemical analysis

Oxygen, ammonium and nitrite concentrations in the water column were measured immediately on board by Winkler titration (O_2), fluorimetric (NH_4^+) (Holmes et al. 1999) and photometric (NO_2^-) analysis (Grasshoff et al. 1999). Water column samples for nutrient analysis were stored in centrifuge tubes at -20°C until measured in the laboratory for nitrate, nitrite, ammonium and phosphate concentrations using a TRAACS 800 autoanalyzer (Bran & Luebbe, Germany). Porewater samples for NO_3^- and NO_2^- were stored frozen in eppendorf vials until measured with a chemoluminescence NOx analyzer (Thermo Environmental Instruments Inc., USA) after Braman and Hendrix (1989). Porewater samples for dissolved inorganic carbon (DIC) and NH_4^+ were amended with 100 µl of saturated $HgCl_2$ solution, stored without headspace at 4°C and measured by flow injection analysis according to Hall and Aller (1992).

Dissolved reduced iron (Fe^{2+}) and hydrogen sulfide (H_2S) in the porewater were measured according to Grasshoff (1999) and Cline (1969). For the Fe^{2+} analysis on board, 1 ml of sample was added to 50 µl of Ferrospectral solution to complex the Fe^{2+} for photometric measurement at 565 nm. Samples with high concentrations of iron (> 1 mg l^{-1}) were pretreated with 10 µl ascorbic acid and diluted with oxygen-free artificial sea-water (1:2 or 1:5) prior to complexation. For H_2S analysis, 1.5 ml subsamples of the pore water were added to a ZnAc solution (600 µl) to fix all H_2S present as ZnS. Sulfide concentrations were then measured photometrically at 660 nm using the methylene blue method (Cline 1969).

The concentrations of organic carbon and nitrogen in the surface sediment were determined in the laboratory. Prior to the analysis, inorganic carbon was removed from the sediment by acidifying with H_3PO_4. The sediment was freeze dried and homogenized before weighed subsamples were combusted using an Elemental Analyzer (Fisons NA 1500 Series 2, Fison Instruments).

^{15}N labeling experiments with intact sediment cores

Sedimentary denitrification and anammox rates were determined using the revised isotope pairing technique (rIPT) described in detail by Risgaard-Petersen et al. (2003). The rIPT is based on ^{15}N labeling incubations of sediment slurries and intact sediment cores: the contribution of anammox to the total N-loss is calculated from the sediment slurry incubation which is then used to calculate total N-loss from incubations of intact sediment cores. In the following, incubation of intact sediment will be referred to as ‘core incubation’.

Experiments with sediment slurries as well as sediment cores were carried out on board. For the core incubations, 15 sediment subcores were taken using Ø 3.6 cm plastic tubes. Sediment height in the cores was adjusted to 13 cm. In each core, the overlying water column of 12.5 cm height was amended with $^{15}NO_3^-$ to a final concentration of 50 µM. The overlying water was mixed by small magnetic stirrers, placed inside the cores and driven by a large external magnet. After pre-incubation of the open cores for ~8 h, all cores were sealed with rubber stoppers and incubated without a gas phase. Five time points were taken between 0 and 15 h. At each time point, 3 cores were sacrificed by first taking of the rubber stopper and injecting 1 ml of 50 % $ZnCl_2$ on to the sediment surface to precipitate dissolved sulfide. Then, the top 6 cm of the sediment were thoroughly mixed with the overlying water and a slurry sample was drawn into 12 ml gas tight vials (Exetainers, Labco) and fixed with 100 µl saturated $HgCl_2$ solution. Measurements were performed in the dark at *in-situ* temperatures.

^{15}N labeling experiments with sediment slurries

Slurry incubations were performed for 4 depth strata and for 2 different treatments. MUC cores (Ø 10 cm) were sliced in 2 cm intervals between 0 and 8 cm depth. Each slice (volume of 157 cm^3) was transferred into a gas tight bag that was subsequently heat-sealed from all sides. To prepare the slurry, 200 ml of degassed bottom water, taken from the overlying water in the MUC cores, were injected through a gas tight port into the bag. The residual air was driven out of the bag and the slurry was thoroughly mixed. After pre-incubating the bags for 2 hours, ^{15}N-labelled substrates were injected into the bags and the slurries were again thoroughly mixed.

For treatment 1 the slurry was enriched with $^{15}NH_4^+$, $^{14}NO_2^-$ and the nitrification inhibitor allylthiourea (ATU) to a final concentration of 200, 100 and 80 µM, respectively. For treatment 2 the slurry was enriched with $^{15}NO_3^-$ to a final concentration of 200 µM. A subsample was drawn from the bags immediately after tracer addition and mixing, representing the time point T0. Between 5 and 7 samples were drawn from the bags during the subsequent 26-28 hours. Slurry samples were drawn into 6 ml gas tight vials (Exetainers, Labco) and fixed with 100 µl saturated $HgCl_2$ solution. Measurements were performed in the dark in a cold room at *in-situ* temperatures.

^{15}N labeling experiments with water column samples

Water column denitrification and anammox rates were determined according to Kuypers et al. (2003). On deployment of the CTD-Rosette and the BWS, samples from 6 specific depths

were chosen at each station for ^{15}N-labeling experiments. After retrieving the sampling instrument, samples were immediately transferred into 250 ml serum vials, avoiding any gas trapping. To facilitate the detection of N_2 production, the N_2 background concentration in the samples were lowered by bubbling with helium for 10 minutes. Subsequently, unlabeled and ^{15}N-labelled nitrite and ammonium were added to final concentrations of 5 µM $^{15}NH_4^+$ + 5 µM $^{14}NO_2^-$ (treatment 1) and 5 µM $^{15}NO_2^-$ (treatment 2). After the addition, the samples were bubbled with helium for another 5 minutes and transferred into 12 ml gas tight vials (Exetainers, Labco) avoiding any gas trapping. The Exetainers were incubated in the dark at *in-situ* temperatures. Samples were taken after 0, 6, 12, 24 and 48 hours. At each time point biological activity in the Exetainer was stopped by adding 100 µl saturated $HgCl_2$ solution.

N_2 isotope measurements

In the laboratory, a 2 ml Helium headspace was introduced into the 12 ml exetainer. A headspace of 1 ml was used for the 6 ml exetainer. The exetainer were shaken vigorously to allow N_2 to equilibrate between the headspace and the water phase. The isotope ratio dinitrogen gas ($^{28}N_2$, $^{29}N_2$, and $^{30}N_2$) in the headspace was determined by gas chromatography-isotopic ratio mass spectrometry by direct injections from the headspace according to Kuypers et al. (2005). Concentrations of $^{30}N_2$ and $^{29}N_2$ were normalized to $^{28}N_2$ and calculated as excess relative to air. N_2 production rates were calculated from the $^{29}N_2$ and $^{30}N_2$ increase over time. Only rates with a significant linear slope ($p<0.05$) were used for further calculations.

Calculation of N-loss in the water column

In treatment 1, the anammox pathway ($NH_4^+ + NO_2^- \rightarrow N_2$) combines either $^{14}NH_4^+$ or $^{15}NH_4^+$ with $^{14}NO_2^-$ to form $^{28}N_2$ and $^{29}N_2$. Anammox activity was indicated when the production of $^{29}N_2$ ($p^{29}N_2$) was measured without any production of $^{30}N_2$ ($p^{30}N_2$). The latter would indicate nitrification coupled with denitrification and/or anammox. Samples with significant $p^{30}N_2$ were not used for further calculations. The total N_2 production via anammox in treatment 1 ($A_{(treat1)}$) was calculated from:

$$A_{(treat1)} = \frac{p^{29}N_2}{F_N} \qquad \text{E 2}$$

where F_N is the labeling percentage of the ^{15}N-substrate ($F_N = {}^{15}NH_4^+ / ({}^{14}NH_4^+ + {}^{15}NH_4^+)$). For treatment 1, F_N was calculated from the measured $^{14}NH_4^+$-background concentrations and the known addition of $^{15}NH_4^+$.

In treatment 2, the addition of $^{15}NO_2^-$ to background concentrations of $^{14}NO_2^-$ and $^{14}NH_4^+$ would produce $^{28}N_2$ and $^{29}N_2$ via anammox and $^{28}N_2$, $^{29}N_2$ and $^{30}N_2$ via denitrification. Thus, the production of $^{30}N_2$ ($p^{30}N_2$) indicates active denitrification. The total N_2 production by denitrification in treatment 2 ($D_{(treat2)}$) was calculated according to Thamdrup and Dalsgaard (2002) from $p^{30}N_2$:

$$D_{(treat2)} = \frac{p^{30}N_2}{(F_N)^2} \qquad \text{E 3}$$

where F_N is the labeling percentage of nitrite ($F_N = {}^{15}NO_2^- / ({}^{14}NO_2^- + {}^{15}NO_2^-)$). In treatment 2, both, anammox and denitrification produce $^{29}N_2$. To calculate anammox from treatment 2, equation 2 is modified to: $A_{(treat2)} = \left(p^{29}N_2 - p^{29}N_{2(Den)}\right)/F_N$, where $p^{29}N_{2(Den)}$ is the $^{29}N_2$ production via denitrification. With $p^{29}N_{2(Den)} = 2\,\frac{(1-F_N)}{F_N}\,p^{30}N_2$ (Thamdrup and Dalsgaard 2002) we derive:

$$A_{(treat2)} = \left(p^{29}N_2 - 2\,\frac{(1-F_N)}{F_N}\,p^{30}N_2\right)\cdot\frac{1}{F_N} \qquad \text{E 4}$$

Calculation of N-loss in the sediment slurries

In general, calculations of N_2 production in sediment slurries do not differ from those of the water column. Therefore, anammox activity in the slurries of treatment 1 was calculated from measured $p^{29}N_2$ and F_N according equation 2. In treatment 2, however, F_N was calculated differently. We had strong indications for the presence of NO_3^--storing organisms releasing stored $^{14}NO_3^-$ in the course of the experiment. An estimate of F_N on the basis of measured $^{14}NO_3^-$ bottom water and porewater concentrations was therefore not possible (for further details, see discussion). Instead, we used the measured anammox rates of treatment 1 ($A_{(treat1)}$) to calculated F_N in treatment 2 from equation 4 by inserting the measured $p^{29}N_2$ and $p^{30}N_2$ and by assuming $A_{(treat1)} = A_{(treat2)}$. The derived F_N value, in the following referred to as F_{N*}, was then used to estimate denitrification according to equation 3. For sediments without the release of stored nitrate we expected F_N equals F_{N*}, whereas $F_{N*} < F_N$ indicated an additional source of $^{14}NO_3^-$, which was not dissolved initially in the porewater. We denoted the additional nitrate as '$^{14}NO_3^-$excess' that was calculated from F_{N*}, F_N and the known concentration of $^{15}NO_3^-$ in the slurry:

$$Excess\,{}^{14}NO_3^- = {}^{15}NO_3^- \left(\frac{1}{F_{N*}} - \frac{1}{F_N}\right) \qquad \text{E 5}$$

Calculation of N-loss in intact sediment cores

The contribution of anammox to the total N-loss (*ra*) was estimated from the slurry incubation ($ra = A_{(treat1)} / (A_{(treat1)} + D_{(treat2)})$). The total N-loss due to denitrification and anammox was calculated according to Risgaard-Petersen et al. (2003) from *ra* and the production of $^{30}N_2$ and $^{29}N_2$ in the core incubations:

$$N - loss = 2 \cdot \frac{(1 - ra)\ R^{29} - ra}{2 - ra} \cdot \left[p^{29}N_2 + p^{30}N_2 \left(1 - \frac{(1 - ra)\ R^{29} - ra}{2 - ra} \right) \right] \qquad \text{E 6}$$

where R^{29} is the ratio between the $^{29}N_2$ and $^{30}N_2$ production.

Results

The water column

The physical structure of the upper water column was characterized by a shallow mixed layer depth of 25 to 35 m (Fig. 2). The mixed layer was separated from the lower water masses by a pronounced pycnocline with a stability frequency of ~10 cycles per hour. From the pycnocline downward, the density gradient decreased with depth. Stratification was due to the decrease of temperature with depth, whereas the simultaneous decrease of salinity counteracted the stability of the water column. From 170 m depth to a maximum of 400 m depth, a salinity maximum was found at all stations, indicating the intrusion of a separate water mass. The depth of the intrusion and the characteristic temperature-salinity signature (Fig. 3) identified it as Persian Gulf Water (PGW) that was gradually mixed with deep water masses.

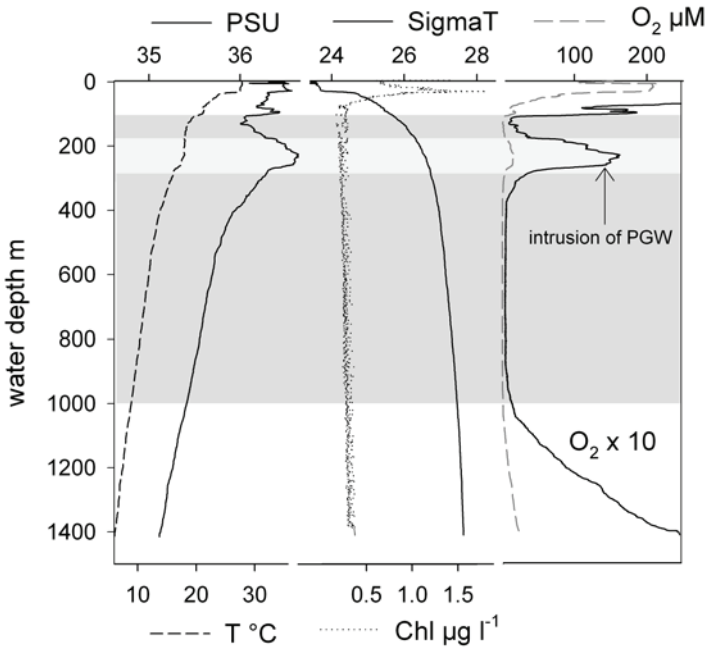

Figure 2: Temperature, salinity, density, chlorophyll a and oxygen concentrations in the water column at station GeoB12208. Gray and light gray areas mark the range of the OMZ and the Persian Gulf Water intrusion, respectively

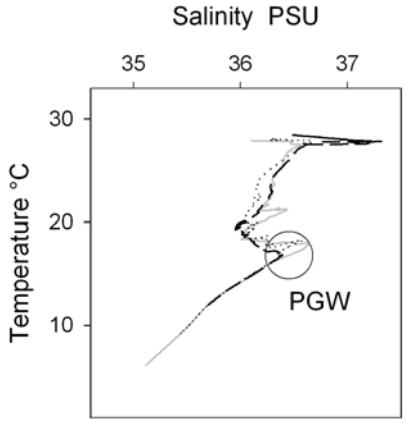

Figure 3: Compiled T-S plot for GeoB12204 (dashed), GeoB12208 (grey) and GeoB12216 (dotted). The circle marks the T-S signature of the Persian Gulf Water intrusion (PGW) at 250 m depth

Chlorophyll concentrations were highest (1.7 to 2.5 µg Chl l^{-1}) in the upper mixed water layer, close to the pycnocline. Integrated chlorophyll concentrations varied between 37 and 60 mg m^{-2} with highest values at the shallow station. Oxygen concentration decreased rapidly from saturation concentration in the mixed layer (200 µM) to less than 20 µM below

the pycnocline at 80 m depth. Below 110 m depth, oxygen concentrations were between 1 and 5 µM before they increased in the PGW to up to 15 µM. Below the PGW, oxygen concentrations decreased towards the detection limit (1 µM) before they increased again below 1000 m depth.

Ammonium and nitrite concentrations were low throughout the water column, ranging from 200 nM (NH_4^+) and 500 nM (NO_2^-) in the mixed layer to 50 nM (NH_4^+) and 100 nM (NO_2^-) in the lower water column (Fig. 4). In the BBL, nitrite and ammonium concentrations increased towards the sediment surface (Fig. 5). Nitrite gradients were found only close to the sediment surface and could, therefore, be measured only from the BBL-Profiler that allowed sampling of high vertical resolution. Due to the limited sample volume, on board ammonium measurements of BBL-Profiler samples were not possible. Ammonium gradients were more pronounced and could be measured from BWS samples. Ammonium and nitrite gradients were most obvious at station GeoB12216.

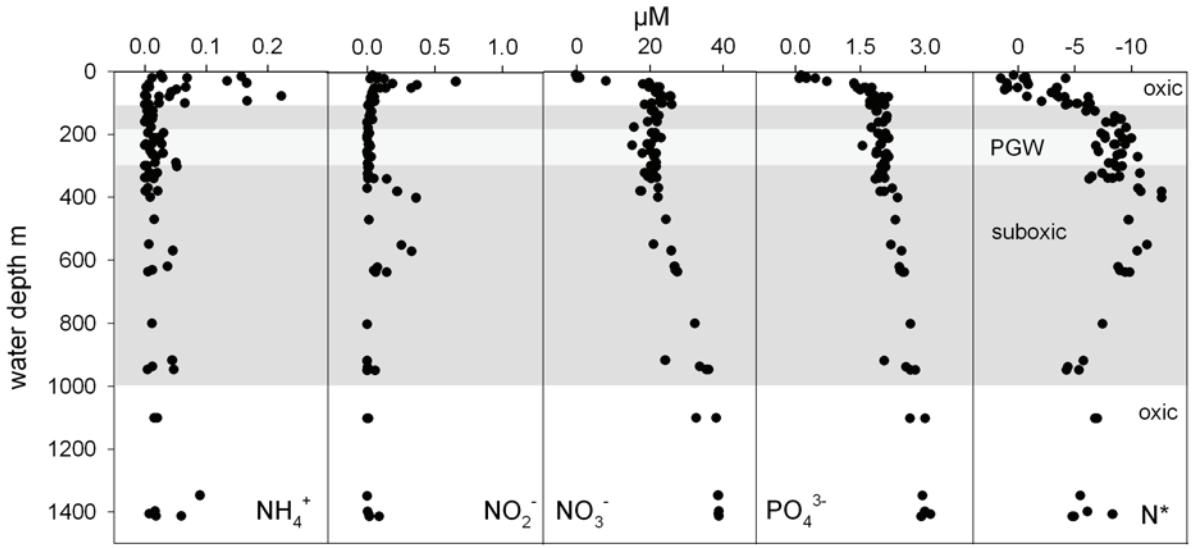

Figure 4: Nutrient concentrations and N* in the water column, compiled from all stations. Gray and light gray areas mark the range of the OMZ and the Persian Gulf Water intrusion, respectively

In the lower oxycline at ~100 m, nitrate and phosphate concentrations were 25 µM and 2 µM, respectively, and decreased to sub-micromolar concentrations towards the water surface. From the oxycline down to the PGW, nitrate concentrations slightly decreased before increasing to maximum concentrations of 38 µM at 1400 m depth. Phosphate concentrations showed a steady increase below the oxycline with maximum concentrations of 3 µM at 1400 m depth. The N-deficit, calculated as N* (Deutsch et al. 2001), decreased from 0 µM in the upper mixed layer to -10 µM in the lower oxycline. N* remained at -10 µM in the PGW,

subsequently decreased to -12 µM at 400 m depth and increased with depth to -5 µM at the lower boundary of the OMZ.

Water column N-loss

N-loss in the water column was low. In 70% of the incubated water samples, N-loss was below the detection limit (~0.1 nM N d^{-1}). Measurable rates were found either in the BBL or at the lower oxycline and varied from 0.1 to 11.0 nM N d^{-1} (Fig. 6). Anammox was the dominant N-loss process. Denitrification rates were detected only twice in the BBL and were found below 0.8 nM N d^{-1}. The integrated areal N-loss rates (see discussion) varied between 0.16 and 0.24 mmol N m^{-2} d^{-1} (Fig. 10).

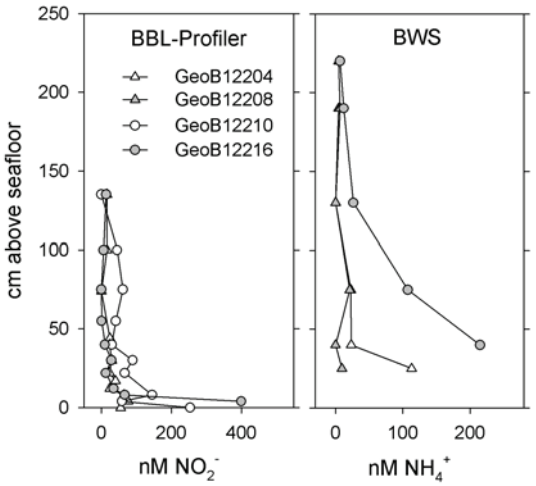

Figure 5: NO_2^- and NH_4^+ concentrations in the BBL, sampled with the BBL-Profiler and BWS, respectively.

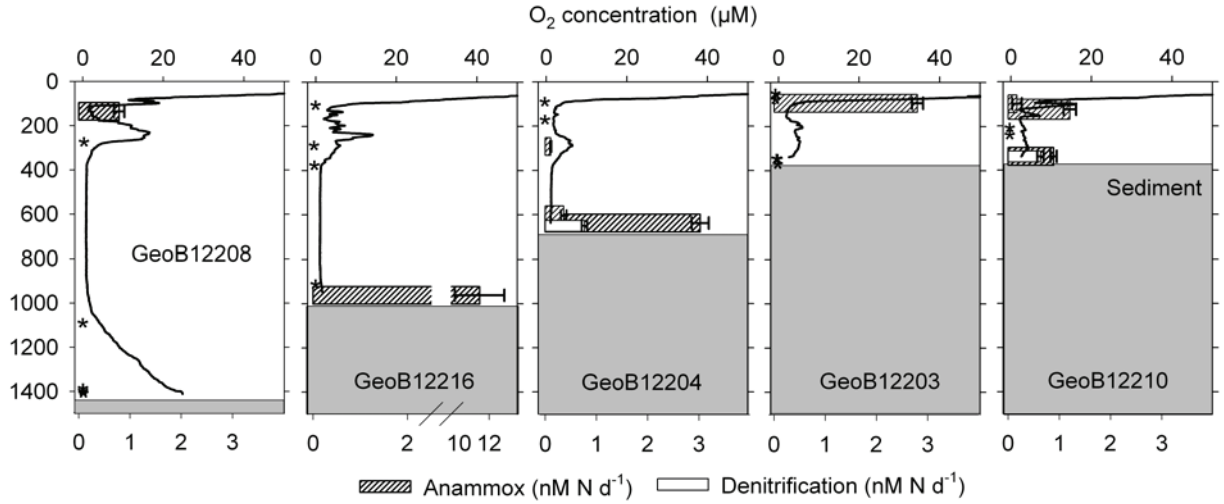

Figure 6: Anammox and denitrification rates (bars) and oxygen concentration (line) in the water column. The asterix mark sample depths without significant rates.

The sediment

The concentrations of dissolved inorganic carbon (DIC) and NH_4^+ in the porewater increased at all stations from the sediment surface down to 30 cm depth (Fig. 7). The gradients of DIC and NH_4^+ concentrations in the porewater decreased with increasing water depth. Nitrate concentration decreased rapidly within the upper sediment layer (0 to 1 cm). At the shallow stations (GeoB12210 and GeoB12204), elevated nitrate concentrations were also found at greater sediment depths. Dissolved reduced iron (Fe^{2+}) was observed at high concentrations between 0-12 cm depth at the shallow station (GeoB12210) and between 0-30 cm depth at the deeper stations (Fig. 7). At the shallow stations, maximum Fe^{2+} concentrations were found close to the sediment surface at 2-3 cm depth. At the deep station, the Fe^{2+} concentration peak was at 10 cm depth. Sulfide (H_2S) was detected below 20 cm depth at the shallow station (GeoB12210), but remained below detection limit in the upper 30-40 cm of the sediment of the other stations.

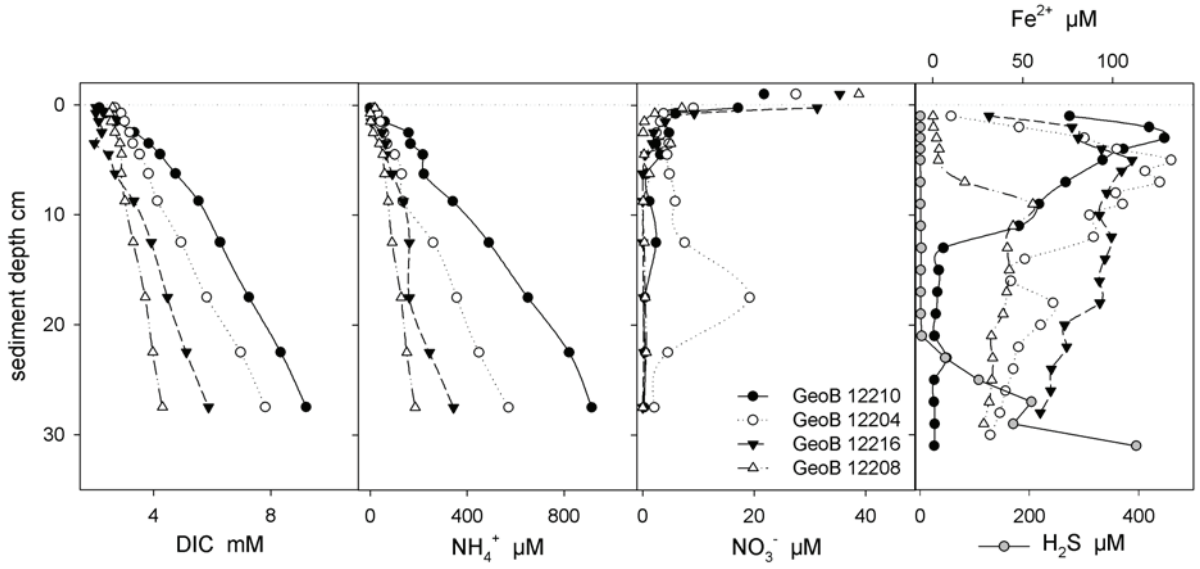

Figure 7: Porewater concentration of dissolved inorganic carbon (DIC), NH_4^+, NO_3^-, Fe^{2+} and H_2S. NO_3^- concentrations above the sediment surface (horizontal dotted line) reflect bottom water concentrations. H_2S concentrations were found only at station GeoB12210.

Sedimentary N-loss

Sedimentary N-loss was detected in both, sediment slurries and intact sediment cores (Fig. 8). In the slurry incubations, denitrification was the dominant N-loss process at all stations. Anammox was responsible for merely 7% of the total N-loss at the shallow station (GeoB12210), but with increasing water depth, the contribution of anammox increased to

over 38% (Fig. 9A). Denitrification and anammox rates were generally highest in the upper sediment layer and decreased rapidly with sediment depth. However, in deep water (GeoB12208), significant N-loss rates were also measured at 2-4 cm depth where anammox and denitrification rates were comparable to those in the upper layer.

We had strong indications for the release of intracellular $^{14}NO_3^-$ during the slurry incubations. The release of stored $^{14}NO_3^-$ was most obvious when we measured the NO_3- concentrations in the fixed subsamples of the first time point (T_0) from the slurry incubations. NO_3^- concentrations at T_0 were significantly above the total sum of bottom water, porewater and labeled NO_3- concentrations indicating an excess of $^{14}NO_3^-$ in the slurry. Unfortunately, the true labeling percentage (F_N) during the slurry incubation could not be determined from these subsamples since any residual intracellular nitrate would have been released after poisoning. For that reason, F_{N*} was calculated from equation 4 (see Methods) and subsequently the excess concentrations of $^{14}NO_3^-$ were calculated according to equation 5. $^{14}NO_3^-$-excess in the upper sediment layer was between 95 and 220 nmol cm^{-3} (Fig. 8) decreasing rapidly with sediment depth. With respect to water depth, highest $^{14}NO_3^-$-excess was found at 970 m depth (GeoB12216, 220 nmol cm^{-3}), whereas at all other stations $^{14}NO_3^-$-excess was around 100 nmol cm^{-3}.

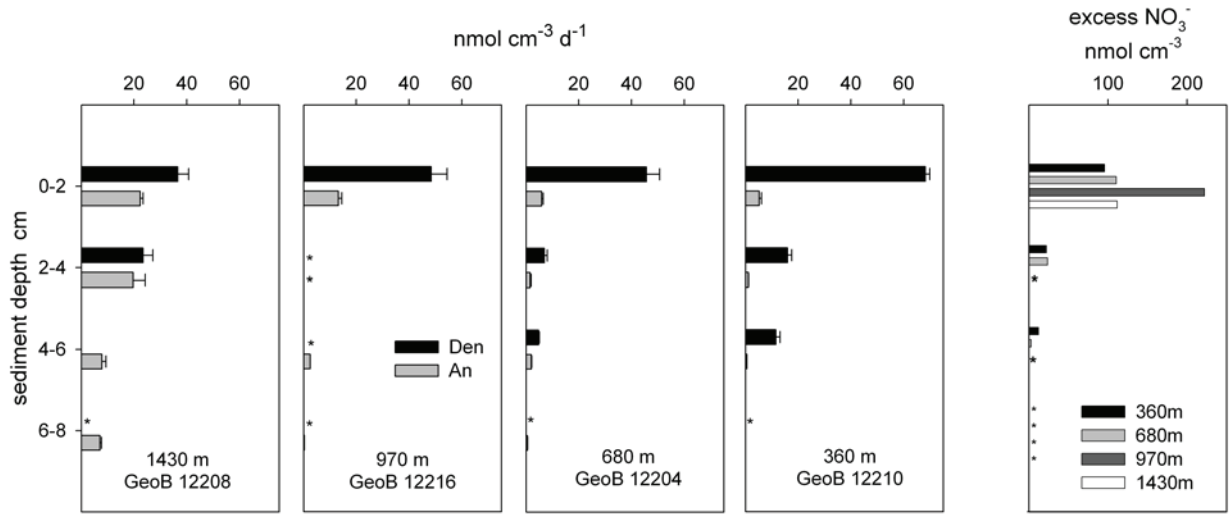

Figure 8: Denitrification and anammox rates in sediment slurries. The asterix marks incubations that were discarded either due to technical difficulties or due to insignificant N_2 production. Right side: Excess $^{14}NO_3^-$ concentrations calculated according to equation 5.

From slurry incubations, the relative contribution of anammox and denitrification to the total N-loss was determined. Applying the anammox contribution, we calculated the areal N-loss rates from the incubations of intact sediment cores (Fig. 9B) according to equation 6. At the shallow station (GeoB12210), total N-loss rates were 0.39 mmol N m^{-2} d^{-1} of which

denitrification and anammox contributed 0.36 and 0.03 mmol N m^{-2} d^{-1}, respectively. At 680 m water depth (GeoB 12204), total N-loss increased to 0.52 mmol N m^{-2} d^{-1}, mostly due to increased denitrification rates. Below 680 m depth (GeoB12208), total N-loss and denitrification rates decreased to 0.18 and 0.11 mmol N m^{-2} d^{-1}, respectively, whereas anammox rates increased to 0.07 mmol N m^{-2} d^{-1}.

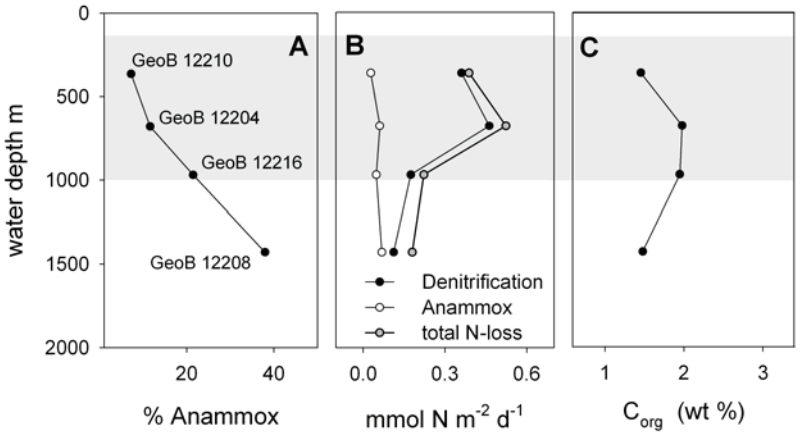

Figure 9: Sedimentary N-loss. A: Contribution of anammox to the total N-loss *vs*. water depth. B: Rates of anammox, denitrification and total N-loss *vs* water depth. For comparison: (C) organic carbont content of the surface sediment.

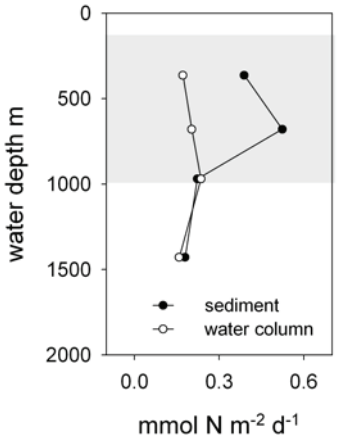

Figure 10: Depth integrated water column N-loss compared to sedimentary N-loss. Gray area marks the range of the OMZ.

Discussion

Sedimentary N-loss

Where the OMZ intersects with the sediment, denitrification was the dominant sedimentary N-loss process, whereas below OMZ waters, anammox accounted for up to 38% of the total N-loss (Fig. 9A). The average sedimentary denitrification rate of 0.33 mmol N m^{-2} d^{-1} was comparable to previously measured rates (0.42 mmol N m^{-2} d^{-1}, Table 2) by Naik and Naqvi (2002) on the West Indian shelf using the acetylene block technique. In a recent study, Schwartz et al. (2009) estimated sedimentary denitrification rates of up to 3.7 mmol N m^{-2} d^{-1} across the OMZ at the Pakistan continental margin. However, these high estimates were derived from sedimentary NO_3^- uptake, not considering nitrification or the uptake of NO_3^- for other processes such as DNRA. Instead, the *in-situ* N_2 production measured by Schwartz in September and October 2003 were between 0.05 and 0.13 mmol N m^{-2} d^{-1}.

Table 2: Estimates of water column and sedimentary N-loss in the Arabian Sea in mmol N m^{-2} d^{-1}

Setting		min	max	average	Method	Source
OMZ	open ocean	0.63	6.30	3.47	budget	Bange, 2000
OMZ	open ocean	2.22	8.40	5.46	ITP	Devol, 2006
OMZ	margin			~ 0.16	ITP	this study
Sediment	Indian shelf	0.15	1.25	0.42	acetylene block	Naik, 2006
Sediment	Pakistan margin	0.07	3.68		NO3- uptake	Schwartz, 2008
Sediment	Pakistan margin	0.22	0.52	0.38	ITP	this study

In our study, denitrification rates varied between the different stations (Fig. 9B). Middelburg et al. (1996) showed that the main factors controlling denitrification are the oxygen and nitrate concentrations in the bottom water as well as the organic carbon content of the sediment. Denitrification is favored by low oxygen concentrations and high nitrate concentrations in the bottom water as well as by high organic carbon availability in the sediment. From the shallow station in the upper OMZ denitrification rates increased towards the core of the OMZ and decreased towards the deepest station. This corresponded with the concentrations of organic carbon (C_{org}) in the sediments (Fig. 9C) that were low at both, the shallow and the deep station, but were increased in the core of the OMZ. However, at the lower boundary of the OMZ (GeoB12216) denitrification rates were decreased although C_{org} concentrations were still high. At the lower boundary, oxygen was present in the bottom water, but concentrations were still low (~2 µM). We therefore assumed that aerobic

mineralization was not high enough to remove considerable amounts of reactive organic carbon on the expense of denitrification. Interestingly, the highest NO_3^--excess was found at the lower boundary (Fig. 8) indicating an increased abundance of nitrate storing organisms. A possible explanation for the decreased denitrification rates is therefore the increased competition for nitrate with nitrate storing organisms.

In the course of this study, we could not identify the source for the excess of $^{14}NO_3^-$ that we found in the slurry incubations. NO_3^--storage is described for the giant filamentous sulfur bacteria such as *Beggiatoa* and *Thioploca* (Jørgensen and Gallardo 1999). Schmaljohann et al. (2001) found *Thioploca* to be present in OMZ sediments off Pakistan. However, in the sediments we sampled, giant sulfide oxidizing bacteria would have to compete for the sulfide with the chemical oxidation of sulfide with dissolved Fe^{2+} (Fig. 7), which makes their presence unlikely. Recently, Risgaard-Petersen (2006) and Høgslund (2008) described NO_3^--storing and denitrifying foraminifera in the OMZ off Chile. They measured intracellular concentrations of several millimoles and suggested that the contribution of sedimentary NO_3^- uptake by foraminifera needs to be considered in these regions.

A possible denitrification of stored NO_3^- by foraminifera would lead to false denitrification estimates if the intracellular labeling percentage (F_N) is not known. However, the increased NO_3^- concentrations in the slurry subsamples at T_0 indicate that most of the stored $^{14}NO_3^-$ was released into the porewater while mixing the slurry at the start of the experiment. Thus, a subsequent uptake of NO_3^- from the porewater would lead to an intracellular F_N that is similar to the porewater F_N. Furthermore, the linear increase of $^{29}N_2$ and $^{30}N_2$ in the slurry with time indicates that either intracellular F_N did not change over time or that the denitrification activity of foraminifera was minor. Next to the complications that nitrate storing organisms such as foraminifera cause for the N-loss measurements it should be mentioned that their relevance for the marine nitrogen cycle is still poorly described as point out by Glud et al. (2009).

In this study, we measured considerable rates of anammox especially in the deep sea sediments. This in fact was the first time that anammox has been described for the sediments of the Arabian Sea. The contribution of anammox to the total N-loss increased with water depth (Fig. 9A). This is in line with several previous studies (Dalsgaard et al. 2005; Rysgaard et al. 2004; Thamdrup and Dalsgaard 2002). However, it remains unclear how anammox activity is regulated in the sediment. Anammox depends on the availability of NH_4^+ and NO_2^-. The degradation of organic matter in the sediments provides sufficient NH_4^+, whereas NO_2^-,

which is released as intermediate during nitrification and denitrification, most likely limits sedimentary anammox. However, in this study and in previous studies no correlation of anammox and denitrification has been observed.

Dalsgaard et al. (2005) suggested that the release of NO_2^- during denitrification is rather coupled to the relative availability of NO_3^- and C_{org} in the sediment: High NO_3^- and low C_{org} concentrations, as found in deep sea sediments, broaden the sediment layer where denitrification is not NO_3^--limited. In this layer, some of the NO_3^- is reduced only to NO_2^- which accumulates in the porewater and fuels anammox. This sediment layer is reduced in size in response to high C_{org} input, as found in shallow waters. The results of our slurry incubations strengthen this hypothesis (Fig. 8). We found low anammox contributions where the bulk of denitrification was situated in the upper sediment layer (shallow stations), whereas the contribution of anammox increased where the bulk of denitrification was found down to 4 cm depth (deep station GeoB12208).

Water column N-loss

The N-deficit in the OMZ was slightly less pronounced when compared with results by Naqvi et al. (2006) who measured N* of up to -15 μM in the western Arabian Sea (Fig. 4). However, despite the prominent N-deficit in the OMZ, N-loss rates in the water column were extremely low and were often below the detection limit (~ 0.1 nM N d^{-1}). These findings were comparable to the very low N-loss estimates measured by Jensen et al. (in prep.) in the central and western Arabian Sea 3 weeks prior to this study. At all stations, anammox was the predominant N-loss process while denitrification was detected only twice (Fig. 6). This is in line with an increasing number of recent studies that identify anammox as the main N-loss process in oxygen-depleted water columns (Dalsgaard et al. 2006; Hamersley et al. 2007; Kuypers et al. 2005; Kuypers et al. 2003; Thamdrup et al. 2006).

In our study, anammox activity was found either in the lower oxycline (80-100 m) or within the BBL. In the core OMZ (150-1000 m), measurable N-loss was found only once (at 290 m depth, GeoB12204) and at very low rates (0.1 nM N d^{-1}). This finding contradicts the N* profile that suggests the main N sink in the core OMZ (Fig. 4). Oxygen inhibition cannot explain the lack of anammox in the core OMZ. In general, oxygen concentrations in the OMZ were well below the inhibiting concentration for the anammox process (10 μM, Jensen et al. (2008)). We suggest that anammox in the core OMZ was indirectly limited by low organic matter concentrations, whereas in the shallower oxycline at 80-100 m depth, anammox

activity was presumably favored by particulate organic matter (POM) that was exported from the overlying mixed layer.

Although autotrophic, anammox depends on heterotrophic mineralization processes that provide NH_4^+ and NO_2^-. This was recently shown by Lam et al. (2009) for the Peruvian OMZ, where a mixture of nitrate reduction to nitrite, dissimilatory nitrate reduction to ammonium (DNRA), micro-aerobic ammonium oxidation and, most probably, micro-aerobic mineralization provided the major fraction of the required NH_4^+ and NO_2^- for the anammox reaction. Lam et al. estimated that mineralized nitrogen accounts for roughly 50% of the N-loss in the Peruvian OMZ. Furthermore they showed that the demand of organic matter, necessary to indirectly fuel the anammox reaction, exceeds the organic matter demands of heterotrophic denitrification.

In our study, the BBL can be seen as another site where NH_4^+ and NO_2^- were supplied from coexisting heterotrophic mineralization processes. Nutrient concentration profiles derived from the BBL-Profiler and the BWS indicated the efflux of NH_4^+ and NO_2^- from the sediment into the BBL (Fig. 5) which could have enhanced the anammox rates in the BBL. In fact, the highest anammox rates were measured in the BBL at station GeoB12216, where the efflux of NH_4^+ and NO_2^- was most pronounced (compare Fig. 5 and 6). It was already suggested by Woebken et al. (2007) that anammox bacteria may find favorable conditions in the BBL and even extend their residence time in the BBL by sticking to particles.

To derive areal N-loss rates we integrated the N-loss over the entire water column, using N-loss averages of 4, 1 and 0.1 nM N d^{-1} in the BBL (only when suboxic), in the lower oxycline and in the rest of the OMZ (background rates), respectively. The vertical dimensions of the oxycline and the BBL were considered with 20 m and 75 m, respectively. The depth-integrated N-loss rates varied between 0.16 and 0.24 mmol N m^{-2} d^{-1} (Fig. 10). The N-loss of 0.16 mmol N m^{-2} d^{-1} at the deepest station (GeoB12208), which may be comparable to the water column N-loss further offshore, is well below the average values of 3.5 and 5.4 mmol N m^{-2} d^{-1} previously estimated by Bange et al. (2000) and Devol et al. (2006) (Table 2), respectively. The estimates from Bange were based on N-deficit measurements during the southwest monsoon season in the central and western Arabian Sea. The estimates from Devol et al. were derived from isotope pairing experiments during various cruises in the central and eastern Arabian Sea. Devol incubated samples from between 200 and 300 m depth of which the average N-loss rate of 9 nM N d^{-1} was then extrapolated to a 600 m strong OMZ. Altogether, the discrepancy between our results and those of Bange and Devol may be

explained in parts by the mode of data extrapolation as well as by the seasonal and spatial variability of N-loss processes.

High temporal and spatial variability of surface chlorophyll concentrations in the Arabian Sea were observed by satellite imaging (Wiggert et al. 2005). The temporal variation of mixed layer depth, primary production and particulate matter export strongly depend on the monsoon cycle (Marra 2002; Rixen et al. 2002; Rixen et al. 2005). In our study, the very shallow mixed layer depth of 25-35 m, the weak winds and the increased sea surface temperatures were typical for the inter-monsoon season in October (Rixen et al. 2005). During inter-monsoon, chlorophyll concentrations in the mixed layer usually decrease (Marra 2002) and the ocean surface waters become oligotrophic (Wiggert et al. 2005). Indeed, chlorophyll concentrations at the same stations measured 24 days later during a subsequent cruise (M74/3) were decreased by 8-10 mg m^{-2}. Furthermore, the mixed layer was well separated from the lower water column by a very pronounced and stable pycnocline with stability frequencies of around 10 cycles per hour which were comparable to those found e.g. in the northern tropical Atlantic (Bahamon et al. 2003). Thus, the strong pycnocline minimized the mixing of nutrients from lower water masses into the mixed layer as well as the export of particulate organic matter from the mixed layer into lower water masses. Further evidence for low mineralization rates in the OMZ was given by the very low oxygen consumption rates in the PGW intrusion that were modeled using salinity and oxygen profiles obtained during this cruise.

Oxygen consumption in the water column

Where oxygen is present, its consumption may be used as proxy for the mineralization rates in the water column (Suess 1980). Oxygen consumption in the Persian Gulf Water (PGW) intrusion was determined from a mixing model using salinity and oxygen concentration profiles. With the PGW, oxygen was laterally transported into the OMZ (Fig. 2). The PGW intrusion and the mixing with deeper water masses was apparently constant over time because no significant deviation was found below 290 m depth for salinity and oxygen profiles obtained from two adjacent sites that were sampled 11 days apart (Fig. 11). Below 290 m, mixing of PGW with deeper water led to a gradual decrease in temperature and salinity (Fig. 12). The linear relationship of temperature versus salinity at these depths was observed for all stations (Fig. 3). Oxygen consumption in the PGW caused a significant non-linear relationship of oxygen versus salinity (Fig. 12).

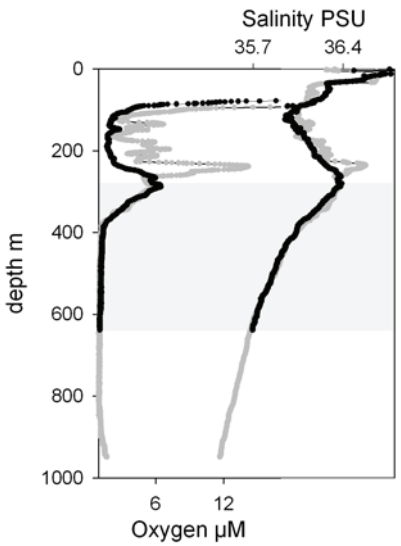

Figure 11: Comparing oxygen and salinity profiles of station GeoB 12204 (black) and GeoB12216 (grey). The grey area marks the depth range of constant mixing

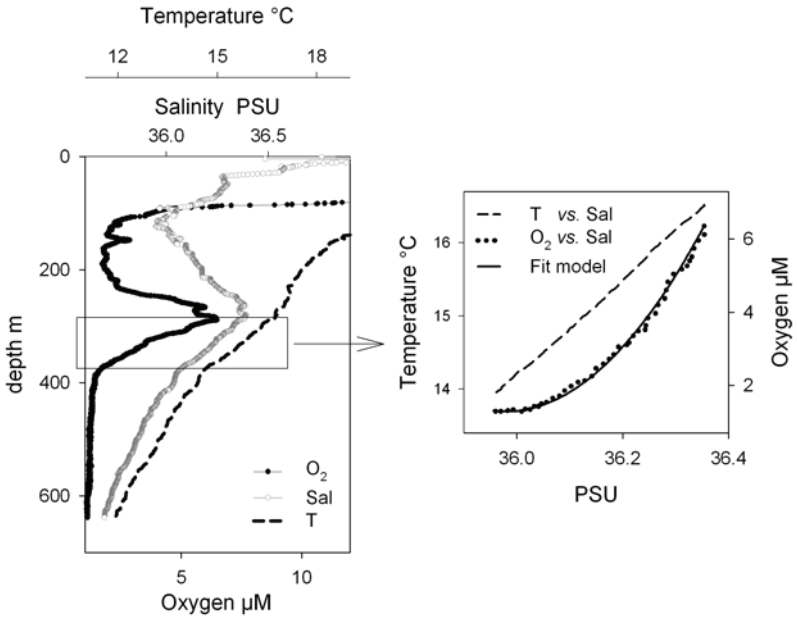

Figure 12: left side: comparing temperature, salinity, oxygen profiles of station GeoB 12204. Right side: Temperature and oxygen as a function of salinity for the depths between 260 and 390m.

The oxygen consumption rates in these depths (from ~260 m to ~390 m) were determined using a simplified 1-dimensional model assuming a steady state situation. Furthermore, we assumed that eddy diffusivities (*Ez*) and oxygen consumption rates (*R*) did not change significantly with depth (see below). The oxygen concentration (C_{ox}) at depth (*z*) can be described by the following second order equation:

$$Ez \cdot \frac{\partial^2 C_{OX}}{\partial z^2} = -R \qquad \text{E 7}$$

For known oxygen concentrations C_{ox}^{up} and C_{ox}^{low} at the upper and the lower boundary of a depth interval *L* we obtained the analytical solution:

$$C_{ox}(z) = -\frac{1}{2}\frac{R}{Ez}z^2 + \left(\frac{1}{L}\left(C_{ox}^{low} - C_{ox}^{up}\right) + \frac{L}{2}\frac{R}{Ez}\right)z + C_{ox}^{up} \qquad \text{E 8}$$

where at the upper boundary $z = 0$ and at the lower boundary $z = L$. Salinity is a conservative tracer with $R = 0$. Thus, for salinity equation 8 simplifies to:

$$C_{sal}(z) = \frac{1}{L}\left(C_{sal}^{low} - C_{sal}^{up}\right)z + C_{sal}^{up} \qquad \text{E 9}$$

where C_{sal}^{up} and C_{sal}^{low} are the salinities at the upper and the lower boundary. Equation 9 can be solved for z and substituted into equation 8 to describe oxygen concentrations C_{ox} as a function of salinity C_{sal} :

$$C_{ox} = -\frac{1}{2}\frac{R}{Ez}\left(\frac{C_{sal} - C_{sal}^{up}}{C_{sal}^{low} - C_{sal}^{up}} L\right)^2 + \left(\frac{1}{L}\left(C_{ox}^{low} - C_{ox}^{up}\right) + \frac{L}{2}\frac{R}{Ez}\right)\left(\frac{C_{sal} - C_{sal}^{up}}{C_{sal}^{low} - C_{sal}^{up}} L\right) + C_{ox}^{up} \quad \text{E 10}$$

Therewith, we replaced water depth, the independent variable in equation 8, with salinity. This accounted for small scale vertical advection (e.g. salt fingers) and variations of *Ez* that caused increased scatter of the O_2-depth profile but did not affect the O_2-salinity profile. *Ez* was calculated according to Gregg et al. (1986) from the Brunt-Väisälä-Frequency N (equation 1) and the turbulent kinetic energy dissipation rate ε :

$$Ez = \frac{\gamma \varepsilon}{N^2} \quad \text{E 11}$$

with the mixing coefficient γ . We applied a mean $\gamma \varepsilon$ of 3.7 x 10^{-10} W kg^{-1}. This value was measured by Gregg et al. (1986) for the open ocean thermocline and was applied in several rate diffusion models (Fennel 1995; Lam et al. 2007).

A precondition for the model application was a linear density gradient for the respective depth range indicating a constant *Ez*. Our model was then applied to the oxygen and salinity profiles of station GeoB12204, GeoB12208 and GeoB12216 for depths with measurable oxygen concentrations (i.e. the PGW intrusions between 265 m and 385 m). The model was not applied to the shallow station GeoB12203/10, because there PGW could not mix with deep waters. In addition, the model was applied to the lower boundary of the OMZ between 950 m and 1400 m depth at station GeoB12208 (see Fig. 2). There, oxygenated bottom water was constantly mixed into the OMZ. Steady state mixing was indicated from identical salinity and oxygen profiles measurements during a subsequent cruise 3 weeks later (data not shown).

All variables in equation 10 could be estimated from measurements except for the oxygen consumption rate (*R*). Oxygen consumption rates were determined by fitting the modelled oxygen concentrations to the measured oxygen concentrations using a least square fit. Table 3 summarizes the input parameters, the modelled oxygen consumption rates and the coefficient of determination of the curve fitting. The calculated eddy diffusivities in the PGW were similar at all stations (average 1.7 x 10^{-5} m^2 s^{-1}) and were comparable to estimates from

Ledwell et al. (1998) who determined eddy diffusivities between 1.2×10^{-5} and 1.7×10^{-5} m² s^{-1} from a tracer release experiment in the subtropical North Atlantic at 300 m depth with density gradients comparable to this study. Similar values of *Ez* (1×10^{-5} m² s^{-1}) estimated from microstructure measurements below the mixed layer in various open ocean settings were reviewed by Wunsch and Ferrari (2004). However, in the lower OMZ (station GeoB12208), eddy diffusivity was increased by a factor of 5 because density gradients were less pronounced.

Table 3: Input parameter for equation 9: water depths of upper (z^{up}) and lower (z^{low}) boundary of the model with the respective salinities (C_{sal}^{up}, C_{sal}^{low}) and O_2 concentrations (C_{ox}^{up} and C_{ox}^{low}). Eddy diffusivity (Ez), calculated from the stability frequency according to equation 1 and 10. Right columns: the modeled O_2 consumption and coefficient of determination (R^2)

Station	z^{up}	z^{low}	C_{ox}^{up}	C_{ox}^{low}	C_{sal}^{up}	C_{sal}^{low}	N	Ez	O_2 consumption	
GeoB	m	m	µM	µM	PSU	PSU	cycles h^{-1}	m² s^{-1}	nM d^{-1}	R²
12204	290	385	6.4	1.5	36.35	36.05	2.79	1.56E-05	1.14	0.992
12216	290	385	5.7	1.2	36.36	36.08	2.66	1.72E-05	1.06	0.982
12208	265	350	13	1.6	36.49	36.10	2.70	1.66E-05	4.20	0.959
12208	950	1400	1.2	24.4	35.45	35.12	1.18	8.66E-05	1.60	0.999

For all stations, very low oxygen consumption rates were determined that varied between 1 and 4 nM d^{-1}. To date, there is no method that could experimentally verify such low rates. However, our results can be compared with estimates derived from organic carbon flux models. Applying the flux model provided by Suess (1980) for a primary production in the surface water between 25 and 120 mmol C m^{-2} d^{-1}, which is comparable to values for the inter monsoon season in the Arabian Sea, (Marra 2002), resulted in oxygen consumption rates between 16 and 52 nM d^{-1} at 350 m water depth. Another flux model, provided by Rixen et al. (2005), is based on sediment trap data from the central Arabian Sea and yielded rates between 1.3 and 32 nM d^{-1}. Our estimates fell within this range.

O_2 consumption was low and could have been limited either by O_2 concentration or by organic matter availability. O_2 concentrations in the PGW were well above 1 µM. The half saturation constant for microbial oxygen respiration (K_{ox}) in these waters is not known, but from respiration experiments (Canfield et al. 2005; Daebel et al. 2007) and bacterial cytochrome oxidase kinetics (Poole 1983) there is evidence that K_{ox} is below 1 µM. To estimate the potential error of the model, the oxygen consumption rate R in equation 10 is replaced by the oxygen-dependent rate $R(C_{ox})$ calculated according to the Michaelis-Menten equation $R(C_{ox}) = R_{\max} \cdot C_{ox} / (K_{ox} + C_{ox})$ with $K_{ox} = 1$ µM. Fitting equation 10 to the

measured oxygen and salinity data resulted in R_{max} that were ~20 % above the previous estimates assuming no limitation. O_2 concentrations, therefore, do not explain the low O_2 consumption rates. Instead, we suggest that rates were limited by low organic matter concentrations due to a decreasing POM export from surface waters.

Concluding remarks

We observed very low anammox and O_2 consumption rates in the OMZ during the inter-monsoon season. Although anammox is a chemoautotrophic pathway it strongly depends on heterotrophic processes and thus on the availability of organic matter (Lam et al. 2009). The export of organic matter to lower water masses could therefore control anammox activity. We suggest that the observed decrease of primary productivity and the strengthening of the pycnocline reduced the flux of particulate organic matter into the OMZ and thus lowered anammox as well as O_2 consumption rates in the PGW. Investigating the link from particulate organic matter flux to N_2 production via anammox will be a challenging task for future studies. To resolve the interactions and temporal dynamics of all related processes, experiments and rate estimates from e.g. incubation experiments become more important. In this study, N-loss estimates were based on incubation experiments and thus reflect the instantaneous N-loss from the water column. These rates were low (0.16 mmol N m^{-2} d^{-1}) compared to the N-loss rate estimates from N* budget calculations that range from 0.63 to 6.3 mmol N m^{-2} d^{-1}, (Bange et al. 2000). In the following, we briefly discuss this discrepancy and offer three explanations:

i) N-loss rates derived from N* budget calculations strongly depend on the estimated residence time of OMZ waters. Olsen (1993) used average trichlorofluoromethane (CFM) concentrations and a simplified box model to calculate a residence time of 10 (+/-4) years for the bulk Arabian Sea. Naqvi (1993) argued that the relatively shallow core of the OMZ must be replaced faster than within 10 years and estimated a residence time of the core OMZ of around 1 year. A residence time between 1 and 10 years was assumed in several publications (Bange et al. 2000; Codispoti et al. 2001; Devol et al. 2006). While N-deficit measurements and calculations were improved in recent years, estimates for the renewal of OMZ waters were hardly reassessed and remain somewhat speculative. It is therefore possible that average N-loss rates based on N-deficit calculations were overestimated due to an underestimation of the residence time of the core OMZ.

ii) While our estimates reflect the instantaneous N-loss rates, those from N* budget calculation reflect the N-loss over long time scales in the range of the residence time of OMZ

waters. Thus, the discrepancy between instantaneous and average N-loss rates might be explained by seasonal variability. Low N-loss rates during the inter-monsoon season may be followed by well above average rates during the monsoon season. Assuming average N-loss rates between 0.63 and 6.3 mmol N m^{-2} d^{-1} (Bange et al. 2000) the low rates during the inter-monsoon (0.16 mmol N m^{-2} d^{-1}) need to be compensated by rates that are increased by a factor of 5 to 50 during the monsoon season. This variability is very high. However, for average N-loss rates based on OMZ residence times of 10 years (0.63 mmol N m^{-2} d^{-1}, (Bange et al. 2000)) a factor of 5 seems reasonable.

iii) In our study, the strong N-deficit at 500-600 m depth (N* Fig. 4) did not match with increased anammox rates in the oxycline and in the BBL. However, the N* profile agreed well with the depth distribution of sedimentary N-loss rates (Fig. 9). Given the sedimentary N-loss rates that were 2 to 3-fold above the water column rates we suggest that the N-deficit in the investigated water column was rather due to sedimentary instead of water column N-loss. The Arabian Sea is a semi-enclosed sea with ~15% of its area consisting of shelf and ocean margin waters (Bange et al. 2000). Thus, a considerable amount of sedimentary N-loss can contribute to the water column N-deficit. How far the sedimentary influence extends into the open ocean, however, depends on the mixing and residence time of OMZ waters.

In summary, our results indicate that water column N-loss in the Arabian Sea is less prominent than previously described and that sedimentary N-loss contributes substantially to the N-deficit in ocean margin waters. Strong seasonal variability of water column N-loss in response to variable primary production and water column stratification needs to be considered. A better understanding of the linkage between organic matter availability in the OMZ and anammox/denitrification is needed as well as more data about the spatial and seasonal variation of water column and sedimentary N-loss in the Arabian Sea.

References

Bahamon, N., Z. Velasquez, and A. Cruzado. 2003. Chlorophyll a and nitrogen flux in the tropical North Atlantic Ocean. Deep-Sea Research Part I-Oceanographic Research Papers **50:** 1189-1203.

Bange, H. W., S. W. A. Naqvi, and L. A. Codispoti. 2005. The nitrogen cycle in the Arabian Sea. Progress in Oceanography **65:** 145-158.

Bange, H. W. and others 2000. A revised nitrogen budget for the Arabian Sea. Global Biogeochemical Cycles **14:** 1283-1297.

Braman, R. S., and S. A. Hendrix. 1989. Nanogram Nitrite and Nitrate Determination in Environmental and Biological-Materials by Vanadium(Iii) Reduction with Chemi-Luminescence Detection. Analytical Chemistry **61:** 2715-2718.

Canfield, D., B. Thamdrup, and E. Kristensen [eds.]. 2005. Aquatic Geomicrobiology. Elsevier.

Cline, J. D. 1969. Spectrophotometric determination of hydrogen sulfide in natural waters. Limnology and Oceanography **14:** 454-458.

Codispoti, L. A. and others 2001. The oceanic fixed nitrogen and nitrous oxide budgets: Moving targets as we enter the anthropocene? Scientia Marina **65:** 85-105.

Daebel, H., R. Manser, and W. Guer. 2007. Exploring temporal variations of oxygen saturation constants of nitrifying bacteria. Water Research **41:** 1094-1102.

Dalsgaard, T., B. Thamdrup, and D. E. Canfield. 2005. Anaerobic ammonium oxidation (anammox) in the marine environment. Research in Microbiology **156:** 457-464.

Dalsgaard, T., B. Thamdrup, and M. M. Jensen. 2006. Nitrogen cycling in sub-oxic water columns. Gayana **70:** 14-18.

Deutsch, C., N. Gruber, R. M. Key, J. L. Sarmiento, and A. Ganachaud. 2001. Denitrification and N2 Fixation in the Pacific Ocean. Global Biogeochem. Cycles **15:** 483-506.

Devol, A. H. and others 2006. Denitrification rates and excess nitrogen gas concentrations in the Arabian Sea oxygen deficient zone. Deep-Sea Research Part I-Oceanographic Research Papers **53:** 1533-1547.

Falkowski, P. G., R. T. Barber, and V. Smetacek. 1998. Biogeochemical controls and feedbacks on ocean primary production. Science **281:** 200-206.

Fennel, W. 1995. A Model of the Yearly Cycle of Nutrients and Plankton in the Baltic Sea. Journal of Marine Systems **6:** 313-329.

Glud, R. N. and others 2009. Nitrogen cycling in a deep ocean margin sediment (Sagami Bay, Japan). Limnology and Oceanography **54:** 723-734.

Grasshoff, K., K. Kremling, and M. Ehrhardt. 1999. Methods of seawater analysis, 3 ed. Wiley-VCH.

Gregg, M. C., E. A. Dasaro, T. J. Shay, and N. Larson. 1986. Observations of Persistent Mixing and near-Inertial Internal Waves. Journal of Physical Oceanography **16:** 856-885.

Gruber, N. 2004. The dynamics of the marine nitrogen cycle and its influence on atmospheric CO2 variations, p. 97-148. *In* M. Follows and T. Oguz [eds.], The ocean carbon cycle and climate. NATO ASI Series. Kluwer Academic.

Gruber, N., and J. L. Sarmiento. 1997. Global patterns of marine nitrogen fixation and denitrification. Global Biogeochemical Cycles **11:** 235-266.

Hall, P. O., and R. C. Aller. 1992. Rapid, Small-Volume, Flow-Injection Analysis for Sigma-Co2 and Nh4+ in Marine and Fresh-Waters. Limnology and Oceanography **37:** 1113-1119.

Hamersley, M. R. and others 2007. Anaerobic ammonium oxidation in the Peruvian oxygen minimum zone. Limnology and Oceanography **52:** 923-933.

Hogslund, S., N. P. Revsbech, T. Cedhagen, L. P. Nielsen, and V. A. Gallardo. 2008. Denitrification, nitrate turnover, and aerobic respiration by benthic foraminiferans in the oxygen minimum zone off Chile. Journal of Experimental Marine Biology and Ecology **359:** 85-91.

Holmes, R. M., A. Aminot, R. Kerouel, B. A. Hooker, and B. J. Peterson. 1999. A simple and precise method for measuring ammonium in marine and freshwater ecosystems. Canadian Journal of Fisheries and Aquatic Sciences **56:** 1801-1808.

Howell, E. A., S. C. Doney, R. A. Fine, and D. B. Olson. 1997. Geochemical estimates of denitrification in the Arabian Sea and the Bay of Bengal during WOCE. Geophysical Research Letters **24:** 2549-2552.

Jensen, M. M., M. M. M. Kuypers, G. Lavik, and B. Thamdrup. 2008. Rates and regulation of anaerobic ammonium oxidation and denitrification in the Black Sea. Limnology and Oceanography **53:** 23-36.

Jørgensen, B. B., and V. A. Gallardo. 1999. *Thioploca spp*: filamentous sulfur bacteria with nitrate vacuoles. Fems Microbiology Ecology **28:** 301-313.

Kuypers, M. M. M. and others 2005. Massive nitrogen loss from the Benguela upwelling system through anaerobic ammonium oxidation. Proceedings of the National Academy of Sciences of the United States of America **102:** 6478-6483.

---. 2003. Anaerobic ammonium oxidation by anammox bacteria in the Black Sea. Nature **422:** 608-611.

Lam, P. and others 2007. Linking crenarchaeal and bacterial nitrification to anammox in the Black Sea. Proceedings of the National Academy of Sciences of the United States of America **104:** 7104-7109.

---. 2009. Revising the nitrogen cycle in the Peruvian oxygen minimum zone. Proceedings of the National Academy of Sciences of the United States of America **106:** 4752-4757.

Ledwell, J. R., A. J. Watson, and C. S. Law. 1998. Mixing of a tracer in the pycnocline. Journal of Geophysical Research-Oceans **103:** 21499-21529.

Marra, J. 2002. Primary Productivity in the Arabian Sea, p. 24-29. *In* L. Watts, P. H. Burkill and S. Smith [eds.], Report of the Indian Ocean Synthesis Group on the Arabian Sea Process Study. JGOFS International Project Office.

Middelburg, J. J., K. Soetaert, P. M. J. Herman, and C. H. R. Heip. 1996. Denitrification in marine sediments: A model study. Global Biogeochemical Cycles **10:** 661-673.

Mulder, A., A. A. Vandegraaf, L. A. Robertson, and J. G. Kuenen. 1995. Anaerobic Ammonium Oxidation Discovered in a Denitrifying Fluidized-Bed Reactor. FEMS Microbiology Ecology **16:** 177-183.

Naik, H., and S. W. A. Naqvi. 2002. Sedimentary nitrogen cycling over the western continental shelf of India. EOS – Transactions of the American Geophysical Union.

Naqvi, S. W. A. 1994. Denitrification Processes in the Arabian Sea. Proceedings of the Indian Academy of Sciences-Earth and Planetary Sciences **103:** 279-300.

Naqvi, S. W. A. and others 2006. Coastal versus open-ocean denitrification in the Arabian Sea. Biogeosciences **3:** 621-633.

Naqvi, S. W. A., and M. S. Shailaja. 1993. Activity of the respiratory electron transport system and respiration rates within the oxygen minimum layer of the Arabian Sea. Deep-Sea Research Part Ii-Topical Studies in Oceanography **40:** 687-695.

Olson, D. B., G. L. Hitchcock, R. A. Fine, and B. A. Warren. 1993. Maintenance of the Low-Oxygen Layer in the Central Arabian Sea. Deep-Sea Research Part Ii-Topical Studies in Oceanography **40:** 673-685.

Poole, R. K. 1983. Bacterial Cytochrome Oxidases - a Structurally and Functionally Diverse Group of Electron-Transfer Proteins. Biochimica Et Biophysica Acta **726:** 205-243.

Risgaard-Petersen, N. and others 2006. Evidence for complete denitrification in a benthic foraminifer. Nature **443:** 93-96.

Risgaard-Petersen, N., L. P. Nielsen, S. Rysgaard, T. Dalsgaard, and R. L. Meyer. 2003. Application of the isotope pairing technique in sediments where anammox and denitrification coexist. Limnology and Oceanography-Methods **1:** 63-73.

Rixen, T., M. V. S. Guptha, and V. Ittekkot. 2002. Sedimentation, p. 65-73. *In* L. Watts, P. H. Burkill and S. Smith [eds.], Report of the Indian Ocean Synthesis Group on the Arabian Sea Process Study. JGOFS International Project Office.

---. 2005. Deep ocean fluxes and their link to surface ocean processes and the biological pump. Progress in Oceanography **65:** 240-259.

Rysgaard, S., R. N. Glud, N. Risgaard-Petersen, and T. Dalsgaard. 2004. Denitrification and anammox activity in Arctic marine sediments. Limnology and Oceanography **49:** 1493-1502.

Sauter, E. J., M. Schluter, J. Wegner, and E. Labahn. 2005. A routine device for high resolution bottom water sampling. Journal of Sea Research **54:** 204-210.

Schmaljohann, R., M. Drews, S. Walter, P. Linke, U. Vonrad, and J. F. Imhoff. 2001. Oxygen-minimum zone sediments in the northeastern Arabian Sea off Pakistan: a habitat for the bacterium *Thioploca* (vol 211, pg 27, 2001). Marine Ecology-Progress Series **220:** 295-295.

Schwartz, M. C., C. Woulds, and G. L. Cowie. 2009. Sedimentary denitrification rates across the Arabian Sea oxygen minimum zone. Deep Sea Research Part II: Topical Studies in Oceanography **In Press, Corrected Proof**.

Suess, E. 1980. Particulate Organic-Carbon Flux in the Oceans - Surface Productivity and Oxygen Utilization. Nature **288:** 260-263.

Thamdrup, B., and T. Dalsgaard. 2002. Production of N-2 through anaerobic ammonium oxidation coupled to nitrate reduction in marine sediments. Applied and Environmental Microbiology **68:** 1312-1318.

Thamdrup, B., T. Dalsgaard, M. M. Jensen, O. Ulloa, L. Farias, and R. Escribano. 2006. Anaerobic ammonium oxidation in the oxygen-deficient waters off northern Chile. Limnology and Oceanography **51:** 2145-2156.

Wiggert, J. D., R. R. Hood, K. Banse, and J. C. Kindle. 2005. Monsoon-driven biogeochemical processes in the Arabian Sea. Progress in Oceanography **65:** 176-213.

Woebken, D., B. A. Fuchs, M. A. A. Kuypers, and R. Amann. 2007. Potential interactions of particle-associated anammox bacteria with bacterial and archaeal partners in the Namibian upwelling system. Applied and Environmental Microbiology **73:** 4648-4657.

Wunsch, C., and R. Ferrari. 2004. Vertical mixing, energy and the general circulation of the oceans. Annual Review of Fluid Mechanics **36:** 281-314.

Aerobic respiration rates in the benthic boundary layer of the Baltic and North Sea

Moritz Holtappels[1], Volker Brüchert[2], Marcel M.M. Kuypers[1]

1) Max Planck Institute for Marine Microbiology, Celsiusstrasse 1, 28359 Bremen

2) Department of Geology and Geochemistry, Stockholm University, 10691 Stockholm, Sweden

Acknowledgement

We thank Lars Umlauf (Leibniz Institute for Baltic Sea Research, Warnemünde) and Sabine Kasten (Alfred Wegener Institute for Polar and Marine Research, Bremerhaven) who provided ship time on *RV Alkor* and *RV Heincke*. We gratefully thank Gabriele Klockgether for analytical assistance and the crews of *RV Heinke* and *RV Alkor* for excellent collaboration. This study was funded through DFG-Research Center / Excellence Cluster „The Ocean in the Earth System" and the Max Planck Society.

Abstract

Oxygen consumption was measured in the benthic boundary layer (BBL) of the German Bight (North Sea) and the Bornholm Basin (Baltic Sea). Samples were collected from different depths above the sediment, and oxygen consumption rates were measured during incubation experiments using oxygen optodes. Oxygen consumption rates were compared to concentrations of suspended particulate matter and to particulate organic matter (POM) composition. Oxygen consumption rates in the BBL of the German Bight (average 20 μM O_2 d^{-1}) were increased compared those in the Bornholm Basin (average 6 μM O_2 d^{-1}). Correlation between oxygen consumption rates and the quantity or quality of particulate organic matter (POM) was poor indicating that POM did not fuel aerobic respiration. Instead, our results may indicate that oxygen consumption was due to the mineralization of dissolved organic matter.

Introduction

In the benthic boundary layer (BBL), the increased shear stress and turbulent mixing favor the re-suspension of sediments and the accumulation of suspended particulate matter (Hill and McCave 2001). The suspended material is eventually transported laterally with the bottom water from sites of increased hydrodynamic energy to sites where decreased current velocities allow the deposition of sediments (Emeis et al. 2002; Inthorn et al. 2006a; van Weering et al. 2001). During the transport, the organic fraction of the suspended material can be altered due to biological mineralization (Inthorn et al. 2006b).

The organic content and biogenic composition of particles in the BBL were described in several studies of Thomsen and Graf (1994), Ritzrau and Thomsen (1997), and Emeis et al. (2002) who found at various settings an increase of particulate organic carbon (POC) in the BBL compared to the adjacent water column. It is assumed that the accumulation of POC in the BBL leads to enhanced mineralization rates that may even exceed sedimentary mineralization rates (Thomsen et al. 2002). However, only a few studies did actually measure POM turnover rates in the bottom water. Ritzrau et al. (1996) measured microbial activity in the BBL off Greenland using ^{14}C-amino acids. They found increased utilization of ^{14}C-amino acids in the BBL that, however, were not correlated to concentrations of particulate organic carbon (POC).

There is no study to our knowledge that uses oxygen consumption measurements to determine the carbon mineralization rates in the BBL. In general, oxygen consumption measurements in the water column are scarce mainly because the rates in the ocean are expected to be low (<1 μM O_2 d^{-1}in the thermocline of the open ocean; Suess 1980) and thus difficult to detect with common Winkler technique over incubation intervals of several hours. Indirect estimates of oxygen consumption such as concentration-flux models (see chapter 3) or the apparent oxygen utilization (AOU) (e.g. Paulmier et al. 2008) work only for the intermediate water column where oxygen concentrations are not biased by the sedimentary oxygen uptake.

Recently, the accuracy of oxygen concentration measurements has been improved by the development of oxygen optodes (Tengberg et al. 2006) and the invention of a drift compensated Clark-type oxygen microsensor (Revsbech et al. 2009) that combine high sensitivity a few nanomole with sufficient signal stability over time. Oxygen optodes were recently used by Warkentin et al. (2007) to measure the respiration rates of plankton

communities in a Freshwater systems. The rates (0.7 to 15.6 μM O_2 per hour) were, however, much above the expected rates in marine systems.

In this study, we measured oxygen consumption rates in the bottom water that was sampled at two sites with very distinct current regimes: in the German Bight (North Sea) where the BBL is influenced by strong tidal currents and in the Bornholm Basin (Baltic Sea) where tides are negligible and currents velocities are low. Water samples were taken from different depths above the sediment. Oxygen consumption was measured over a time course of several hours using oxygen optodes and compared to concentrations of suspended particulate matter and particulate C/N ratios. The influence of POM quantity and quality on the oxygen consumption is discussed.

Methods

Study site and sampling procedure

Bottom water samples were collected during a cruise with the *RV Heincke* to the German Bight (GB) in September 2007 and during a cruise with the *RV Alkor* to the Bornholm Basin (BB) in April 2008 (Table 1). Four stations were sampled in the German Bight (Table 1) of which stations GB 1, GB 2 and GB 4 were located in areas with sandy sediment and station GB 3 was located in the Helgoland mud area (Hebbeln et al. 2003). In the German Bight, bottom water was sampled 1.5 m, 3 m, 5 m, and 10 m above the sediment using Niskin bottles attached to a cable with a bottom weight. Once the weight reached the seafloor the Niskin bottles were closed by a messenger weight. At the shallow station (GB 2, 14 m depth) bottom water was sampled only in the lower 5 m above the sediment. After retrieving the samples the water was transferred into 5 L Duran bottles and stored in the dark at *in-situ* temperature until further treatment.

Six stations were sampled in the Bornholm Basin of which BB 3, BB 5 and BB 6 were in areas with sandy sediment, station BB 2 and BB 4 were in areas with muddy sediment and station BB 1 was in an area with muddy/clayish sediment (Table 1). Bottom water was sampled using the BBL-Profiler (see chapter 2). The BBL-Profiler consisted of a sampling frame carrying an oxygen optode (Model 3830, Aanderaa), a CTD (SBE 16 SeaCat, Sea-Bird Electronics), an acoustic Doppler velocimeter (Vectrino, Nortek AS) and a horizontally attached Niskin Bottle. The BBL-Profiler was deployed to the sea floor for 2-5 hours while connected to a surface marker buoy. The automatic sampling procedure started with a delay of at least 30 minutes to allow the drift of artificially resuspended sediment from the

Table 1: List of stations, positions, water depths and corresponding sediment characteristics, temperatures and salinities.

Station	Date	Lat N	Lon E	Water depth m	Sample depth m above seafloor.	Sediment type	Temp. °C	Salinity PSU
GB 1	05.09.2007	54°10.77'	8°2.37'	28.5	1.5, 3, 5, 10	mixed sand	17.0	31.4
GB 2	07.09.2007	54°13.60'	8°23.55'	14	1.5, 3, 5	mixed sand	17.2	28.3
GB 3	09.09.2007	54°5.02'	8°0.00'	30	1.5, 3, 5, 10	mud	17.3	31.8
GB 4	11.09.2007	54°8.00'	7°50.30'	43	1.5, 3, 5, 10	mixed sand	17.1	31.1
BB 1	01.04.2008	55°15.02'	16°20.77'	65	0.5	clay/mud	7.5	14.2
BB 2	03.04.2008	54°56.50'	16°05.91'	67	0.1	mud	8	13.8
BB 3	04.04.2008	54°54.00'	16°14.34'	35	0.5	mixed sand	4.5	8.1
BB 4	05.04.2008	54°55.86'	16°08.98'	56	0.5	mud	7.2	11.4
BB 5	06.04.2008	55°10.06'	16°59.92'	58	0.5	mixed sand	5.8	10.3
BB 6	07.04.2008	55°11.13'	17°00.05'	71	0.5	mixed sand	5.6	9.7

BBL-Profiler deployment. Bottom water was sampled with the Niskin bottle at the end of the deployment at 0.5 m above the sediment, except at station BB 2 where the BBL-Profiler sank into the muddy sediment and water was sampled at approximately 0.1 m above the sediment. After retrieving the samples, the water was transferred into 5 L Duran bottles and stored in the dark at *in-situ* temperature until further treatment.

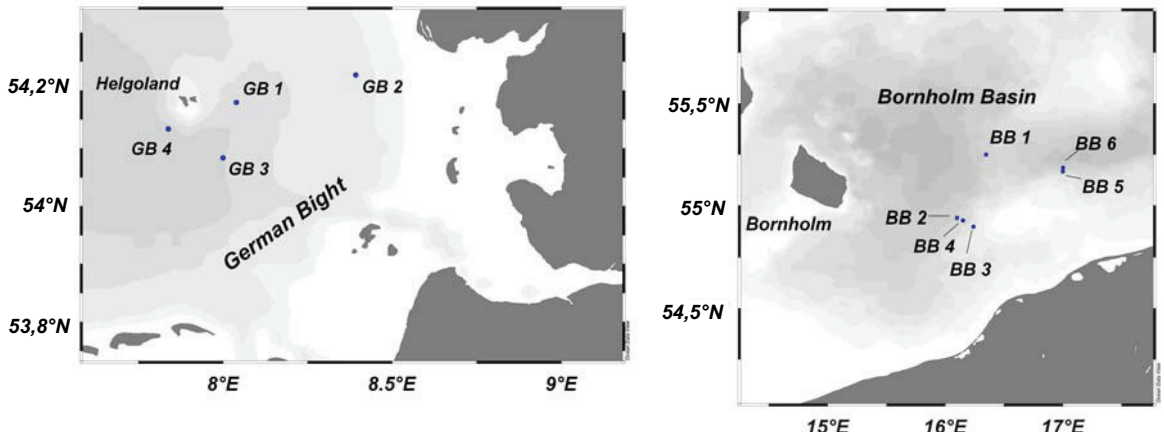

Figure 1: Sites in the German Bight (GB, left) sampled in September 2007 and sites in the Bornholm Basin (BB, right) sampled in April 2008.

Oxygen consumption measurement

Within two hours after sampling, the water sample was carefully transferred into a 3000 ml glass incubation chamber (Figure 2). Before sub sampling, the water samples were carefully stirred to evenly distribute the suspended particulate matter. The incubation chamber was subsequently sealed with a butyl stopper leaving no gas phase inside. An oxygen optode (Model 3830, Aanderaa Data Instruments, Norway) was situated inside the chamber. The electric cable was connected through the butyl stopper to a computer. The chamber content was gently stirred by a magnetic stirrer. The incubation chamber was kept in a water bath at *in-situ* temperatures. Respiration measurements were performed in the dark with oxygen concentrations being measured every 10 seconds for up to 40 hours.

The oxygen consumption rate was calculated from oxygen concentrations over time using the slope of the linear regression. As a control measurement, water samples at one station in the German Bight and in the Bornholm Basin were poisoned after the respiration measurement by injecting either 30 ml of 50% ZnCl (GB 4) or 15 ml of 18% HCl (BB 1). After each measurement, the glass incubation chambers and the optodes were thoroughly

cleaned using ethanol and deionized water. In the German Bight, samples from four different depths were incubated in parallel. Additionally, aerobic respiration rates were measured for filtered bottom water for a sample from station GB 2 (sampled at 3 m above sediment) and for all samples from station GB 4.

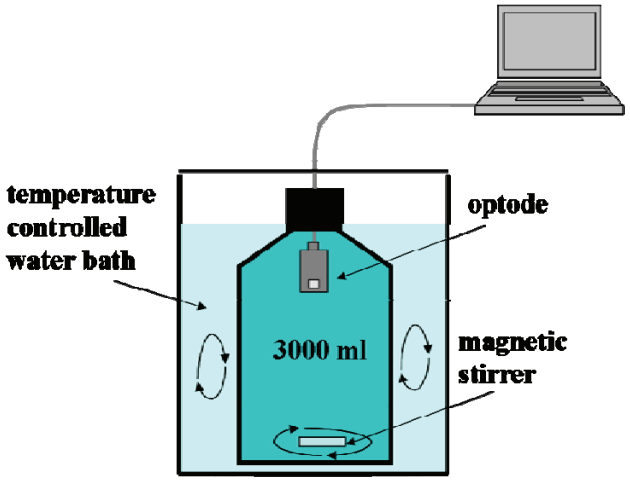

Figure 2: Schematic drawing of the set-up used for aerobic respiration rate measurements. Oxygen concentrations were measured online using an oxygen optode. The sample was kept in the dark at constant temperatures

Analysis of particulate matter

For the analysis of particulate matter, a subsample of ~1 L was drawn from the water samples. Before sub sampling, the water samples were carefully stirred to evenly distribute the suspended particulate matter. The samples for particle analysis were filtered on board onto precombusted and weighted Whatman glass fiber filters (GF/F) and stored frozen at –20°C. In the laboratory, filters were freeze dried and weighed to determine the concentration of suspended particulate matter. Inorganic carbon was removed by HCl-vapor treatment for 24 h in an exsiccator. Particulate organic carbon (POC) and particulate nitrogen were determined using an Elemental Analyzer (Fisons NA 1500 Series 2, Fison Instruments).

To express the aerobic respiration rates in relation to the concentration of particulate organic carbon the aerobic respiration rates were first converted to carbon mineralization rates assuming a respiratory quotient (RQ) of 106/138 = 0.77 (Froelich et al. 1979). Subsequently, the carbon mineralization rates were divided by the POC concentration to derive the POC specific respiration rates (in units: d^{-1}).

Results

In the German Bight, water temperatures ranged from 16.5 to 17.3 °C (Table 1, Figure 3) and salinity ranged from 28 to 33 PSU between the stations. In the German Bight the warmer and more saline bottom waters were separated from the cooler and less saline surface waters by a pycnocline situated at ~10 m water depth (Figure 3). Oxygen concentrations decreased from 220 µM at the surface to 200 µM at the bottom. Current velocities of the bottom water were not measured but are known to vary between 30 and 35 cm s^{-1} due to strong tidal currents

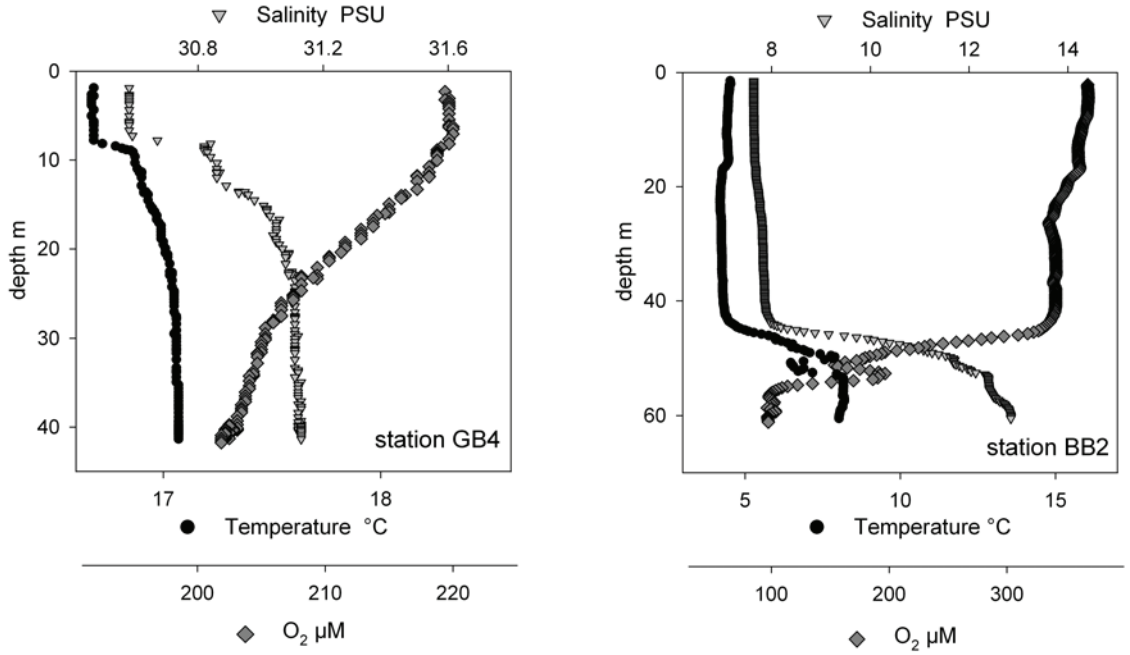

Figure 3: Depth profiles of temperature, salinity and oxygen of station GB4 (German Bight) and of station BB2 (Bornholm Basin).

(Klein 1995). Aerobic respiration rate measurements for stations in the German Bight are shown in Figure 4. Each plot shows the measurements from four different depths. The oxygen concentrations of the water samples were altered during sample transfer and as such the oxygen concentrations in the incubation chambers do not reflect the exact *in-situ* concentration. At stations GB 3 and GB 4, a decrease of oxygen concentrations was measured from the start of the experiment, whereas at stations GB 1 and GB 2 oxygen concentrations remained constant for up to 10 hours before values started decreasing. Some of the respiration

rate measurements showed high frequency fluctuations in oxygen concentrations which were probably due to a defect magnetic stirrer. Aerobic respiration rates were calculated from time intervals that showed a linear decrease in oxygen concentration (yellow box in Figure 4). In general, correlation coefficients (R^2) for the linear regressions were above 0.9 (Table 2).

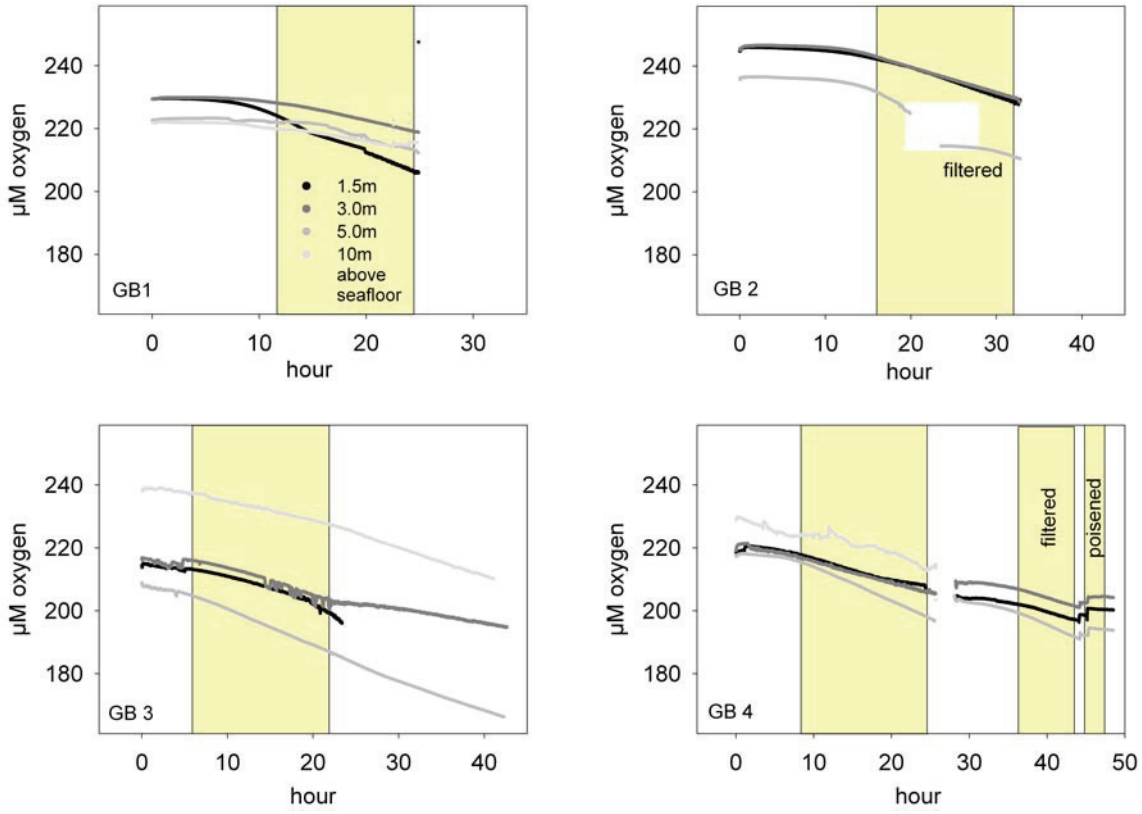

Figure 4: Change of oxygen concentrations over time in the benthic boundary layer of the German Bight. Water samples were taken in 1.5, 3, 5 and 10m above seafloor. The yellow background marks the time interval used to calculate aerobic respiration rates. At GB 4 and at GB 2 (at 3 m above sediment) aerobic respiration rates were also measured in filtered seawater. At GB 4, samples were poisoned at the end of the experiment and oxygen concentrations were monitored over time in the poisoned samples as control.

The respiration rates in the German Bight were high, ranging from 13 to 34 µM O_2 d^{-1}. At three stations (GB 2, GB 3 and GB 4), respiration rates maximized at 5 m above the sediment (Figure 5), whereas at station GB 1, the highest rate was found at 1.5 m above the seafloor. At station GB 4, suspended particles were removed by filtration after 24 hours and aerobic respiration rates were measured in the filtered seawater (Figure 4). The aerobic respiration rates in the filtered seawater were similar to the rates in the unfiltered seawater (Table 2). Adding ZnCl or HCL to the samples fully stopped aerobic respiration (Figure 4). In contrast to station GB 4, the aerobic respiration rates in the filtered seawater at station GB 2

(5 m depth) were decreased (10 µM O_2 d^{-1}) compared to the unfiltered seawater (34 µM O_2 d^{-1}).

In the German Bight, concentrations of suspended particulate matter in the samples ranged from 4 to 26 mg l^{-1} and correlated significantly ($p < 0.01$) with the particulate organic carbon (POC) and particulate nitrogen concentrations that ranged from 0.3 to 0.8 mg l^{-1} and from 0.05 to 0.11 mg l^{-1}, respectively (Table 2). The organic fraction of suspended particulate matter was between 2 and 10% and the molar C/N ratios ranged from 6.3 to 8.8. The vertical distributions of suspended particulate matter, POC and C/N ratios are shown in Figure 5. In general, suspended particulate matter concentrations were increased at 1.5 m above the sediment compared to those at 3 m above the sediment. However, at GB1 and GB2, highest suspended particulate matter concentrations were found at 5 m above the sediment. The POC concentrations at GB1, GB3 and GB4 showed a similar trend with increasing concentrations towards the sediment. The POC concentrations at GB2, however, maximized in the upper most sample. No trend was found for the vertical distributions of molar C/N ratios. Both, highest and lowest C/N ratios were found close to the sediment. Distant from the sediment C/N ratios were constant between 7.1 and 8.

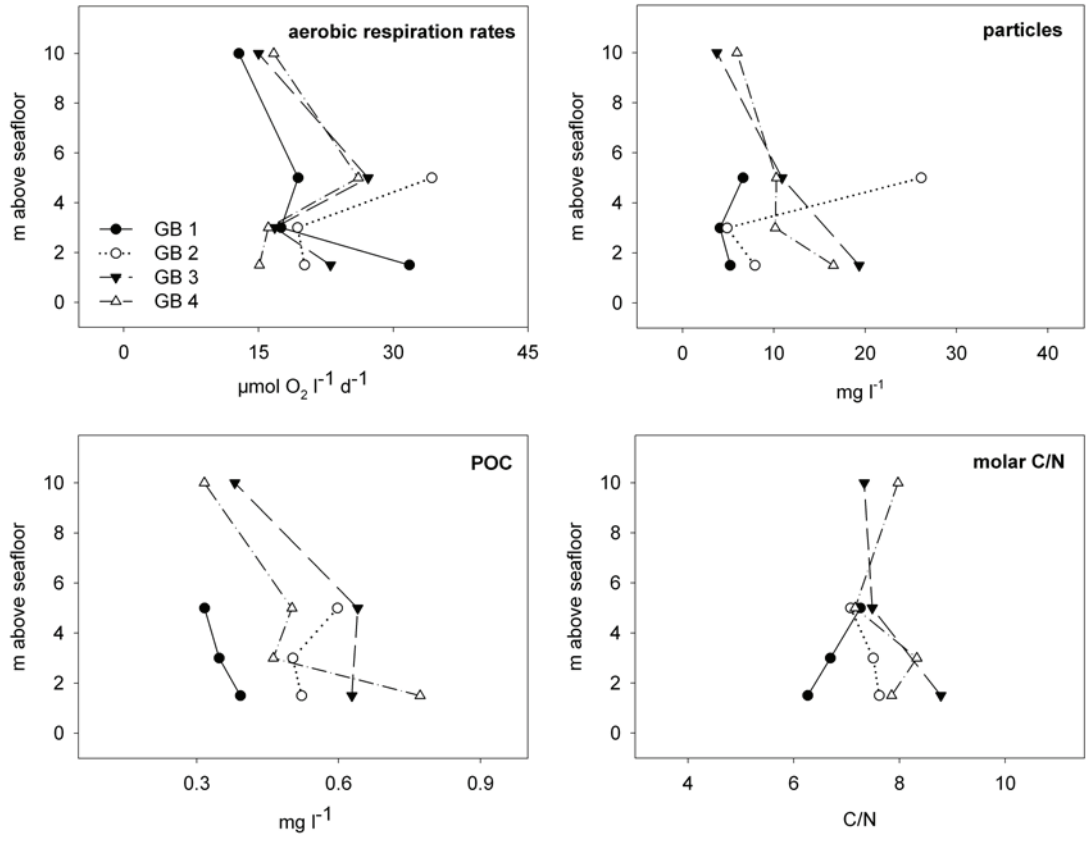

Figure 5: Profiles of aerobic respiration rates, suspended particle concentration, particulate organic carbon (POC) and molar C/N ratios in the benthic boundary layer of the German Bight.

Table 2: Compiled aerobic respiration rates and corresponding concentrations of suspended particulate matter (SPM), particulate organic carbon (POC) and particulate nitrogen as well as the molar C/N ratio and the POC specific respiration.

Station	Depth	O_2 consumption	R^2	SPM	POC	particulate nitrogen	C/N	POC specific rates
		µmol l^{-1} d^{-1}		mg l^{-1}	mg l^{-1}	mg l^{-1}	mol/mol	d^{-1}
GB 1	1.5	31.8	0.995	5.23	0.39	0.07	6.27	0.75
GB 1	3	17.5	0.996	4.09	0.35	0.06	6.69	0.46
GB 1	5	19.4	0.959	6.62	0.32	0.05	7.26	0.57
GB 1	10	12.8	0.981	failed	-	-	-	
GB 2	1.5	20.1	0.994	7.93	0.52	0.08	7.62	0.36
GB 2	3	19.4	0.999	4.88	0.50	0.08	7.50	0.35
GB 2	5	34.3	0.995	26.15	0.60	0.10	7.08	0.53
GB 2	filtered 5	10.3	0.977	-	-	-	-	
GB 3	1.5	23.0	0.952	19.34	0.63	0.08	8.78	0.34
GB 3	3	16.8	0.957	failed	-	-	-	
GB 3	5	27.2	0.999	10.89	0.64	0.10	7.48	0.39
GB 3	10	15.0	0.995	3.75	0.38	0.06	7.33	0.36
GB 4	1.5	15.1	0.984	16.52	0.77	0.11	7.85	0.18
GB 4	3	16.1	0.997	10.15	0.46	0.06	8.33	0.32
GB 4	5	26.1	0.999	10.28	0.50	0.08	7.16	0.48
GB 4	10	16.7	0.921	5.95	0.32	0.05	7.97	0.49
GB 4	filtered 1.5	17.2	0.997	-	-	-	-	
GB 4	filtered 3	18.3	0.999	-	-	-	-	
GB 4	filtered 5	26.1	0.999	-	-	-	-	
BB 1	0.5	1.1	0.932	42.84	1.88	0.23	9.40	0.005
BB 2	0.1	23.2	0.999	2.98	0.27	0.03	10.46	0.785
BB 3	0.5	9.2	0.99	16.52	0.27	0.03	9.21	0.311
BB 4	0.5	3.6	0.974	9.15	0.28	0.04	8.27	0.120
BB 5	0.5	0.5	0.723	1.44	0.15	0.03	6.61	0.031
BB 6	0.5	1.3	0.955	1.50	0.18	0.03	7.71	0.065

In the Bornholm Basin, the water column was separated by a pronounced pycnocline at 45 m depth (Figure 3). Temperature and salinity in the surface waters were ~ 5°C and ~8 PSU, respectively. Oxygen concentrations ranged from 340 to 370 µM. In the bottom waters below the pycnocline, salinity and temperatures increased up to 12 PSU and 8°C, respectively. At the same time oxygen concentrations decreased to around 100µM. At the different stations in the Bornholm Basin, temperatures and salinities in the bottom water ranged from 4.5 to 8.0°C and from 8.1 to 14.2 PSU, respectively (Table 1). Current velocities of the bottom waters ranged from 2 to 8 cm s^{-1}. Aerobic respiration rate measurements for the stations in the Bornholm Basin are shown in Figure 6. At station BB 2, the respiration rate (23 µM O_2 d^{-1}) was comparable to the rates observed in the German Bight. All other stations showed lower rates between 9.2 µM O_2 d^{-1} (BB 3) and 0.5 µM O_2 d^{-1} (BB 5). Correlation coefficients (R^2) from the linear regression were above 0.94. The only exception was BB 5,

where $R^2 \sim 0.72$ (Table 2). Nonetheless, the linear decrease in O_2 concentration was significant ($p < 0.0001$) at this station. The aerobic respiration rate measurements revealed an initial increase in O_2 concentrations in all Bornholm Basin samples until a plateau was reached after 1 to 5 hours (Fig. 6). In some of the respiration rate measurements for the German Bight we observed also an initial increase in O_2 concentrations that, however, is not resolved in Figure 4.

Suspended particulate matter concentrations in the Bornholm Basin ranged from 1.4 to 43 mg l^{-1} and correlated significantly ($p < 0.01$) with the POC and particulate nitrogen concentrations that ranged from 0.15 to 1.9 mg l^{-1} and from 0.03 to 0.23 mg l^{-1}, respectively (Table 2). The organic fraction of suspended particulate matter was between 2 and 12% and the molar C/N ratios ranged from 6.6 to 10.5.

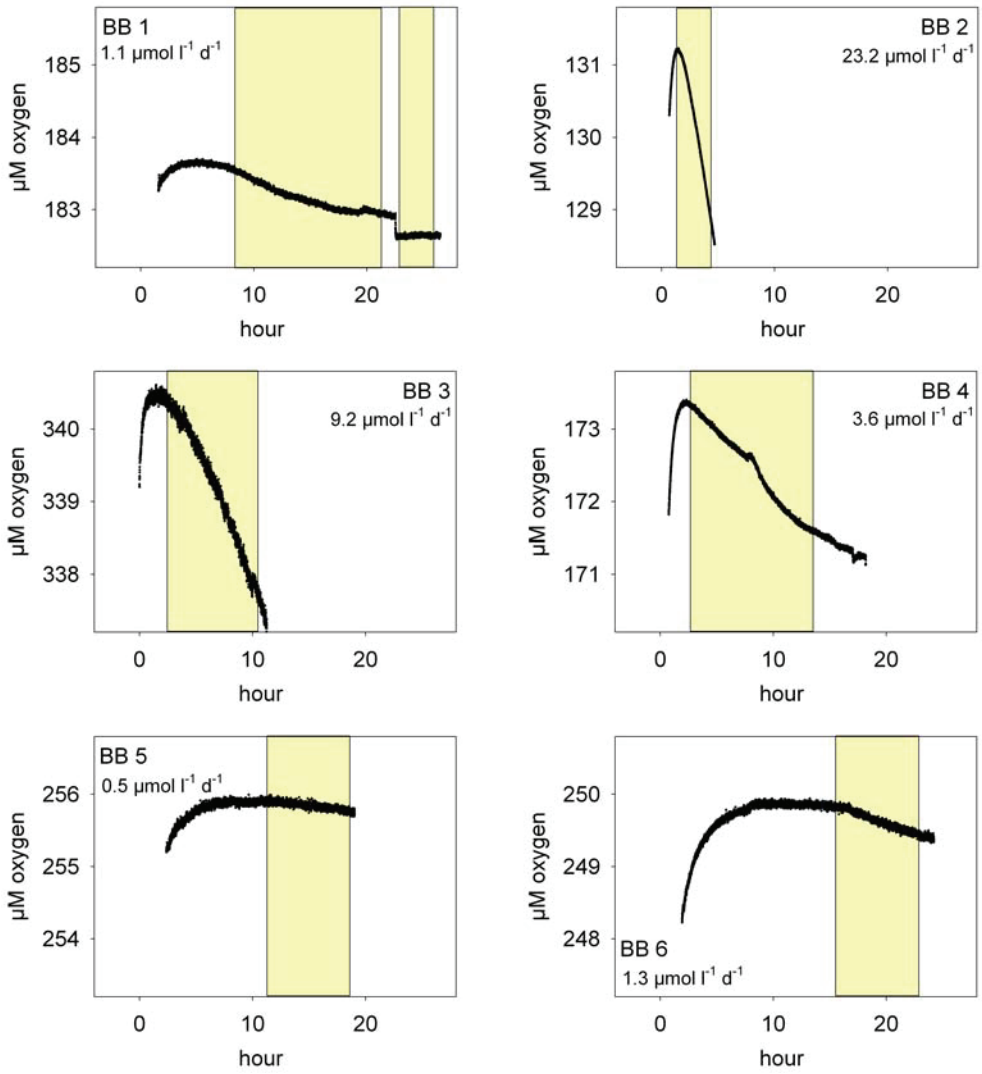

Figure 6: Aerobic respiration rates in the benthic boundary layer in the Bornholm Basin. The yellow background marks the time interval used for linear regression.

Discussion

Aerobic respiration rate measurements

The high accuracy of the oxygen optodes (Tengberg et al. 2006) allows to resolve aerobic respiration rates < 1 μM O_2 d^{-1} during a reasonable incubation time of 10 to 20 hours. Compared to the traditional Winkler technique, the high precision and the high temporal resolution of the optode measurement (one measurement every 10 seconds in this study) allowed to observe the temporal variations in oxygen concentrations. These variations can be due to biologically and non-biologically induced changes in oxygen concentrations. The observed increase in oxygen concentrations at the start of the incubations was, presumably, non-biologically induced. An initial increase in oxygen concentrations was observed in almost every experiment. At the moment we can only speculate about the cause of the initial increase in oxygen concentrations. Temperature is known to have a strong affect on the optode measurement (Tengberg et al. 2006). However, the initial temperature compensation between the water bath and the sample took less than 2 hours and during the experiment, temperature was kept constant within +/- 0.1 °C. Moreover, the optodes we used measure temperature in the water sample and automatically correct oxygen concentrations for changes in temperature.

Interestingly, the artifact was most obvious in samples from the Bornholm Basin, where oxygen consumption rates were low (Fig. 6). High oxygen consumption rates as found in the German Bight probably masked the artifact. The observed gradual change from an initial increase of oxygen concentrations to a linear decrease after several hours suggests an oxygen source from which the dissociation of oxygen was initially high but decreased with time until it became negligible. The oxygen source was probably recharged after every opening and cleaning of the incubation chamber. With regard to this artifact the method needs some further testing and improvement. Nevertheless, the cease of oxygen consumption in response to the poisoning of the sample indicates that the observed decrease of oxygen concentrations after several hours was caused by biological oxygen consumption.

Aerobic respiration rates versus particle abundance and composition

The high aerobic respiration rates in the German Bight (13 and 34 μM O_2 d^{-1}) agree well with pelagic respiration rates of 10 to 30 μM O_2 d^{-1}measured during the summer in the Wadden Sea (List Tidal Basin) by Loebl et al. (2007). The concentrations of suspended particulate matter (average 10 mg l^{-1}) were in the range of previous findings of Puls et al. (1997) who

reported average suspended particulate matter concentration in the German Bight of 2-10 mg l^{-1} at 3-5 m above the sediment. Aerobic respiration rates in the BBL of the Bornholm Basin were, on average, three times lower than those found in the German Bight. Average respiration rates (6 µM O_2 d^{-1}) as well as average suspended particulate matter concentrations (12 mg l^{-1}) in the Bornholm Basin were comparable to respiration rates of 2 to 5 µM O_2 d^{-1} and suspended particulate matter concentrations of 8 mg l^{-1} measured previously in the BBL of the Arkona Basin (see chapter 2).

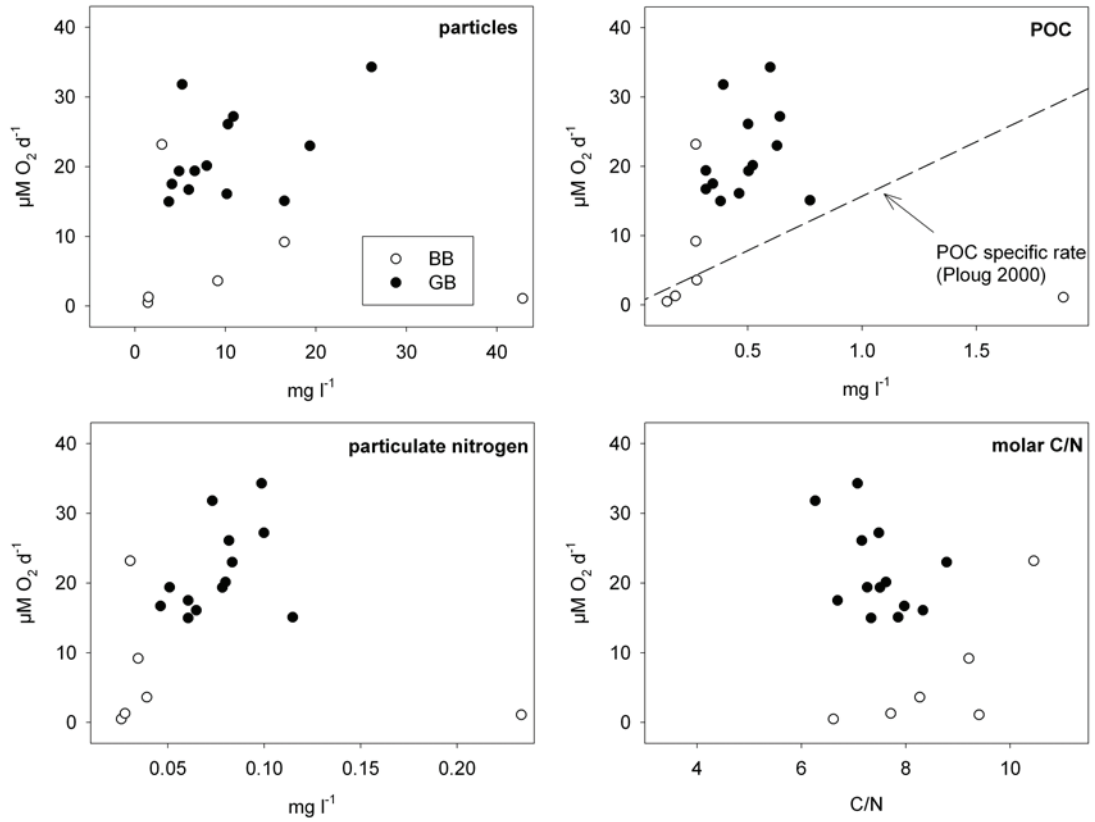

Figure 7: Compiled aerobic respiration rates from stations in the German Bight (black dots) and Bornholm Basin (white dots) *versus* concentrations of suspended particles, particulate organic carbon (POC), particulate nitrogen and molar C/N ratios. The dashed line marks the POC specific rates (i.e. the ratio of respiration rate to POC concentration) as found by Ploug et al. (2000) for diatom aggregates.

In the German Bight, the respiration rates were poorly correlated with the particle abundance and composition (Fig. 7). Neither the concentrations of suspended particulate matter, POC, particulate nitrogen nor the C/N ratios could explain the variability in aerobic respiration rates (all correlations: $p > 0.05$). A correlation between respiration rates and POC was found only at GB2 ($p < 0.05$) (compare with Fig. 5). The poor overall correlation with the particle abundance and composition was unexpected and suggests that respiration was to a large extent controlled by other factors such as dissolved organic matter (DOM)

concentrations. This is supported by the fact that aerobic respiration rates at GB4 did not show any significant change after removal of the particulate matter. However, it can not be excluded that the filtered seawater at GB4 was enriched in DOM due to the release of DOM from particles during filtration.

Nevertheless, the measured respiration rates were extremely high when compared to the POC concentrations. The calculated POC specific respiration rates of 0.18 to 0.75 d^{-1} (Table 2) were increase by factors of up to 10 when compared to POC turnover rates of 0.083 d^{-1} previously observed for microbial mineralization of diatom aggregates (Ploug and Grossart 2000; see also Fig. 7). Since the diatom aggregates consist of reactive organic matter and since the POC turnover rates were measured at maximum bacterial abundance on the aggregates, the POC specific respiration rates of 0.083 d^{-1} can be seen as maximum rates. The mineralization of dissolve organic matter is therefore a likely explanation for the observed high respiration rates in the German Bight. Dissolved organic carbon (DOC) is an important part of the total organic carbon pool in aquatic systems and DOC concentrations of 100-500 µM can be found in coastal waters (Canfield et al. 2005). The most prominent source for DOC is phytoplankton. It was shown by Biddanda and Benner (1997) that 10 to 30% of the total carbon fixed by a phytoplankton bloom can be released as DOC. Carlson et al. (1998) measured a DOC release of 85% of the total fixed carbon during a phytoplankton bloom in the Sargasso Sea. The phytoplankton biomass in the German Bight can be high (8-16 mg m^{-3} chlorophyll) (Joint and Pomroy 1993) even in the late summer due to the nutrient input through the rivers Elbe, Weser and Ems (Hickel et al. 1993). In the shallow waters of the German Bight, primary production occurs at all water depths and chlorophyll concentrations in the bottom water can occasionally exceed the chlorophyll concentrations in the surface waters (Jones et al. 1998). Furthermore, the rivers Elbe, Weser and Ems are a source for terrestrial DOC. It is, therefore, likely that the DOM based mineralization rates exceed the POM based mineralization rates in the German Bight. Further investigations are needed to more accurately distinguish and quantify the respiration due to the mineralization of particulate and dissolved organic matter.

Compared to the German Bight, average respiration rates as well as average concentrations of suspended particulate matter, POC and particulate nitrogen were lower in the Bornholm Basin. In the Bornholm Basin, bottom water current velocities were low (2 to 8 cm s^{-1}) and insufficient to re-suspend substantial amounts of sediment (Seibold 1974). Furthermore, samples in the Bornholm Basin were taken at water depths that were below the euphotic zone in which the phytoplankton spring bloom is usually observed (0-35 m, van

Beusekom et al. 2009). Bottom waters, therefore, were well separated from the major DOM source in the surface waters. POC specific respiration rates at station BB4, BB5 and BB6 (Table 2) were comparable to those reported by Ploug and Grossart (2000) for the diatom aggregates. Only at these stations in the Bornholm Basin respiration rates correlated with POC and particulate nitrogen concentrations ($p < 0.02$, Fig. 7). For the other stations in the Bornholm Basin no positive correlation was found between aerobic respiration rates and suspended particulate matter, POC or particulate nitrogen. In fact, the respiration rates and POC concentrations at BB1 and BB2 were negatively correlated showing lowest respiration rates and highest POC concentrations at BB1 and low POC concentrations but highest rates at BB2 (Table 2, Fig. 7). The sediment at site BB2 was very soft and organic rich ($C_{org} > 5\%$wt, data not shown) causing the BBL-Profiler to sink 30-40 cm into the sediment. It is possible that the suspended matter collected at approximately 10 cm above the sediment was artificially resuspended surface sediment rather than suspended particles from the BBL. The C/N ratios were significantly increased at BB2 compared to the other stations (Table 2) which may be also indicative for the resuspension of less reactive surface sediments. Additionally, the increased respiration rates could be due to enhanced fluxes of dissolved organic matter from the organic rich sediment as described by Burdige and Homstead (1994) who measured a diffusive DOM flux from Chesapeake Bay sediments of up 3 mmol m^{-2} d^{-1}.

Interestingly, respiration rates in the Bornholm Basin were positively correlated with particulate C/N ratios ($p < 0.05$). This is surprising since high C/N ratios are believed to be indicative for a decreased reactivity of organic matter (Richardson 1996). At the moment we can only speculate about the cause of this discrepancy. In the Bornholm Basin, the phytoplankton spring bloom co-occurred with our cruise. At the end of the cruise decreased C/N ratios were observed and we speculate that sedimented phytoplankton aggregates caused a decrease of C/N ratios over time. However, this decrease in C/N ratios of suspended particular matter did not increase the aerobic respiration rates.

In summary, our results from the German Bight and from the Bornholm Basin indicate that aerobic respiration rates in the BBL cannot be explained solely by the availability of particulate organic carbon. Our results provide evidence for the mineralization of DOM. Especially in coastal waters DOM concentrations are increased due to the DOM input from terrestrial sources, the high DOC release from increased phytoplankton production and high DOM fluxes from organic rich sediments (Guo et al. 1995). Nevertheless, suspended particulate matter may provide bacteria with a substrate to grow on, which retains them close to the sediment where concentrations of dissolved organic matter and other solutes are

increased. Furthermore, Ritzrau (1996) argued that the mass transfer of dissolved substrates to a microbial cell that is attached to a particle can be enhanced due to the increased shear in the BBL.

The respiration rate measurements presented in this study were the first in the BBL and revealed that the specific role of the BBL as zone of enhanced solute exchange between sediments and water column is not fully understood. Microbial activity in the BBL may alter concentrations and composition of solutes such as nutrients, thereby controlling the nutrient flux to the surface waters. The strategies and the quantity of the microbial utilization of dissolved substrates in the BBL, therefore, need to be investigated in future studies.

References

Biddanda, B., and R. Benner. 1997. Carbon, nitrogen, and carbohydrate fluxes during the production of particulate and dissolved organic matter by marine phytoplankton. Limnology and Oceanography **42:** 506-518.

Burdige, D. J., and J. Homstead. 1994. Fluxes of Dissolved Organic-Carbon from Chesapeake Bay Sediments. Geochimica et Cosmochimica Acta **58:** 3407-3424.

Canfield, D., B. Thamdrup, and E. Kristensen [eds.]. 2005. Aquatic Geomicrobiology. Elsevier.

Carlson, C. A., H. W. Ducklow, D. A. Hansell, and W. O. J. Smith. 1998. Organic carbon partitioning during spring phytoplankton blooms in the Ross Sea polynya and the Sargasso Sea. Limnology and Oceanography **43:** 375-386.

Emeis, K. and others 2002. Material transport from the near shore to the basinal environment in the southern Baltic Sea - II: Synthesis of data on origin and properties of material. Journal of Marine Systems **35:** 151-168.

Froelich, P. N. and others 1979. Early oxidation of organic matter in pelagic sediments of the eastern equatorial Atlantic: suboxic diagenesis. Geochimica et Cosmochimica Acta **43:** 1075-1090.

Guo, L., P. H. Santschi, and K. W. Warnken. 1995. Dynamics of dissolved organic carbon (DOC) in oceanic environments. Limnology and Oceanography **40:** 1392-1403.

Hebbeln, D., C. Scheurle, and F. Lamy. 2003. Depositional history of the Helgoland mud area, German Bight, North Sea. Geo-Marine Letters **23:** 81-90.

Hickel, W., P. Mangelsdorf, and J. Berg. 1993. The human impact in the German Bight: Eutrophication during three decades (1962-1991). Helgoländer Meeresuntersuchungen **47:** 243-263.

Hill, P. S., and I. N. McCave. 2001. Suspended particle transport in benthic boundary layers, p. 78-103. *In* B. P. Boudreau and B. B. Jørgensen [eds.], The Benthic Boundary Layer: Transport Processes and Biogeochemistry. Oxford University Press.

Inthorn, M., M. R. van der Loeff, and M. Zabel. 2006a. A study of particle exchange at the sediment-water interface in the Benguela upwelling area based on Th-234/U-238 disequilibrium. Deep-Sea Research Part I-Oceanographic Research Papers **53:** 1742-1761.

Inthorn, M., T. Wagner, G. Scheeder, and M. Zabel. 2006b. Lateral transport controls distribution, quality, and burial of organic matter along continental slopes in high-productivity areas Geology **34:** 205-208.

Joint, I., and A. Pomroy. 1993. Phytoplankton biomass and production in the southern North Sea. Marine Ecology Progress Series **99:** 169-182.

Jones, S. E., C. F. Jago, A. J. Bale, D. Chapman, R. J. M. Howland, and J. Jackson. 1998. Aggregation and resuspension of suspended particulate matter at a seasonally stratified site in the southern North Sea: physical and biological controls. Continental Shelf Research **18:** 1283-1309.

Klein, H. 1995. On the current profile in the German Bight: A two-month BroadBand ADCP time series of high vertical resolution. Ocean Dynamics **47:** 77-92.

Loebl, M., T. Dolch, and J. E. E. van Beusekom. 2007. Annual dynamics of pelagic primary production and respiration in a shallow coastal basin. Journal of Sea Research **58:** 269-282.

Paulmier, A., D. Ruiz-Pino, and V. Garcon. 2008. The oxygen minimum zone off Chile as intense source of CO2 and N2O. Continental Shelf Research **28:** 2746-2756.

Ploug, H., and H.-P. Grossart. 2000. Bacterial growth and grazing on diatom aggregates: Respiratory carbon turnover as a function of aggregate size and sinking velocity. Limnology and Oceanography **45:** 1467-1475.

Puls, W., H. Heinrich, and B. Mayer. 1997. Suspended particulate matter budget for the German Bight. Marine Pollution Bulletin **34:** 398-409.

Revsbech, N. P., L. H. Larsen, J. Gundersen, T. Dalsgaard, O. Ulloa, and B. Thamdrup. 2009. Determination of ultra-low oxygen concentrations in the oxygen minimum zone by the STOX sensor. Limnology and Oceanography: Methods **7:** 371-381.

Richardson, K. 1996. Carbon flow in the water column. Case study: The southern Kattegat, p. 95-114. *In* B. B. Jørgensen and K. Richardson [eds.], Eutrophication in Coastal Marine Ecosystems. American Geophysical Union.

Ritzrau, W. 1996. Microbial activity in the benthic boundary layer: Small-scale distribution and its relationship to the hydrodynamic regime. Journal of Sea Research **36:** 171-180.

Ritzrau, W., and L. Thomsen. 1997. Spatial distribution of particle composition and microbial activity in benthic boundary layer (BBL) of the Northeast Water Polynya. Journal of Marine Systems **10:** 415-428.

Seibold, E. 1974. Der Meeresboden. Ergebnisse und Probleme der Meeresgeologie. Springer.

Suess, E. 1980. Particulate Organic-Carbon Flux in the Oceans - Surface Productivity and Oxygen Utilization. Nature **288:** 260-263.

Tengberg, A. and others 2006. Evaluation of a lifetime-based optode to measure oxygen in aquatic systems. Limnology and Oceanography: Methods **4:** 7-17.

Thomsen, L., and G. Graf. 1994. Boundary-Layer Characteristics of the Continental-Margin of the Western Barents Sea. Oceanologica Acta **17:** 597-607.

Thomsen, L., T. Vanweering, and G. Gust. 2002. Processes in the benthic boundary layer at the Iberian continental margin and their implication for carbon mineralization. Progress in Oceanography **52:** 315-329.

van Beusekom, J., D. Mengedoht, C. Augustin, M. Schilling, and M. Boersma. 2009. Phytoplankton, protozooplankton and nutrient dynamics in the Bornholm Basin (Baltic Sea) in 2002–2003 during the German GLOBEC Project. International Journal of Earth Sciences **98:** 251-260.

Van Weering, T. C. E. and others 2001. Benthic dynamics and carbon fluxes on the NW European continental margin. Deep Sea Research Part II: Topical Studies in Oceanography **48:** 3191-3221.

Warkentin, M., H. M. Freese, U. Karsten, and R. Schuhmann. 2007. New and Fast Method To Quantify Respiration Rates of Bacterial and Plankton Communities in Freshwater Ecosystems by Using Optical Oxygen Sensor Spots. Applied and Environmental Microbiology **73:** 6722-6729.

Conclusions and Outlook

The chapters of this thesis can be divided in two main parts. Part one focuses on the dynamics of turbulent transport in the benthic boundary layer, which was mainly discussed in Chapters 2 and 3. Part two focuses on mineralization processes and microbial turnover rates in BBL, sediment and water column, which was mainly discussed in Chapters 4 and 5.

The physical properties of the flow in the benthic boundary layer were described in Chapter 3. It was shown that variable current velocities can cause highly variable turbulent diffusivities that were not predicted by common hydrodynamic models such as the logarithmic Law of the Wall. When the benthic boundary layer exhibited stable density stratification or decreased current velocities a disproportionally high decrease of turbulent diffusivity was found. Although the findings of Chapter 3 are based on measurements in a freshwater lake the conditions that cause such low diffusivities were also found during the expeditions to the Baltic Sea. Stratified boundary layers as found at station A1 and low current velocities as found at station A2 (see Chapter 2) are common in the Baltic Sea and may be found in other regions that exhibit decreased tidal currents or high freshwater input. As pointed out in Chapter 3, the resulting reduction in turbulent diffusivity in the BBL in combination with a moderate to high sedimentary oxygen uptake rate can cause a significant decrease in oxygen concentration at the sediment surface. The decrease in oxygen concentrations found in the lowermost meter of the BBL in the Baltic Sea (see Chapter 2) point in this direction. As a consequence, oxygen concentrations at the sediment surface may decrease so much that they affect the abundance and diversity of macrofauna, and may even cause the release of sulfide into the overlying water column. It would, therefore, be particularly interesting to examine the role of decreased turbulent diffusivity in the BBL for the development of bottom water hypoxia.

In Chapter 2, it was shown that solute gradients in the BBL can be used to distinguish between solutes that are released and solutes that are consumed by the sediment. Since the gradients are measured at some distance above the sediment they readily integrate the mineralization rates at the sediment surface, which can be enhanced in the presence of a fluffy, organic rich surface layer. For example it was shown in Chapter 2 how the release of nitrate from sediment, which was inferred from the nitrate profile in the BBL, provided direct evidence for nitrification at the sediment surface in the Baltic Sea.

High turbulent diffusivities, such as those found in parts of the North Sea (~10^{-3} m^2 s^{-1}) make it difficult to resolve nutrient and oxygen concentration gradients in the BBL. In general, the measurement and use of nutrient and oxygen concentrations gradients to distinguish between sedimentary solute release and consumption is restricted to low and moderate turbulent diffusivities (<10^{-4} m^2 s^{-1}). Under these conditions one may derive flux ratios from the measured gradients as described in Chapter 2 or, alternatively, calculate the absolute fluxes by multiplying the gradients with the turbulent diffusivity that can be measured as described in Chapter 3. As pointed out in Chapters 2 and 3, the advantages of flux measurements in the BBL are that the measurements are non-invasive and consider the diffusive as well as advective flux across the sediment surface. In view of the potential impact of low turbulent diffusivity on the oxygen flux it may be even regarded as imperative to estimate fluxes with such non-invasive methods, since it is virtually impossible to simulate a natural, flux limiting BBL in closed chamber incubations.

The role of the BBL in microbial mineralization and nitrogen loss was investigated in Chapters 4 and 5. In Chapter 5 it was shown that oxygen respiration rates in the BBL could not be explained by the sole availability of particulate organic matter. Instead, the results provide evidence that microorganism in the BBL may utilize considerable amounts of dissolved organic matter, which was eventually released from the sediments. In Chapter 4 it was shown that anammox rates in the oxygen minimum zone of the Arabian Sea were increased in the oxycline but also in the suboxic benthic boundary layer. In fact, the anammox rates in the BBL exceeded those observed in the oxycline. In addition, the efflux of ammonium and nitrite from the sediment was indicated by the increase in concentration with depth in the BBL. These substrates that are released from the sediment may feed anammox bacteria growing in the suboxic BBL. Alternatively, anammox bacteria may stick to particulate organic matter and feed on the ammonium and nitrite released during POM mineralization.

The combined results from Chapters 4 and 5 suggest that the specific role of the BBL as interface between reduced sediments and the oxic water column is not fully understood. As such, the BBL is a favorable niche for microbes that benefit from the different redox potentials of dissolved substrates. As nutrients are transported across the BBL, the redox processes in the BBL may alter the nutrient stoichiometry and as such control the primary production and the species composition of the phytoplankton community in the surface waters.

Acknowledgements

First of all I have to say that this work would have been virtually impossible without the sharing of enthusiasm, skill and knowledge and without the atmosphere of easy collaboration that I have experienced in the entire Institute. I would like to thank all those who contributed to this spirit of open mindedness.

In particular, I would like to thank Bo Barker Jørgensen for accepting me as a PhD student, for his advice and comments in the committee meetings and for reviewing the thesis.

I am most grateful to my two mentors Volker Brüchert and Marcel Kuypers who greatly supported me in numerous ways. It was due to Volker Brüchert that I walked the first steps into the field of Biogeochemistry and I am thankful for his support and teamwork during various expeditions. Very special thanks go to Marcel Kuypers for sharing is experience in the field nitrogen cycling and for the numerous enthusiastic and encouraging discussions. It was his ability to separate important from irrelevant things that helped me a lot especially over the last period of the thesis. Hartelijkt bedankt!

Many thanks go to Andreas Lorke from the University of Koblenz-Landau for his extra lessons on fluid dynamics. His advice and encouragement was essential for major parts of the thesis.

I also would like to thank Michael Schlüter for his teamwork during various cruises and for sharing ideas and equipment. He was much involved in all the challenging technical aspects that were important for the thesis. I also thank him very much for the examination of the thesis.

I want to thank Gaute Lavik for introducing me to the mysteries of mass spectrometry. He was the main and most important support in the cellar dwelling times of isotope measurements.

I would further like to thank Hans Røy, Felix Janssen and Frank Wenzhöfer for their advice and encouragement in many technical aspects of the work as well as Arzhang Khalili for his help in mathematics.

Many thanks go to Gavin Collins from the University of Galway for his friendship and collaboration and for the relaxing and fun time after work.

For their help and technical assistance and for the many practical advices in the laboratory I want to thank especially Gabi Klockgether, Daniela Franzke, Martina Meyer, Jaqeline Schmidt, Kirsten Imhoff and Andrea Schipper. Very special thanks go also to all technicians who contributed to the construction of the sampling devices: Volker Meyer, Paul Färber, Harald Osmers, Georg Herz, Volker Asendorf, Jörn Patrick Meyer, Axel Nordhausen and Marc Viehweger. Without their skills and dedication this work would have never been possible.

I would further like to thank the captains and crews of *RV Heincke*, *RV Alkor*, *RV Meteor*, and *RV Professor Albrecht Penck* for their support and excellent collaboration. I am indebted to Bernd Schneider, Anne Loeffler and Lars Umlauf from the Leibniz Institute for Baltic Sea Research, Warnemünde as well as to Sabine Kasten, Michael Schlüter and Volkhard Spieß from the Geoscience Department of the University of Bremen who organized the various expeditions.

All dear colleagues in the Nutrient Group and the BioGeo Group are thanked for their open mind and warmth which made the last years a very pleasant time. My long term office members Phyllis Lam and Hang Gao are thanked very much for a lot of help, discussions and latest news. I also want to thank Jan Fischer, Alberto Robador, Casey and Anna-Maria Hubert, Simone Böer, Friederike Hoffmann, Gunter Wegener, Anna Lichtschlag, Ireen Viehweg and Sarah Sokoll for their friendship and the spare time that we spent together.

Most of all I want to thank my family as well as Patrick, Hans and Gülay, my spare time divers Uwe and Matilda and my dear friends Lars and Stefan for their support and for their curiosity and interest which kept me from feeling like a scientific nerd. My very special thanks go to my lovely Rita for her love and support especially at the end of this work.

Finally I would like to acknowledge the DFG-Research Centre / Excellence Cluster „The Ocean in the Earth System" and the Max Planck Society for providing funding of the work.

Titles and Abstracts not included in the Thesis

Environmental Microbiology (2009)

Complex nitrogen cycling in the sponge *Geodia barretti*

Friederike Hoffmann[1], Regina Radax[2], Dagmar Woebken[1], Moritz Holtappels[1], Gaute Lavik[1], Hans Tore Rapp[3], Marie-Lise Schläppy[1], Christa Schleper[2,3] and Marcel M. M. Kuypers[1]

1) Max Planck Institute for Marine Microbiology, Celsiusstr. 1, 28359 Bremen, Germany.

2) Department of Genetics in Ecology, Faculty of Life Sciences, Althanstr. 14, 1090 Vienna, Austria.

3) Centre for Geobiology, Department of Biology, University of Bergen, PO Box 7803, 5020 Bergen, Norway.

Received 3 October, 2008; accepted 30 March, 2009.

Abstract

Marine sponges constitute major parts of coral reefs and deep-water communities. They often harbour high amounts of phylogenetically and physiologically diverse microbes, which are so far poorly characterized. Many of these sponges regulate their internal oxygen concentration by modulating their ventilation behaviour providing a suitable habitat for both aerobic and anaerobic microbes. In the present study, both aerobic (nitrification) and anaerobic (denitrification, anammox) microbial processes of the nitrogen cycle were quantified in the sponge *Geodia barretti* and possible involved microbes were identified by molecular techniques. Nitrification rates of 566 nmol N cm^{-3} sponge day^{-1} were obtained when monitoring the production of nitrite and nitrate. In support of this finding, ammonia-oxidizing *Archaea* (crenarchaeotes) were found by amplification of the *amoA* gene, and nitrite-oxidizing bacteria of the genus *Nitrospira* were detected based on rRNA gene analyses. Incubation experiments with stable isotopes ($^{15}NO_3^-$ and $^{15}NH_4^+$) revealed denitrification and anaerobic ammonium oxidation (anammox) rates of 92 nmol N cm^{-3} sponge day^{-1} and 3 nmol N cm^{-3} sponge day^{-1} respectively. Accordingly, sequences closely related to *'Candidatus Scalindua sorokinii*' and *'Candidatus Scalindua brodae*' were detected in 16S rRNA gene libraries. The amplification of the nirS gene revealed the presence of denitrifiers, likely belonging to the *Betaproteobacteria*. This is the first proof of anammox and denitrification in the same animal host, and the first proof of anammox and denitrification in sponges. The close and complex interactions of aerobic, anaerobic, autotrophic and heterotrophic microbial processes are fuelled by metabolic waste products of the sponge host, and enable efficient utilization and recirculation of nutrients within the sponge–microbe system. Since denitrification and anammox remove inorganic nitrogen from the environment, sponges may function as so far unrecognized nitrogen sinks in the ocean. In certain marine environments with high sponge cover, sponge-mediated nitrogen mineralization processes might even be more important than sediment processes.

J. Phys. D: Appl. Phys. **40** (2007) 6850–6856

A new working principle for ac electro-hydrodynamic on-chip micro-pumps

Marco Stubbe[1], Moritz Holtappels[2] and Jan Gimsa[1]

1) Chair of Biophysics, Faculty of Biology, University of Rostock, D-18057 Rostock, Germany

2) Max Planck Institute for Marine Microbiology, Celsiusstrasse 1, D-28359 Bremen, Germany

Received 21 August 2007, in final form 19 September 2007, Published 19 October 2007

Abstract

Our new type of on-chip micro-pump exploits the ac electro-kinetic forces acting in the volume of a fluid in the presence of a temperature gradient. No mechanically movable parts are used. The velocity of the pump flow observed depends on the frequency and strength of the driving ac field and on the temperature gradient across the pump channel. An integrated heating element allows the temperature gradient to be adjusted. Both ac field electrodes and heating element are platinum structures processed on a glass chip. The pump-channel walls and cover are made from polymer and thin-glass, respectively. In this paper, we present measurements of the fluid velocity as functions of the medium conductivity (0.1-1.3 S m^{-1}) and field frequency (300 kHz-52 MHz), voltage across the field-electrode voltage (0-35 Vrms) and the heating element (1.1-3.6 V). Velocities of up to 120 μm s^{-1} were observed in the pump channel. The advantage of our new design is an evenly shaped cross-section of the pump channel, which reduces the risk of the channel becoming clogged by debris. Ac-electro-osmosis is not a predominant effect in our structures. Pumping could only be observed when the heating current and ac-pump field were applied simultaneously. The effects observed were simulated with the COMSOL Multiphysics program.

PHYSICAL REVIEW E **79**, 026309 (2009)

AC-Field-Induced Fluid Pumping in Microsystems with asymmetric Temperature Gradients

Moritz Holtappels[1], Marco Stubbe[2] and Jan Gimsa[2]

1)Max Planck Institute for Marine Microbiology, Celsiusstrasse 1, D-28359 Bremen, Germany

2)Chair of Biophysics, Faculty of Biology, University of Rostock, D-18057 Rostock, Germany

Received 27 May 2008; revised manuscript received 4 December 2008; published 12 February 2009

Abstract

We present two different designs of electrohydrodynamic micropumps for microfluidic systems. The micropumps have no movable parts, and their simple design allows for fabrication by microsystems technology. The pumps are operated by ac voltages from 1 to 60 V and were tested with aqueous solutions in the conductivity range of 1–112 mS m^{-1}. The pump effect is induced by an ac electric field across a fluid medium with an inhomogeneous temperature distribution. It is constant over a wide range of the ac field frequency with a conductivity-dependent drop-off at high frequencies. The temperature-dependent conductivity and permittivity distributions in the fluid induce space charges that interact with the electric field and induce fluid motion. The temperature distribution can be generated either by Joule heating in the medium or by external heating. We present experimental results obtained with two prototypes featuring Joule heating and external heating by a heating filament. Experimental and numerical results are compared with an analytical model.